



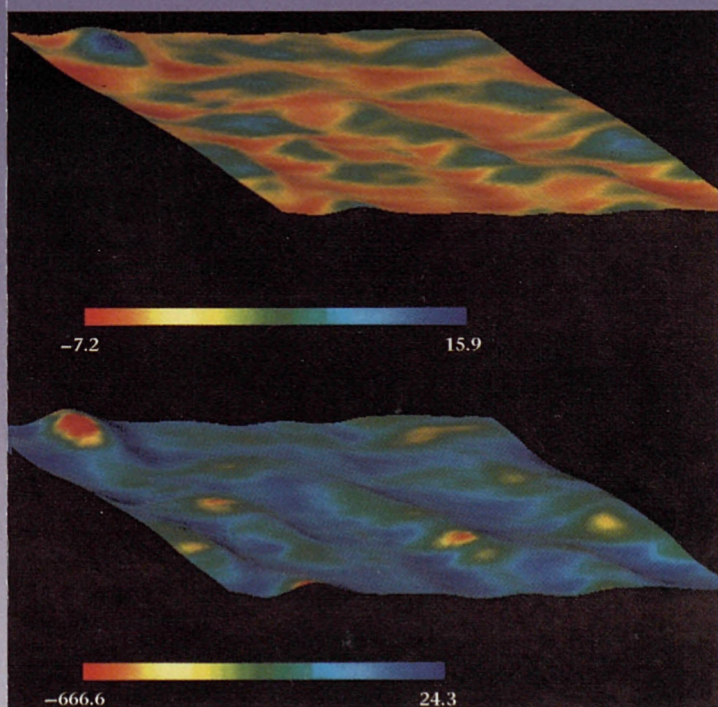
EUROPEAN
COMMISSION

SCIENCE
RESEARCH
DEVELOPMENT

Environment and climate programmes

Investigations of the coupling fluxes at the air-ocean interface

■
Research results



EUR 18356 EN



Cover photos: Streaky structure (top) and shear stress (bottom) at the air-ocean interface



EUROPEAN COMMISSION

Edith CRESSON, Member of the Commission
responsible for research, innovation, education, training and youth
DG XII/B.1 — RTD actions: Environment — Climatology and natural hazards

Contact: Dr Claus Brüning

*Address: European Commission, rue de la Loi 200 (SDME 7/41)
B-1049 Brussels — Tel. (32-2) 29-54484; fax (32-2) 29-63024*

European Commission

Investigations of the coupling fluxes at the air-ocean interface

Edited by Paolo Andreussi and Sanjoy Banerjee

Project No EV5V-CT93-0291
August 1997

Final report

Directorate-General
Science, Research and Development

1998

EUR 18356 EN

LEGAL NOTICE

Neither the European Commission nor any person acting on behalf of the Commission is responsible for the use which might be made of the following information.

A great deal of additional information on the European Union is available on the Internet. It can be accessed through the Europa server (<http://europa.eu.int>).

Cataloguing data can be found at the end of this publication.

Luxembourg: Office for Official Publications of the European Communities, 1998

ISBN 92-828-4878-7

© European Communities, 1998

Reproduction is authorised provided the source is acknowledged.

Printed in Belgium

PRINTED ON WHITE CHLORINE-FREE PAPER

Foreword

An important aim of climate research is to better understand the processes at the ocean-atmosphere interface, since air-sea exchange processes play an important role in the dynamics of the climate system. They are crucial when coupling Ocean and Atmosphere General Circulation Models, which provide the basis for reliable climate change predictions. The ever-increasing resolution of numerical climate models requires detailed description and computation of the air-sea fluxes and their perturbation by the ocean surface wave field on a global scale.

Observations based on satellite retrievals have become the main data source, satisfying the growing demand for continuous global measurements of ocean waves and other climate relevant parameters. The development and application of advanced wind-wave data assimilation systems combining satellite observations, field and model data, is also an important milestone towards improved model predictions. It is a particular useful tool for model validation and development. Also, measurements in wind-wave channels add to the understanding of the physical processes. Further progress in this research area requires the combination of these tools and the close co-operation of experimentalist and modellers.

The present publication is a result of an EC project under the Environment and Climate Programme of DGXII. Research teams of 8 European institutions have combined their experiences to tackle this complex issue. The results of this project prove the usefulness of satellite data for wave predictions and model development underpinning the importance of air-sea exchange processes for climate model predictions.

We congratulate the authors on their achievements and are confident that this report will find the expected resonance in the scientific community.

A. Ghazi and C. Brüning
Climate and Natural Hazards Unit
DGXII/D/2
Environment and Climate Programme
European Commission

Contents

PREFACE	iii
CHAPTER 1. OVERVIEW OF THE PROJECT	1
1.1 Issues and State of the Art	1
1.2 Modelling approaches	4
CHAPTER 2. DEVELOPMENTS RELATED TO MODELLING AND REMOTE SENSING OF OCEAN WAVES	5
2.1 Introduction	5
2.2 Retrieval of wave spectra from ERS-1 SAR data	7
2.3 Global validation of satellite and WAM model data	10
2.3.1 Analysis of altimeter data	10
2.3.2 A three year global validation of the WAM model using ERS-1 SWM spectra	13
2.4 Assimilation of satellite data into the WAM model	16
2.4.1 The optimal interpolation scheme	16
2.4.2 The Green's function assimilation method	17
2.5 The adjoint modelling technique	17
2.5.1 Application of the adjoint technique to model tuning	18
2.5.2 The use of SWADE data for adjoint wave modelling	18
2.5.3 Towards an integrated wind and wave data assimilation	19
2.6 Future directions: Tests using the adjoint of WAM and the ECAWOM	19
CHAPTER 3. MOMENTUM AND SENSIBLE HEAT EXCHANGE AT THE AIR-SEA INTERFACE	20
3.1 Introduction	20
3.2 Reynolds averaged modelling of air-sea exchange of momentum and sen- sible heat	21
3.2.1 Interpretation of field data	21
3.2.2 A one dimensional model	23
3.2.3 Results	25
3.3 Air Flow over Waves: Numerical Developments	29
3.4 High frequency / high wavenumber wind-wave spectra and breaking waves	31
CHAPTER 4. GAS AND MOISTURE EXCHANGE AT AIR-WATER INTERFACES	32
4.1 Introduction	32
4.2 Scalar transfer models – a brief history	33
4.3 Turbulence Structure near flat gas liquid Interfaces	35
4.4 Turbulence structure near wavy surfaces	37
4.5 Scalar transfer rates	39
4.5.1 Simulation Results: flat interface	39
4.5.2 Simulation Results: Wavy surface	42
4.5.3 Scalar flux parametrization	42

CHAPTER 5. SEA SPRAY EFFECTS ON LATENT HEAT EXCHANGE AT THE AIR-SEA INTERFACE	45
5.1 Introduction	45
5.2 Mechanism of droplet generation	46
5.3 Droplet production	49
5.3.1 Method of calculating droplet production	49
5.3.2 Flow over waves	50
5.3.3 Droplet simulations and estimates of droplet production	51
CHAPTER 6. CONCLUSIONS AND FUTURE DIRECTIONS	56
6.1 Wave-Climate Models	56
6.2 Wave Forecasting	57
6.3 Wind-Wave Momentum Coupling	58
6.4 Heat and Mass Exchange	60
6.5 Exchange Processes due to Marine Spray	61
6.6 Future Work	62
REFERENCES	63

PREFACE

The atmosphere and the oceans respond at very different rates to stimuli such as additions of heat. This allows climate, over the short term, to be predicted by calculations of atmospheric conditions that are largely uncoupled from calculations of the general oceanic circulation. Over the long term, however, the oceans act something like flywheels, storing information about past climatic conditions that cumulatively impact their large-scale motions. Therefore, for century-long climate predictions, interactions between the atmospheric and the oceanic circulations become critical. In fact, a key uncertainty in such predictions arises from incomplete understanding of the atmosphere-ocean coupling, which entails exchanges of heat, momentum and mass.

The rates at which such exchanges occur affect quantities, vital to climate, such as atmospheric concentrations of water vapor and greenhouse gases like CO_2 , as well the oceanic circulation itself – which is largely driven by stresses at the surface imposed by the wind, i.e. by momentum exchange with the atmosphere.

The lack of understanding, and hence, of reliable quantitative estimates of ocean-atmosphere exchange rates is related to the complex nature of the interface between the two systems. The interface moves and deforms into waves with a substantial range of lengthscales, some of which may break, forming spray and entraining bubbles. This makes it difficult to measure relevant quantities like concentrations of various species, fluid velocities and temperature. It is as difficult to develop theories, the problem being exacerbated by both the atmosphere and ocean being turbulent – a state that continues to baffle researchers even in its simplest manifestations far from boundaries.

The problem is compounded by the different length scales of fluid motion that impact the exchanges. For example, momentum exchange occurs primarily due to drag exerted by the wind on the ocean surface. The drag itself depends on the state of the surface, i.e. the sizes and lengths of the waves – which in turn depend on the drag. A portion of the drag is primarily associated with the form of the waves – the “form” drag – and is controlled by the relatively large amplitude waves with lengths of the order of meters. A portion of the drag is also associated with the friction between the wind and the water, and this “frictional” drag is affected primarily by waves with length scales of the order of millimeters and centimeters, rather than meters.

If we consider now the other exchanges of interest, the controlling resistance to moisture transfer, in the absence of sprays, lies in layers with thickness of the order of millimeters – similar to the length scales affecting frictional drag, but two or three orders of magnitude smaller than those of primary interest for form drag. On the other hand, exchanges of gases, like CO_2 , are controlled by resistances in layers, now on the water side, that have thickness of the order of one hundredth of a millimeter – length scales, therefore, four to five orders of magnitude smaller than those of primary interest for form drag.

These considerations associated with ocean-atmosphere coupling, and its importance in climate prediction, prompted a group of meteorologists, oceanographers, fluid dynamicists and chemical engineers to initiate an informal dialogue on the subject in early 1991. The rationale for forming such a multidisciplinary group arose naturally from the multiplicity of scales involved in the exchange processes. At one end of the spectrum were members of the group interested in modelling the general circulation of the atmosphere and oceans, and the nature of the global wave field — meteorologists and oceanographers. At the other end were chemical engineers interested in the micro-physics of transport processes dominated by fine-scale turbulence, *e.g.* in gas exchange which is controlled by layers of the order of one hundredth of a millimeter thick.

Out of this dialogue arose the PISA (Pisa-coordinated Investigation of Sea/Air Coupling) project funded by the EU under Contract EV5V-CT93-0291 (DG XII). The project has been coordinated by Consorzio Pisa Ricerche, a research institution associated with the University of Pisa. The other members of the consortium and active participants were the Max Planck Institut für Meteorologie, Hamburg, Germany, and from the UK, the Meteorological Office, Reading University and Imperial College, London. At a later stage, the Royal Netherlands Meteorological Institute (KNMI) acted as a subcontractor.

The main scientists involved in the project were: Paolo Andreussi, Sanjoy Banerjee, Paolo Lombardi, Valerio De Angelis, Maria Vittoria Salvetti, Angela Rossodivita and François Beux from *Consorzio Pisa Ricerche*; Klaus Hasselmann, Patrick Heimbach and Georg Barzel from *Max Planck Institut*, Vladimir Makin and C. Mastenbroeck from *Royal Netherlands Meteorological Institute*; Geoffrey Hewitt and Martin Pattison from *Imperial College*; Stephen Belcher, Derek Stretch and Nicola Harfield from *University of Reading*; Julian Hunt, Steve Foreman and Nigel Wood from *UK Met Office*.

The present work tries to summarize the main results of the project, avoiding derivations and details which are believed to be of minor impact to the scientific community to which this work is addressed. In order to have a more complete understanding of the project, reference should be made to the three Annual Reports, which contain the periodic reports from individual partners, and to the list of scientific papers generated by or directly related to the project, here enclosed.

This report is organized as follows: Chapter 1 presents a brief survey of what was known about air-sea interactions when the project was initiated. Chapter 2, 3, 4 and 5 report the main results obtained at the Max Planck Institut (Chapter 2), Reading University with support from the Royal Netherlands Meteorological Institute (Chapter 3), Consorzio Pisa Ricerche (Chapter 4) and the Imperial College (Chapter 5). To the extent possible, the discussions in Chapters 2, 3, 4 and 5 have been made “stand-alone,” *i.e.* they are relatively self-contained, and can be read without reference to the others. The last chapter presents the conclusions and main achievements of the project. The directions in which further work is desirable are also indicated.

The developments themselves, of course, have already proved useful and will be incorporated in coupled-atmosphere-wave-ocean models in the future. This was the main objective of the present project and the results obtained allowed this objective to become within reach.

Paolo Andreussi and Sanjoy Banerjee

Pisa, July 1997.

CHAPTER ONE

OVERVIEW OF THE PROJECT

1.1 Issues and State of the Art

Reliable prediction of changes to the global climate, in response to both human activities and natural causes, is crucial to the development of policies to mitigate effects on the economy and society. Although the climate system is very complex, considerable progress has recently been made in modelling its changes and understanding its sensitivity to many phenomena and processes. Clearly the ocean has an enormous influence on the atmosphere, from moderating the diurnal cycle to controlling the climate of continents. This necessitates good representations in models of climate of the internal dynamics, thermodynamics and biology of oceans, and of the fluxes across the ocean surface.

The overall objective of this project was to elucidate the mechanisms governing exchanges of momentum, heat and chemical species (CO_2 , moisture, etc.) between the atmosphere and the oceans, as these appeared to be crucial in making reliable long-term climate predictions. In particular, the role of ocean-surface waves in mediating these exchanges was to be clarified, as this appeared to be an aspect that was poorly understood at the time the PISA project was initiated. At the outset, it was clear that momentum exchange rates and the ocean-wave field were strongly coupled, and therefore, further development of numerical wave-forecasting models was an essential ingredient of the work.

Global climate change studies are increasingly turning to Coupled Ocean-Atmosphere General Circulation Models (CGCMs) for improved simulations, *e.g.* Washington and Meehl (1989), Stouffer *et al.* (1989) and Hasselmann (1991). These CGCMs represent significant advances over atmosphere general circulation/mixed-layer ocean models used previously to estimate climatic response to increased greenhouse gas concentrations by Hansen *et al.* (1988), Manabe and Wetherald (1987) and Washington and Meehl (1984). A key uncertainty in CGCMs relates to the fluxes of momentum, energy and species (*e.g.* water vapour and CO_2) at the air-ocean interface — the coupling between OGCMs and AGCMs primarily being through these fluxes.

Except very recently in regional simulations like ECAWOM (about which, more later), the present state of the art is almost entirely to phrase these fluxes in terms of local (grid-averaged) parameters. The ocean state (or the wave field) is not explicitly introduced into the expressions — though it is implicit, in that the wind speed dependence in the flux expressions is thought to capture the ocean state. However, the ocean-surface wave-field depends on the spatio-temporal history of the wind and therefore requires solution of a transport equation for the two-dimensional wave spectrum. The transport equation has source and sink terms related to wind input and dissipation. Consequently, the ocean-surface wave field, which is known to influence the air-ocean fluxes, cannot be simply related by algebraic relationships to the wind and various stability parameters — which is the present approach! It is clear that good coupling models between Ocean GCMs (OGCMs) and Atmosphere GCMs (AGCMs) must be dynamic in the sense that at least a simplified transport equation is solved for the global wave field, and the expressions for the fluxes explicitly contain wave parameters in addition to the conventional ones, such as wind velocity, sea surface temperature (SST), air temperature and air humidity.

In more detail, consider that the following fluxes must be estimated:

- Air-side sensible and latent moisture heat fluxes.
- Momentum flux.
- CO₂ and other greenhouse gas fluxes.

We include in the latent heat/moisture flux a contribution due to evaporation of sprays. Alternatively, a droplet flux can be separated out with evaporation calculations being done in the AGCM rather than in the air-ocean coupling model. Certainly, for prediction of latent heat/moisture, sensible heat, momentum and greenhouse gas fluxes, the ocean-surface state is likely to be important in mechanistically-based expressions.

At present, for heat and momentum exchange the usual framework adopted for the calculation of the fluxes is based on Monin-Obukhov theory (Businger, 1973), or some variation that is related to it. This results in vertical profile functions for wind velocity, temperature and humidity (water vapour concentration) which involve a number of constants and stability parameters (the Monin-Obukhov length which requires the surface stress and heat flux). The expressions also involve “roughness” length scales. Models such as those of Liu *et al.* (1979) essentially solve the system of equations by iteration, given wind speed, sea surface temperature, air temperature and air humidity. Implicit in these calculations is that the ocean-surface state is in equilibrium with the wind, *i.e.* is only a function of the current wind conditions, not of the history of the wind.

Reviews of similar methods of estimating the exchange coefficients have been provided by Blanc (1985) and Smith (1989). Without going into detail, suffice it to say that these expressions are extremely difficult to verify since open-ocean flux measurements are difficult.

In particular, it is clear that very large deviations are obtained from the various models *e.g.* Liu *et al.* (1979), Geernaert *et al.* (1990) and Kondo (1975, 1976), in conditions when the wind speed is changing. See for example the very large deviations in drag coefficients, from the predictions, measured by Bradley *et al.* (1991) and which they attributed to rising winds in the period preceding the runs. It is precisely because

the ocean-surface state is not in equilibrium with the wind in such situations, that a dynamic wave model is needed for predictions of the various fluxes.

A second factor that complicates calculation of the latent heat/water vapour flux at the ocean surface arises from the formation of sprays from breaking waves. There are two main mechanisms by which droplets are produced. Breaking waves entrain air and the resulting bubbles rise to the surface where they burst, forming small droplets. At wind speeds above about 9ms^{-1} , the stress on the waves becomes high enough to tear liquid directly from the wave crests, forming spume drops — this is believed to be the primary mechanism of spray generation at high wind speeds. The bursting of bubbles has been studied experimentally by, for example, Blanchard (1982) and Resch and Afeti (1992), and the mechanisms by which the droplets are produced are now relatively well understood. Much less is known about the formation of spume droplets, though some photographic observations have been made in a wind/wave tank by Koga (1981, 1987). The underlying mechanism is thought to be the Kelvin-Helmholtz instability.

The key problem in quantifying the spray contribution to the fluxes is that the rate at which droplets are produced is not at all well known. To this end, a number of experiments have been performed in which droplet concentrations and size distributions have been measured. These have included both field trials (*e.g.* DeLeeuw, 1990 and Smith *et al.*, 1990) and laboratory-scale investigations using wind/wave tanks (*e.g.* Lai and Shemdin, 1974; Wang and Street, 1978). A number of researchers have used such data to construct models for the rate of droplet generation, but the predictions of different models vary by several orders of magnitude (Wu, 1993).

We turn now to the subject of air-ocean gas transfer. This subject has been extensively researched but there remains large differences between JASIN, BOMEX and GEOSECs when the gas transfer velocity is correlated with wind velocity (see Liss and Merlivat, 1986; Takahashi, 1989; Murphy *et al.*, 1991). The GEOSECs Antarctic Summer and Antarctic Winter experiments are at relatively high wind speed ($>10\text{ms}^{-1}$) whereas JASIN and BOMEX are well below 10ms^{-1} . Part of the problem undoubtedly arises from using wind velocity as a correlating parameter — instead of, as we will discuss later, the wind stress — and part may be due to bubble entrainment becoming an important transport mechanism at high wind velocity. The situation requires clarification, particularly in view of the rapid developments in our understanding of near surface turbulence structure that have occurred in several laboratories (*e.g.* , Komori *et al.*, 1989; Banerjee, 1990a). These developments emphasize the need for knowledge of the ocean-surface state, as discussed earlier. This is also highlighted by Murphy *et al.* (1991) who show the variability in gas transfer flux when correlated against wind velocity, without directly introducing the ocean-state effects.

To repeat, the wind velocity, which is conventionally used, is in any case the wrong correlating parameter to collapse the data and second, under the higher winds there may be breaking waves giving rise to entrainment of bubbles. The first is a serious problem since, as will be shown later, form drag plays almost no role in affecting heat and mass transfer. The bubble entrainment effect must be taken into account (see Broecker and Siems, 1984 and Merlivat and Memery, 1983 for early discussions of the effect) and also requires explicit consideration of the ocean surface state.

To summarise, most current models for the coupling fluxes are phrased in terms of algebraic relationships between averaged variables (such as wind speed, SST, air temperature and air humidity). However, consideration of the ocean surface state is necessary. This requires solution of at least a simplified wave evolution equation.

From this, grid-averaged wave parameters may be obtained and explicitly included in expressions for the fluxes. With regard to latent heat/moisture flux, it is necessary also to consider the formation of sea spray.

1.2 Modelling approaches

With the advent of ever more powerful computers, many of the mechanisms governing transport processes are becoming amenable to elucidation by approaches that combine computation and experiments. For relatively low Reynolds numbers, or phenomena governed by length scales such that they can be characterized by low Reynolds numbers, Direct Numerical Simulation (DNS) becomes possible. These are essentially “numerical experiments” provided resolution and numerical accuracy are made sufficient. Since scalar transfer at continuous interfaces occur over length scales that lead to relatively low Reynolds numbers when these are based on thicknesses of the layers containing the main resistances DNS may well clarify the important transport mechanisms for such problems. On the other hand, DNS cannot be done, in the foreseeable future, over length scales like those governing form drag – or the upper end of the range affecting frictional drag. Here, models are required for the turbulence in the fine scales, and only the large flow structures can be computationally resolved. Such Large Eddy Simulations (LES) can indicate, for example, whether separation occurs behind wave crests, and can, also, indicate what types of simpler models might be most successful in capturing the governing phenomena. Such LES depends, to some extent, on DNS for the subgrid scale models — an area in which much research is still necessary before reliable results can be expected.

For more routine calculations, averaging of motions over all scales is necessary leading to what are called Reynolds-averaged models. These usually cannot clarify physical mechanisms, but when “tuned” against experiments and DNS, may provide sets of results on turbulence statistics that are valuable for mechanistic and theoretical developments that lead to relatively simple parametrizations for the coupling fluxes.

At the end of the process that builds on such a cascade of approaches, starting with DNS and progressing through perhaps LES and Reynolds-averaged modelling to mechanistic/theoretical models, is the requirement that the results be simple enough to incorporate in coupled general circulation models. Ideally, the resulting model or theory must be phrased in terms of the variables calculated by atmospheric and oceanic general circulation models, and perhaps a wave model of the type incorporated in ECAWOM.

In the chapters where the coupling fluxes are discussed, some subset of these approaches will be adopted. For example, DNS will be of value in developing simple parametrizations for the scalar fluxes when there is no wave breaking or spray formation, whereas Reynolds-averaged models will be used in studying the effects of sprays, and momentum and heat exchange over waves. LES is of less utility at present, though attempts were made to use it during this project to study momentum exchange over waves. From the results it is clear that more resolution and better subgrid scale models would be needed.

CHAPTER TWO

DEVELOPMENTS RELATED TO MODELLING AND REMOTE SENSING OF OCEAN WAVES

2.1 Introduction

Recent developments in climate modelling confirm the central role played by the air-sea interaction processes in the dynamics of the climate system. With the advent of sophisticated Coupled atmosphere-ocean General Circulation Models (CGCMs) of ever increasing spatial and temporal resolution, the accurate description of the air-sea fluxes has become very important. However, the simple bulk formulae used presently to parametrize the coupling fluxes ignore the detailed influence of the wave field on the transfer processes at the air-sea interface. These include, for example, modifications of the drag coefficient and roughness length through the wave induced stress, a changed heat transfer and enhanced gas exchange rates due to white-capping dissipation, a modified sea surface albedo for rough sea surfaces and the formation of sea-salt aerosols in sea spray. A necessary step in using field data on exchange rates is then to predict the wave field using a well-verified wave-forecasting program. Validation of such models, therefore, is an important ingredient of the PISA project.

To reiterate global continuous measurements of the sea surface state represent an indispensable ingredient in understanding and interpreting transfer processes field experiments at the air-sea interface, in the presence of surface waves. The only way to obtain data which meet these requirements is by means of satellite measurements. One main objective, therefore, was the development of algorithms to enable a correct interpretation of these data, a quantitative retrieval of geophysical parameters and their efficient use in models through appropriate data assimilation schemes. Since the launch of the first European Remote Sensing satellite ERS-1 in July 1991 and of the Franco-American TOPEX/POSEIDON mission in December 1992, data sets are available on wind speed and direction from the ERS-1 scatterometer, on significant wave height and the sea surface level from the ERS-1 and TOPEX altimeter, on two-dimensional wave spectrum and sea surface images from the ERS-1 SAR. A necessary prerequisite for using these was the development of accurate sensor algorithms. Of particular interest

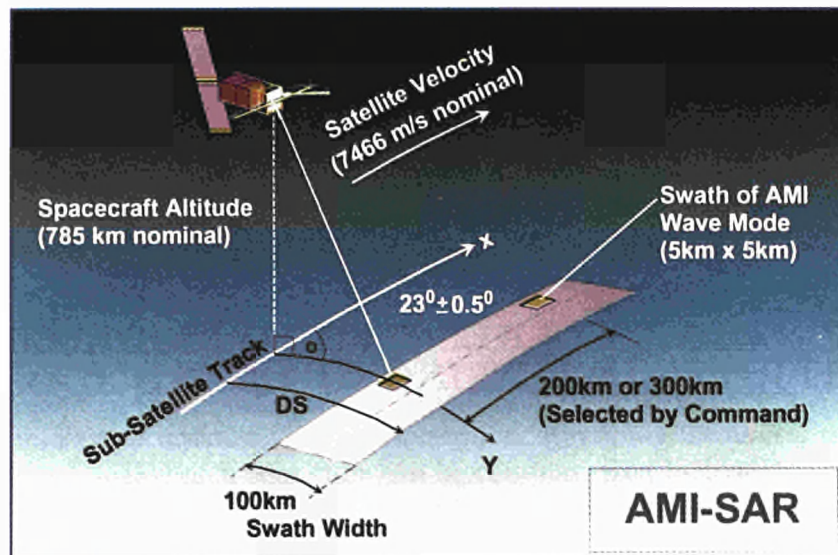


Figure 2.1 : ERS-1 SAR Wave Mode geometry.

was the development of an algorithm to retrieve 2-D ocean wave spectra from SAR imagette spectra (section 2.2).

An appropriate way to combine observation and model data for model validation and improvement, is by means of data assimilation techniques. Different methods were developed which all take into account spectral properties of the principal wave systems within a wave spectrum (section 2.4). Complementary, several global and regional statistical intercomparisons were performed to validate both satellite measurements and model results. These include integral comparisons of altimeter data from ERS-1 and TOPEX with ERS-1 SWM-derived data and spectral comparisons of the latter data with WAM model data (section 2.3). The overall process is sketched in Figure 2.2

A further major task was the development and use of an adjoint model of the wave model WAM (section 2.5). The adjoint modelling technique offers a variety of applications-related model testing and tuning, including sensitivity analyses, inverse modelling for testing and optimizing free model parameters, calculation of unstable modes of dynamical systems and dynamically consistent data assimilation in the sense of a 4-D variational approach.

The benefit of the afore mentioned efforts for the development of coupled atmosphere-wave-ocean models such as the ECAWOM is described in section 2.6. The PISA project adds notably to this overall goal in that it provides new insights into the air-sea interaction processes which lead to new parametrizations that can be tested with the ECAWOM model.

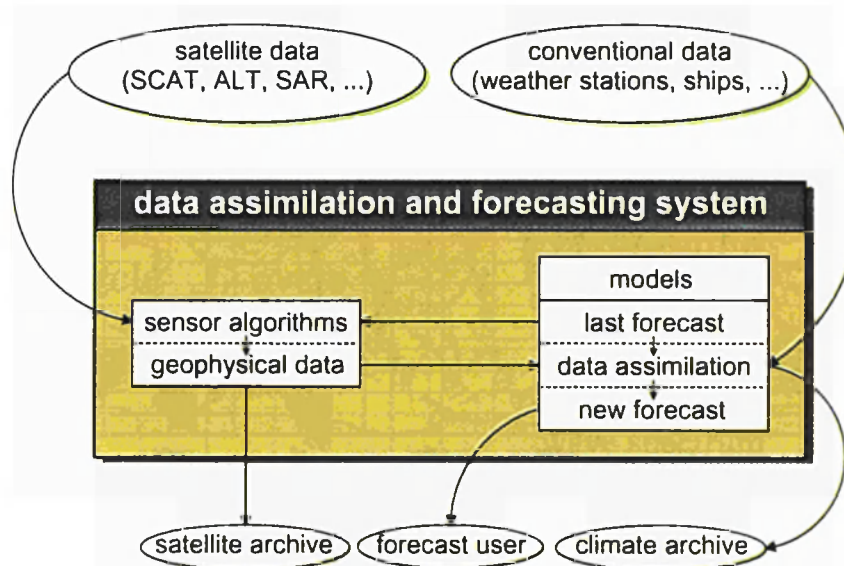


Figure 2.2 : Sketch of the data assimilation and forecasting system.

2.2 Retrieval of wave spectra from ERS-1 SAR data

With the development of the third generation wave model WAM a powerful tool has become available for research and forecasting applications (WAMDI, 1988, and Komen *et al.*, 1994). The model runs at many operational forecasting centres such as the ECMWF in Reading, UK, and is implemented at more than 100 research institutions. Although the model has been extensively validated in the past, prior to the first European Remote Sensing satellite ERS-1 launched on 21 July 1991, no data had been available which provided both dense global coverage and information on the full 2-D ocean wave spectrum over a long time period. Thus, validation of the WAM against observations was limited to a few field experiments and sparse wave buoy data. The operation of the ERS-1 Synthetic Aperture Radar (SAR) in the intermittent sampling mode, so-called "SAR Wave Mode" (SWM), provided for the first time global 2-D wave spectral data in near real-time. During SWM operation 10×6 km snapshot imagerettes are collected every 200 km along the satellite track (see Figure 2.1) which are processed to polar wavenumber power spectra and disseminated via the Global Telecommunication System (GTS) together with altimeter and scatterometer data as fast delivery product (FDP) in near real-time to the major forecasting services. An example of a one day coverage of ERS-1 SWM data is given in Figure 2.3 . On 21 April 1995 ERS-2 was launched replacing ERS-1. The continuity and operational application of global SAR wave data will be ensured in the future through the launch of ENVISAT scheduled for 1999 which will deploy an Advanced SAR (ASAR).

The retrieval of ocean wave spectra from the SWM imagerette spectra is not straightforward, since the SAR imaging mechanism is strongly nonlinear due to the distortions induced by the long-wave orbital motions (so-called "velocity-bunching" mechanism). Nevertheless, the derivation of a closed nonlinear integral describing the mapping of ocean wave spectra into SAR image spectra and the development of an efficient inver-

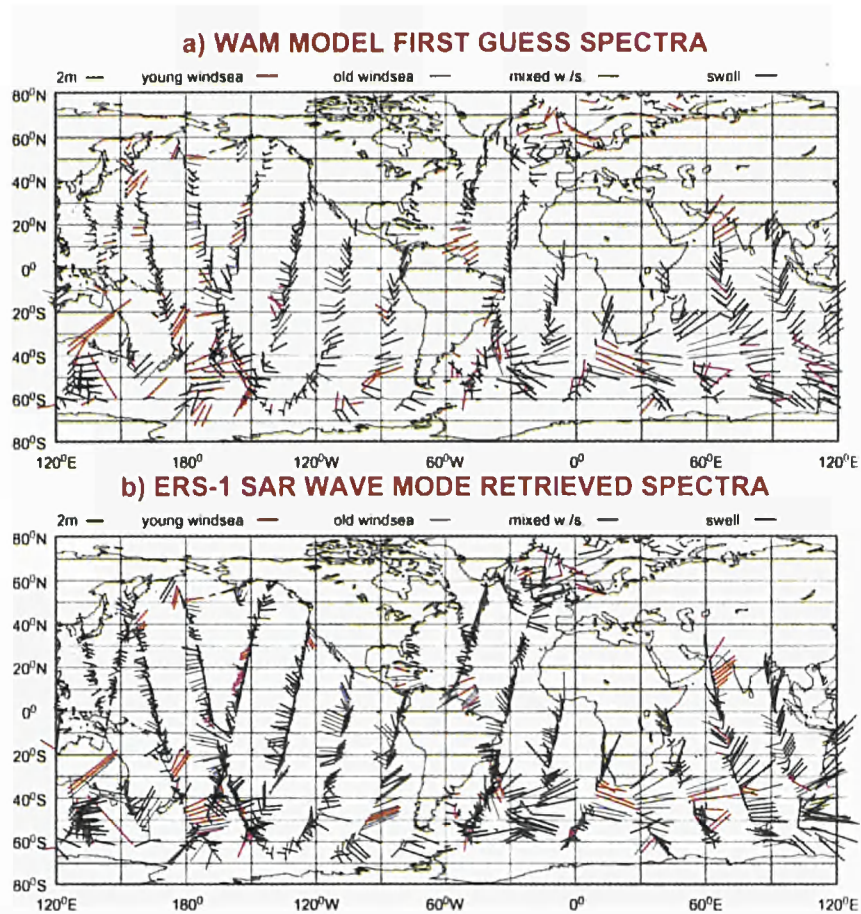


Figure 2.3 : Example of a one day coverage of WAM model first guess spectra (panel a), collocated to ERS-1 SAR wave mode retrieved spectra (panel b).

sion algorithm based on the iterative minimisation of a least square error cost function by Hasselmann and Hasselmann (1991) has enabled the implementation of a reliable retrieval algorithm within the computational constraints of real-time operational applications. Despite the successful validation of the original inversion algorithm (Brüning *et al.*, 1994) shortcomings were occasionally revealed. The algorithm has therefore recently been improved (Hasselmann *et al.*, 1996a/c and Heimbach *et al.*, 1996a/b). The input spectrum is now iteratively modified with the aid of a spectral partitioning scheme which subdivides a complex spectrum into its principal wave systems. Furthermore, the limitation imposed by the azimuthal smearing is partially overcome by including an explicit penalty term in the minimisation cost function for errors in the azimuthal cut-off. Figure 2.4 depicts the intermediate steps of the retrieval of an ocean wave spectrum from an ERS-1 SWM spectrum including the inversion and partitioning procedure in 2-D wavenumber domain. An example of the wave spectral partitioning is given in Figure 2.5 . The retrieval algorithm was applied to some 1.2 million ERS-1 SWM spectra for the period 1 January 1993 to 31 December 1995.

Iterative wave spectral retrieval operation


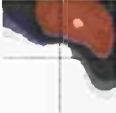


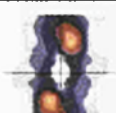




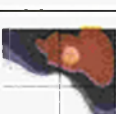
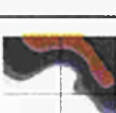
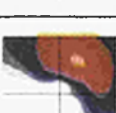
0-th cycle	best cycle	Inversion and partitioning cycle
		input wave spectrum
		SAR spectrum computed from input wave spectrum
		observed SAR spectrum
		SAR spectrum computed from inversion
		wave spectrum from inversion
		retrieved wave spectrum after partitioning operation

Figure 2.4 : Example showing the intermediate steps of the retrieval of an ocean wave spectrum from a SAR imagette spectrum in 2-D wavenumber domain. Each column represents an inversion cycle of the nonlinear spectral transform. The last row depicts the inverted wave from the inversion after the partitioning and readjustment procedure, which serves as new input spectrum in a subsequent cycle.

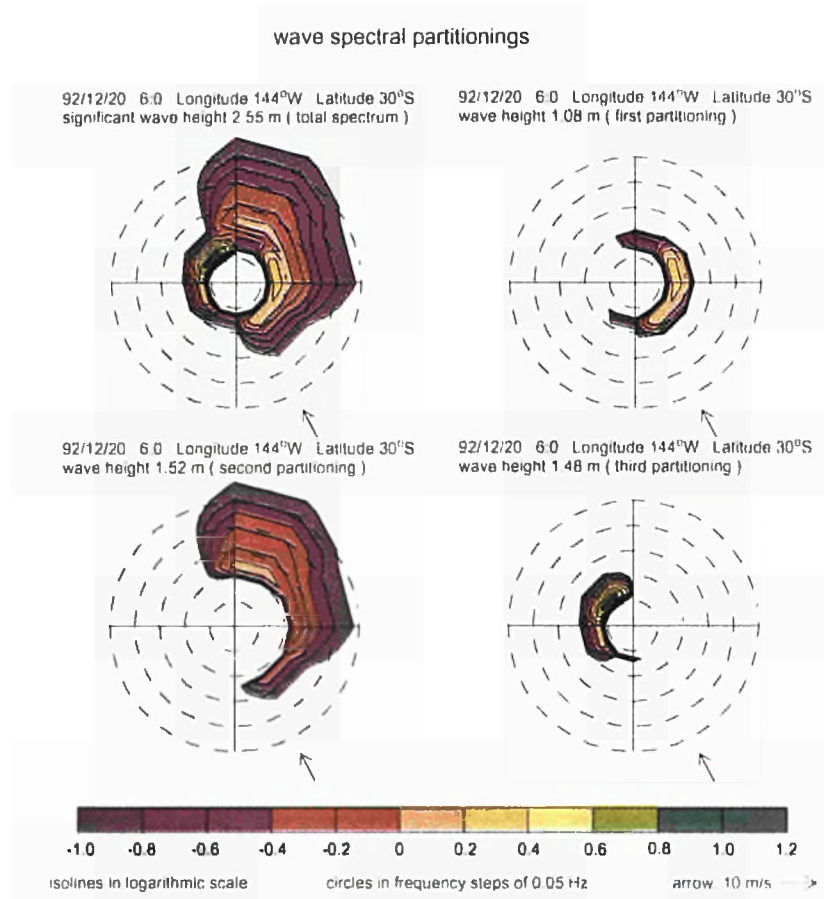


Figure 2.5 : Wave spectral partitionings.

2.3 Global validation of satellite and WAM model data

2.3.1 Analysis of altimeter data

A systematic cross-validation of all available altimeter data from 1978 to 1994 (from SEASAT, GEOSAT, ERS-1 AND TOPEX), together with WAM model data, was performed by Bauer and Staabs (1996) to obtain an estimate of changes in wave statistics from the various altimeters. The purpose was both to estimate the degree of accuracy between the different instruments by a cross-validation and to see whether climate trends in the wave height statistics could be detected. This study provided a sound basis for the accurate interpretation of a detailed comparison of ERS-1 SAR wave mode data with collocated altimeter data from ERS-1 and TOPEX (Hansen *et al.*, 1994 and Bauer and Heimbach, 1996). An example of the validation is shown in Figure 2.6 .

Significant wave height data retrieved from ERS-1 SWM data for the period 1994 were compared to altimeter wave heights from the TOPEX and the ERS-1 collocated in space and time. This study represents a first global continuous one-year validation of ERS-1 SWM-retrieved data. The values of SWM-derived monthly mean significant

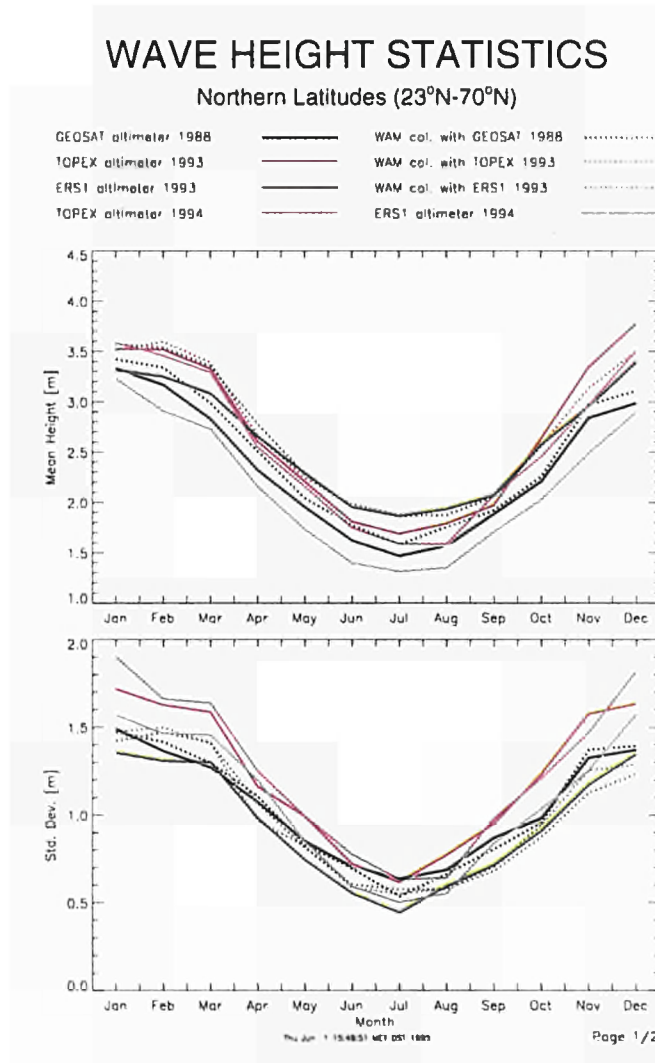


Figure 2.6 : One year time series of monthly mean significant wave heights derived from different altimeters. Corresponding H_s of WAM are also shown for reference.

wave heights are generally higher than those of the ERS-1 altimeter and slightly lower than those of the TOPEX altimeter. The agreement to the TOPEX altimeter data which are well calibrated is found to be very good, especially in the Tropics, deviations being limited to ± 5 to 10 percent. The systematic deviations with respect to the ERS-1 altimeter data is explained by a systematic low bias of the ERS-1 altimeter after a new sensor algorithm had been implemented in January 1994 (see Bauer and Heimbach, 1996). Thus, for the significant wave height as the main single wave parameter the SAR retrieval algorithm could successfully be validated, as shown in Figure 2.3.1.

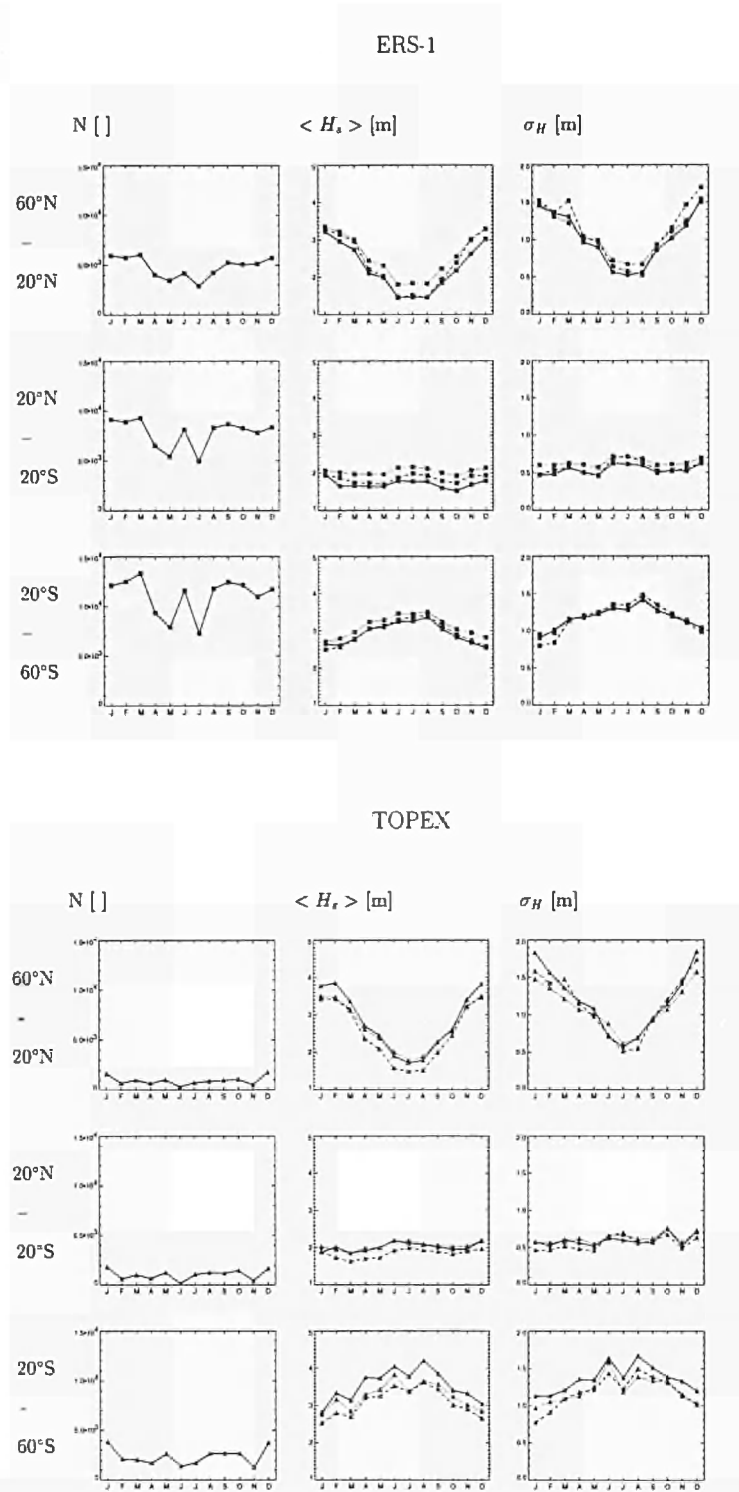


Figure 2.7 : One year time series of significant wave heights (middle columns) and standard deviations (right columns) retrieved from ERS-1 SWM (dotted lines), derived from the ERS-1 (upper part of Figure) and the TOPEX (lower part of Figure) altimeters (solid lines) and computed with the WAM model (dashed lines) for the Northern Extra-Tropics (top row), the Tropics (middle rows) and the Southern Extra-Tropics (bottom rows).

2.3.2 A three year global validation of the WAM model using ERS-1 SWM spectra

A statistical analysis of ERS-1 SWM-retrieved spectra was carried out for the three-year period January 1993 to December 1995 and the data compared with WAM model spectra. Complementary to the validation of significant wave height data described in the previous section, a combined quality analysis of the satellite data and performance analysis of the retrieval algorithm was performed. The assessment yielded about 75 % successful retrievals (Heimbach *et al.*, 1996a/b and Hasselmann *et al.*, 1996). Comparison of significant wave height revealed good overall agreement. Typical seasonal and regional synoptic conditions were represented. However, a more detailed investigation of the windsea and swell content of the spectra revealed a small but systematic model overprediction of windsea and a small underprediction of swell systems. Whereas the overpredicted windsea can be attributed to incorrect wind fields as suggested by data assimilation studies (Bauer *et al.*, 1996b and Hasselmann *et al.*, 1996b) the underpredicted swell could be due to an incorrect dissipation behaviour in the WAM model at low frequencies. Several detailed investigations support this hypothesis.

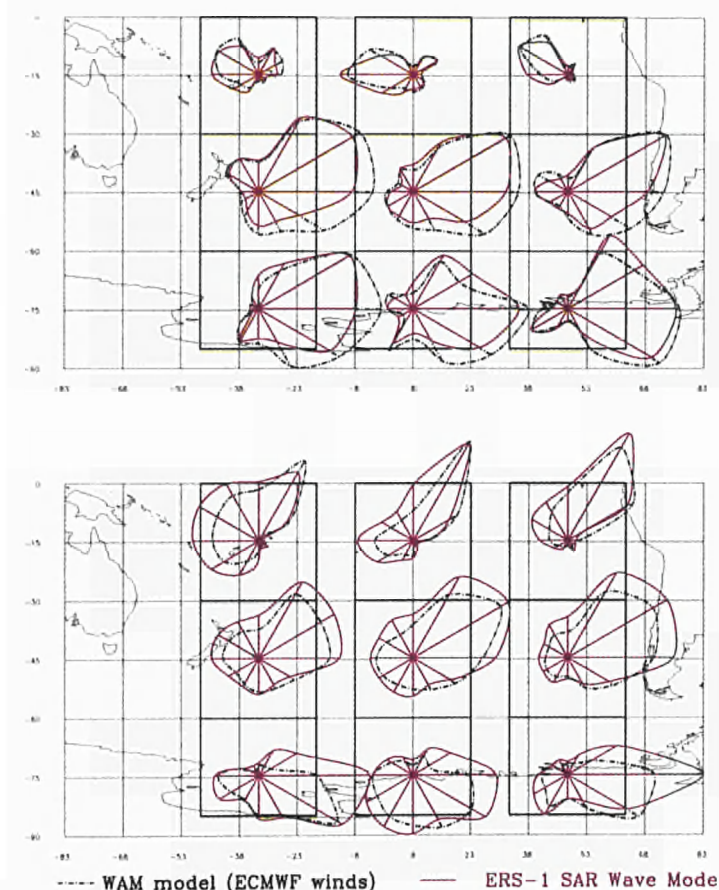


Figure 2.8 : Seasonal mean directional windsea (top panel) and swell (bottom panel) energy distribution in different parts of the South Pacific for JJA 1994. Blue curves: WAM model, red curves: ERS-1 SWM retrieved.

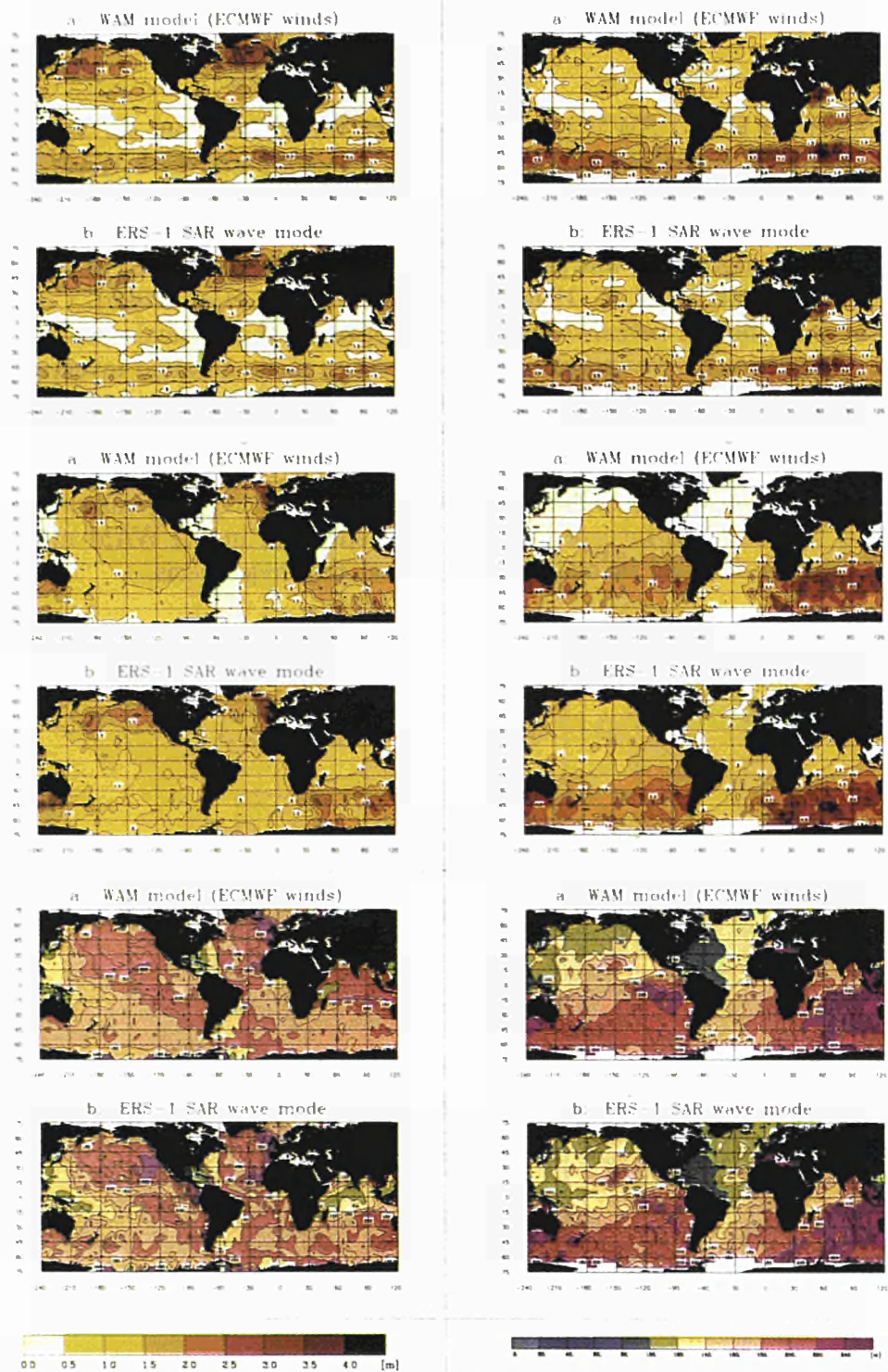


Figure 2.9 : Global maps of seasonal mean windsea wave heights (top panels), seasonal wave heights of swell of longest wavelengths (middle panels) and seasonal mean swell wavelengths (bottom panels) for DJF 1993/94 (left row) and JJA 1994 (right row). Map pairs represent WAM model (a) and ERS-1 SWM retrieved (b) data.

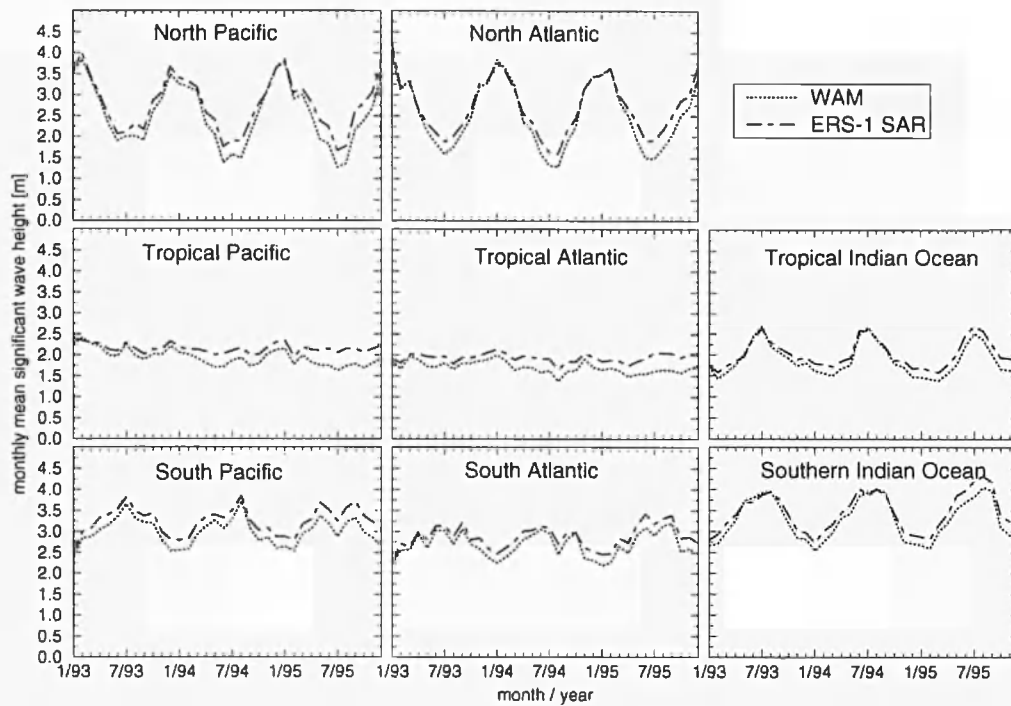


Figure 2.10 : Time series of monthly mean significant wave heights between January 1993 and December 1995 for different ocean basins.

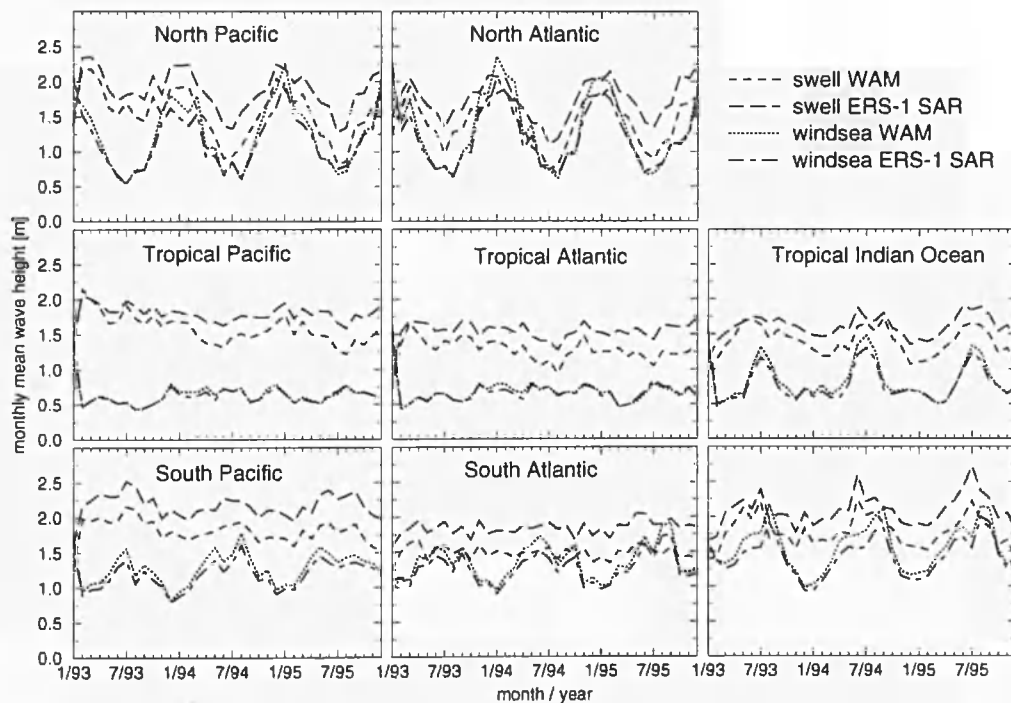


Figure 2.11 : Same as Figure 2.10 for monthly mean windsea and swell wave heights.

2.4 Assimilation of satellite data into the WAM model

Before wave data assimilation schemes for SAR wave mode spectral data were developed experiences with the assimilation of altimeter wave heights were gained. Although a single parameter is of limited value in updating the full 2-D wave spectrum, its assimilation already yielded improved results (Bauer *et al.*, 1992).

2.4.1 The optimal interpolation scheme

At ECMWF an OI scheme was implemented operationally for altimeter data (Lionello *et al.*, 1992). This scheme can be readily generalized to wave spectral data derived from ERS-1 SWM spectra (Hasselmann *et al.*, 1996b). For this purpose, both the WAM model and SAR-retrieved wave spectra are partitioned into a small number of windsea and swell systems, each of which is characterized by a few mean wave parameters. After cross-assigning the observed and model wave systems, analysed fields of the wave system parameters can be constructed by standard optimal interpolation. The updated full wave spectra in the vicinity of the observation point are recovered by superimposing the corrected wave systems. From the corrected windsea, errors in the driving wind field can be inferred using empirical laws for growing windseas. Figure 2.12 shows the example of the wind correction in the Atlantic inferred from a 6 hour assimilation.

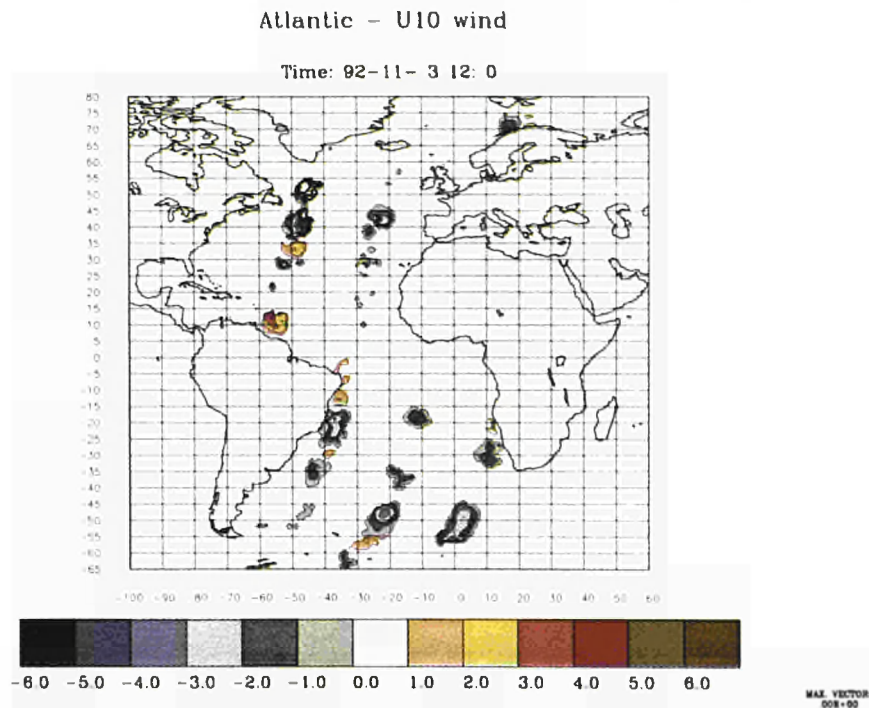


Figure 2.12 : Correction of local wind vector along the ERS-1 satellite track inferred from a 6 hour assimilation of SWM retrieved wave spectra via optimal interpolation.

2.4.2 The Green's function assimilation method

Bauer *et al.* (1996a/b) take a step further towards a dynamical rather than interpolative assimilation scheme using a Green's function method. The basic idea is to correct the wind field which drives the wave field, thereby obtaining dynamically, and mutually consistent, corrected wind and wave fields. Both windsea and swell data are used, the wind being corrected also in the past. An analysis for the entire Atlantic revealed substantial errors in the driving wind fields. The method was corroborated by the repeated identification of the same wind corrections at the same position from different observed spectra at different times and places (see Figure 2.13). Using the wave age for each spectral grid point it is possible to trace back the erroneous swell system to its origin in space and time, i.e. to the original, erroneous windsea.

2.5 The adjoint modelling technique

The adjoint technique is an efficient method to compute the derivatives of a given model with respect to some specific control variables, *e.g.* free model parameters. Such

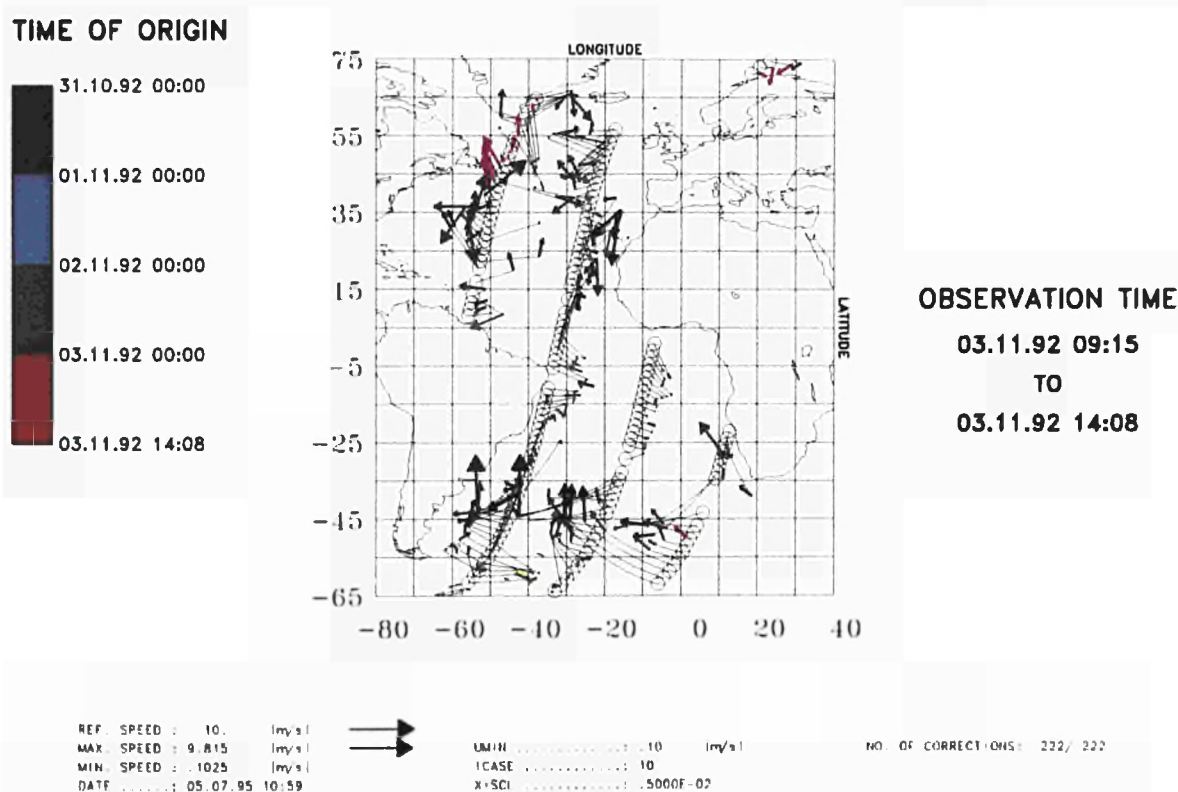


Figure 2.13 : Wind field correction inferred from assimilation of ERS-1 wave spectral retrievals by means of the Green's function method. Corrections are also applied non-locally by tracing back erroneous swell in space and time to its origin of generation (cf. the different colors in the Figure).

derivatives are needed for inverse modelling purposes in which model parameters are optimised by minimising a suitably defined cost function. Furthermore they are a basic ingredient for a dynamically consistent 4-D variational data assimilation. Finally, the adjoint model can serve as a tool for sensitivity analyses and for computing the most unstable modes of a model (singular value decomposition). For a large set of control variables the adjoint technique avoids the prohibitive computation costs incurred in the determination of the cost gradient by direct finite differences.

At the MPI a Tangent linear and Adjoint Model Compiler (TAMC) was developed (Giering and Kaminski, 1996) which for a given FORTRAN program of a model automatically computes the FORTRAN code of the model derivatives with respect to some given control variables and its adjoint. This tool is of great help if different model approaches are to be tested and tuned.

A hierarchy of data set was established for inverse modelling and data assimilation purposes with the WAM model. These include 1-D fetch-limited data, 2-D wind and wave data from Lake George (Australia), data from the SWADE experiment, carried out in the western part of the North Atlantic in 1991 and global ERS-1 SWM data between January 1993 and December 1995. These data can be used for different studies involving the adjoint technique.

2.5.1 Application of the adjoint technique to model tuning

In a first step, an adjoint model for a 1-D version of the WAM model was developed and applied to inverse modelling studies (Barzel *et al.*, 1993, and Barzel, 1994). A total of five free parameters in the source terms of the energy balance equation were optimised by fitting the model to fetch-limited wave data. The latest WAM model cycle 4 was compared with the former WAM cycle 3 and with a boundary layer model. The comparison revealed that there is substantial ambiguity in the choice of the wind input term in combination with a suitably adjusted dissipation term, at least in fitting to fetch-limited wave data. The resolution of this ambiguity requires data involving inhomogeneous or non-stationary wind fields and the adjoint of the full 2-D wave model. The extension of the adjoint to the full spatial dimensions of WAM has been carried out in a joint work between MPI and KNMI. First model tests have been performed using data from Lake George (Hersbach, 1996 and 1997).

2.5.2 The use of SWADE data for adjoint wave modelling

With the availability of more complex data from the Surface Wave Dynamics Experiment (SWADE) in the North Atlantic (Cardone *et al.*, 1996), together with the 2-D adjoint of the WAM, it should be possible to determine the source terms individually. Instruments involved in the wave measurements include the SAR (Synthetic Aperture Radar) from the Canadian Center for Remote Sensing, the RESSAC (Radar pour l'Etude du Spectre des Surfaces par Analyse Circulaire) from Météo-France, the

SRA (Scanning Radar Altimeter) from Goddard Space Flight Center, ROWS (Remote Ocean Wave Scanner) from Johns Hopkins APL and pitch-roll buoys. All data are currently being evaluated. Work to utilize them for inverse modelling purposes is in progress. A hierarchy of nested model grids with different spatial and temporal scales was set up. The prediction of the wave field was done on a 1° basin scale, a 0.25° regional scale and a 0.05° fine-resolution scale for a limited domain. Wind field descriptions were performed using six different models (ECMWF, FNOC, NMC, NASA and UKMO). The SWADE wind data include measurements of the surface meteorology of sufficient accuracy to largely eliminate the errors in the wind fields which have traditionally hindered accurate tuning of wave models. This allows detailed comparison of the observed and modelled wave field to be done with high accuracy.

2.5.3 Towards an integrated wind and wave data assimilation

As part of the efforts to construct an adjoint model for ECAWOM model the application of the adjoint model technique for wave data assimilation is envisaged in the near future. Ultimately, a dynamically consistent assimilation scheme has to include both an atmospheric and a wave model, as wind and wave field corrections are intimately related to each other and to their respective dynamical history.

2.6 Future directions: Tests using the adjoint of WAM and the ECAWOM

Within the framework of the European Coupled Atmosphere-Wave-Ocean model project (ECAWOM) a community coupled model is being developed which incorporates the state-of-the-art model physics and provides an integrated data assimilation system for application in European seas.

It is made up of the HIRLAM (High Resolution Limited Area Model) atmosphere model modified with the Hamburg physics package (HIRHAM), the wave model WAM and the 3-D baroclinic ocean circulation model HAMSOM (Hamburg Shelf Ocean Model). One of the main objectives is to study the effect of surface waves on the momentum, latent and sensible heat transfer at the air-sea interface and on the mixing through the upper layer of the ocean. The new parametrizations developed within the PISA project for the sensible heat and momentum fluxes across the air-sea interface, taking into account the effect of the local wave field (see Makin *et al.*, 1995), can now be tested using the adjoint of the WAM and the ECAWOM model.

The efforts presented should lead to improved analyses and forecasts of global wave models, of wind fields which drive the ocean circulation and to a better understanding of transfer processes at the air-sea interface. In the long term, a significant impact on the modelling of coupled ocean-atmosphere climate phenomena can be expected.

CHAPTER THREE

MOMENTUM AND SENSIBLE HEAT EXCHANGE AT THE AIR-SEA INTERFACE

3.1 Introduction

One of the central issues in coupling atmosphere and ocean general circulation models is related to the transfer of momentum by the wind to the ocean. This has a large effect both on ocean circulation and, through the surface stress boundary condition, on atmospheric motions. Similarly, sensible heat exchange between the ocean and atmosphere can also impact climate dynamics – particularly in the long term because of the substantial heat capacity of the oceans.

To improve our understanding of how waves affect momentum and heat exchange between the ocean and atmosphere, several studies were undertaken as part of the PISA project. These were an example of the cascade of approaches discussed in Chapter 1, where modelling of varying degrees of complexity was discussed as a way to clarify specific aspects of a problem. Here, Reynolds-averaged modelling, large eddy simulation (LES) and theoretical approaches were all used to clarify aspects of the problem. We will start with the Reynolds averaged approach (actually based on the $k - \varepsilon$ turbulence model). It will become clear from the discussion that knowledge of the wave spectrum and growth rate are required for this level of modelling. These subjects will be taken up in subsequent sections, particularly with regard to situations where waves propagate at an angle to the wind, and for the high frequency/high wavenumber portion of the wave spectrum.

3.2 Reynolds averaged modelling of air-sea exchange of momentum and sensible heat

3.2.1 Interpretation of field data

The experimental observation that the drag coefficient above the sea increases considerably with increasing wind speed, while the exchange coefficient for sensible heat (Stanton number) remains virtually independent of wind speed, can be explained by a different balance of the turbulent and the wave-induced part in total flux of momentum and sensible heat. Organised motions induced by waves form the wave-induced stress which dominates the surface momentum flux. Such organised motions do not contribute to the vertical flux of heat. The heat flux above waves is determined by how the diffusivity of turbulence is affected by waves.

The dependence of the exchange coefficient for heat on wind speed is usually parametrized in terms of a constant Stanton number. However, an increase of the exchange coefficient with wind speed is not ruled out by field measurements and could be parametrized in terms of a constant temperature roughness length. The large scatter of field data do not allow the determination of the actual dependence.

In bulk parametrization, the fluxes are related to the measured variables (wind speed U , potential temperature T) at the surface and at a certain reference height via exchange coefficients. For the momentum flux τ , the exchange coefficient is called the drag coefficient C_D , for the sensible heat flux H , the Stanton number C_H :

$$\frac{\tau}{\rho_a} = C_D(\Delta U)^2, \quad (3.1)$$

$$\frac{H}{\rho_a c_p} = C_H \Delta U \Delta T, \quad (3.2)$$

In (3.1) and (3.2) ρ_a is the air density, c_p is the heat capacity of the air and Δ denotes the difference between the variable measured at height h , normally 10 meters, and its surface value. In a neutrally stratified surface boundary layer the distribution of velocity and temperature with height is described by the logarithmic profiles:

$$U(z) = \frac{u_*}{\kappa} \ln \frac{z}{z_0}, \quad T(z) = \frac{t_*}{\kappa} \text{Pr}_t \ln \frac{z}{z_0 t}, \quad (3.3)$$

($u_* = \sqrt{\tau/\rho_a}$ is the friction velocity, κ is the von Karman constant, $t_* = H/\rho_a c_p u_*$ is the scale temperature, $\text{Pr}_t = K/K_t$ is the turbulent Prandtl number; K , K_t are the turbulent diffusivity for momentum and heat). The exchange coefficients can be now related to the roughness lengths of momentum z_0 (sea roughness) and heat z_{0t}

$$C_D = \frac{\kappa^2}{\ln^2 \frac{h}{z_0}}, \quad C_H = C_D^{1/2} \frac{\kappa}{\text{Pr}_t \ln \frac{h}{z_{0t}}}, \quad (3.4)$$

At present it is well established that the drag coefficient depends strongly on wind speed (see the reviews of Garratt, 1977; Geernaert, 1990; recent field experiments of Smith *et al.*, 1992; Anderson, 1993). In the wind speed range of $5 < U_{10} < 20$ m/s the drag coefficient increases roughly linearly with wind speed. The variation of C_D in this range is about 100%-150%. The increase of the drag coefficient with the wind has been explained using the analogy between waves and roughness elements (*e.g.* Phillips, 1977). With increasing wind speed waves grow and sea surface becomes rougher. The increase of the sea roughness with wind speed is described by the Charnock relation (1955):

$$z_0 = z_0^* \frac{u_*^2}{g} \quad (3.5)$$

where z_0^* is the Charnock constant and g is the acceleration due to gravity. (The Charnock 'constant' can in principle be a function of the sea state (*e.g.* Smith *et al.*, 1992).

Measurements of sensible heat flux give a clear indication that the Stanton number C_H is much less dependent on wind speed than the drag coefficient. These measurements include open ocean measurements of Large and Pond (1982), Smith (1980, 1989), Geernaert (1990), Anderson (1993); coastal measurements obtained during the Humidity Exchange over the Sea Main Experiment (HEXMAX) and reported by Smith and Anderson (1988), DeCosmo (1991), DeCosmo *et al.* (1996), and measurements of Francey and Garratt (1979). However, the difficulties in heat flux measurements result in a considerable scatter of the data (30%-60% of the mean), which obscures the actual dependence of the Stanton number on wind speed.

The most common parametrization of the field data is to assign a constant value to the Stanton number (Pond *et al.*, 1971; Smith, 1980 and 1988; Large and Pond, 1982; DeCosmo, 1991; Anderson, 1993). However a dependence on wind speed is not ruled out by the field measurements. Large and Pond (1982) argue that for wind speeds above 10 m/s the parametrization of the Stanton number in terms of a constant temperature roughness length is more appropriate, though the statistical improvement of such a fit to their data is not significant compared to the constant Stanton number parametrization. However such a choice makes a difference. What immediately follows from equation (3.4) is that $C_H \sim C_D^{1/2}$ which could increase the Stanton number up to 50% for high wind speeds, compared to the constant value of C_H , and increase estimates of heat exchange between atmosphere and ocean.

In the bulk parametrization the water surface is regarded as a 'solid' boundary with the principal problem being to determine the characteristic roughness lengths of the water surface. The bulk parametrization is based on empirical relationships for the exchange coefficients and does not explain the physics which determine those relations.

The first attempt to obtain theoretically the drag coefficient (or the sea roughness) by explicitly taking into account the sea state and the impact of waves on the atmospheric boundary layer was made by Janssen (1989) and later by Chalikov and Makin (1991). However both had to use a Charnock-type relation for the 'background' roughness parameter entering their theories. This ensures proper values of the drag coefficient when seas are fully developed. Caudal (1993) bypassed this problem by assuming that the total surface stress is supported only by waves. This assumption does not hold in general. A consistent theory to calculate the sea drag which accounts for balance between the wave-induced and the turbulent stress at the surface and avoids

the use of a Charnock-type relation for the 'background' roughness was introduced by Makin *et al.* (1995).

It has been shown (Janssen, 1989; Makin *et al.*, 1995) that for typical sea conditions the wave-induced stress at the surface (the form drag) contributes a considerable fraction of the total surface stress. The wave-induced flux decays rapidly with height. Therefore the turbulent stress above waves is no longer constant with height. In this way the organized wave-induced stress alters the diffusivity of turbulence above waves. This effect was not taken into account in Janssen (1989), Chalikov and Makin (1991) and Makin *et al.* (1995), as they used a mixing length theory to parametrize the turbulent stress. Chalikov and Belevich (1993) use a one-equation eddy-viscosity model to account for a proper balance of the TKE but needed to specify the mixing length.

In this work we introduce a model which explicitly accounts for the impact of waves on the fluxes of sensible heat and momentum. The model is based on the previous work by Makin *et al.* (1995). The proper balance of the TKE and of the dissipation rate is accounted for by using a two-equation eddy viscosity scheme to parametrize the turbulent stresses in the balance equations of momentum and heat.

3.2.2 A one dimensional model

The lowest part of the marine atmospheric surface layer where the wave-induced motion can be detected, is considered. The height of this surface 'wave boundary layer' or WBL scales with the wave length of energy containing waves. The $h = 10$ metre height is a good estimate for the upper boundary of the WBL (Makin *et al.*, 1995).

The balance equation of momentum above waves is

$$\frac{\partial}{\partial z}(\tau^t + \tau^w) = 0, \quad (3.6)$$

where the mean turbulent stress τ^t is

$$\tau^t = -\overline{u'w'}, \quad (3.7)$$

the mean wave-induced stress τ^w can be expressed as:

$$\tau^w = \tau_w^p + \tau_w^a \quad (3.8)$$

and stresses are scaled with the density of air. z is a vertical coordinate and is relative to (and follows) the water surface. Expressions for τ_w^p and τ_w^a are given by Makin (1990). At $z = 0$, $\tau_w^a = 0$, and the term τ_w^p is called the form drag.

In a stationary WBL the total stress $\tau = \tau^t + \tau^w$ is constant over height

$$\tau = \text{Const.} = u_*^2 \quad (3.9)$$

and by definition equals the square of the friction velocity. In the upper part of the WBL (far enough from the waves) the wave-induced stress $\tau^w = 0$ and the friction velocity relates to the turbulent stress τ^t . In this part of the WBL the bulk formalism can be applied: by measuring the turbulent stress and the wind velocity the roughness

length follows from (3.3). Near the wave surface the wave-induced stress τ^w supports a considerable part of the total stress τ and the local friction velocity related to the local turbulent stress $u_*^t(z) = \sqrt{\tau^t(z)}$ varies with height. If the turbulent stress is measured in the layer of the WBL affected by the waves, no bulk formalism can be applied for the estimation of the sea roughness.

The wave-induced stress decays rapidly with height. For each wave component the vertical decay can be approximated by $\exp(-z/r(k))$, where r is a decay length and k is a wave number. The 2D numerical calculations of Makin (1989), based on a mixing length theory to parametrize the turbulent stress, have shown that the decay length can be approximated by $r(k) = 1/2k$. However, the rapid distortion theory of the turbulent air flow above waves (Belcher and Hunt, 1993) indicates that the wave-induced flux decays much faster due to the smearing of the wave fluctuations of turbulent stresses in the outer region. Mastenbroek *et al.* (1995) have used the 2nd order LRR (Launder *et al.*, 1975) closure scheme which accounts for the rapid distortion effects to model turbulence above waves. Their calculations show that the wave-induced flux indeed decays faster and that the decay length can be related to the height of the inner region. For short waves which support most of the surface stress (Makin *et al.*, 1995), the height of the inner region and hence the decay length can be approximated by $r = 1/5k$ (Mastenbroek *et al.*, 1995).

The form drag at the sea surface $\tau_w^p = \tau_0^w$ and the distribution of the wave-induced stress $\tau^w(z)$ with height can be calculated according to:

$$\tau^w(z) = \int_0^\infty \int_{-\pi}^\pi \omega^2 S \beta \cos \theta k d\theta e^{-z/r} dk, \quad (3.10)$$

Equation (3.10) presumes that:

1. All undulations of the sea surface are considered as waves, which can then be statistically described by a directional wave spectrum $S(k, \theta)$, where the wave number k satisfies the dispersion relation

$$\omega^2 = gk + \mathcal{T}k^3, \quad (3.11)$$

where \mathcal{T} is the dynamical surface water tension, θ is the propagation direction of the k - wave component, and ω is the wave frequency.

2. The energy input to waves from the atmosphere is known and can be described in terms of the growth rate parameter $\beta(k, \theta)$.
3. The decay rate of the wave-induced flux of the individual wave component is known. Note the importance of the growth rate parameter and wave spectrum in determining the wave induced flux.

It has been shown (Janssen, 1989; Makin *et al.*, 1995) that for the typical sea conditions the form drag contributes a considerable fraction of the total surface stress. The value of the coupling coefficient - the ratio of the form drag to the total stress

$$\alpha = \frac{\tau_0^w}{u_*^2}, \quad (3.12)$$

is about 0.5 for a wind speed of 6 m/s and increases to about 0.95 for a wind speed of 20 m/s (see Figure 3 in Makin *et al.*, 1995). What immediately follows from (3.9) and (3.10) is that the turbulent stress is significantly smaller near the sea surface than at the top of the WBL. Due to the fact that the wave-induced stress decreases rapidly with height, the turbulent stress will increase rapidly with height compared to its surface value to satisfy the conservation of momentum (3.6). Such a distribution of τ^t will change the balance of the TKE and the dissipation rate of turbulence ε , compared to the logarithmic boundary layer, and will therefore influence the diffusivity of turbulence near the wave surface. In this indirect way the wave-induced stress has an impact on the diffusivity of turbulence above waves. In order to properly calculate the diffusivity of turbulence above waves the balance equations for the TKE and the dissipation rate are to be considered in the description of the WBL, but are omitted here, except to present the results.

The wave-induced flux in the balance equation for momentum is calculated by means of (3.10). For this a wave spectrum $S(k, \theta)$ and the growth rate parameter $\beta(k, \theta)$ are to be defined. For the wave spectrum $S(k, \theta)$ we use the model adopted in Makin *et al.*, (1995). For the growth rate parameter $\beta(k, \theta)$ we adopt the following relationship:

$$\beta = 16 \left(\frac{u_{*r}}{c} \right)^2 \cos^2 \theta \quad (3.13)$$

where u_{*r} is the friction velocity at the height of the inner region $r(k) = 1/5k$. For waves travelling with the speed of the wind, the parametrization (3.13) overpredicts the growth rate (Mastenbroek *et al.*, 1995). Mastenbroek *et al.* (1995) have shown that for fast waves the energy flux is supported to a large extent by the work of tangential stress on the orbital velocity and is negative, meaning that waves lose their energy to the atmosphere. We therefore take for waves travelling with the phase speed $c > 28u_* \cos \theta$

$$\beta = -4 \frac{u_{*r}}{c} \frac{u_{*r}}{u_r} \cos^2 \theta, \quad (3.14)$$

where u_r is the wind velocity at the height of the inner region. Note the key role of the wave growth parameter and wave spectrum in determining the wave-induced flow.

The momentum and sensible heat flux, as well as the drag coefficient C_D and the Stanton number C_H follow from the model.

3.2.3 Results

The impact of waves on the height dependence of the momentum flux is shown in Figure 3.1 for a wind speed of 15 m/s. The total stress $\tau = u_*^2$ is constant with height (as stress is normalized on u_*^2 it equals 1). The total stress is supported by the wave-induced stress τ^w and the turbulent τ^t . In this example at the surface more than 60% of the stress u_*^2 is supported by waves. The wave-induced flux decays rapidly with height supporting only 20% of the total stress at 0.1 m height. Correspondingly the turbulent stress τ^t increases rapidly with height. At the top of the WBL where the

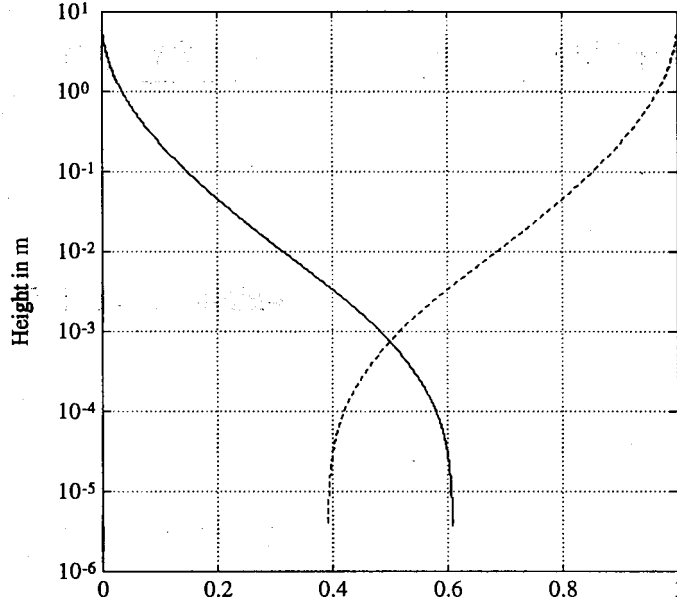


Figure 3.1 : Momentum flux. Turbulent stress τ^t/u_*^2 - dashed line, wave-induced flux τ^w/u_*^2 - solid line, total stress $\tau/u_*^2 = 1$.

wave-induced stress is negligible, the turbulent stress equals u_*^2 , almost three times the surface value of τ^t .

The TKE, which is roughly proportional to the turbulent stress, is no more constant with height as it should be in the logarithmic boundary layer. Present computations relative to a wind speed of 15 m/s show that in the layer about 1 m above the waves, the TKE experiences a 40% increase in its surface value. The dissipation rate, normalized by $u_*^3/(z\kappa)$, is constant with height in the logarithmic boundary layer. In the WBL it increases to twice the surface value.

In the mixing length model the eddy-viscosity K is derived from the assumption that the dissipation rate $\varepsilon = K^3/l^4$ (l is the mixing length) equals the TKE production due to the interaction of the turbulent stress and mean velocity gradient $P^t = \tau^t \partial u / \partial z = K(\partial u / \partial z)^2$. An equation for K then follows: $K = l^2 |\partial u / \partial z|$. Such calculation of the eddy-viscosity above waves leads to underestimate K near the surface. The reason is that the production of the TKE due to the dissipation of the mean motion is only a part (which is small for high wind speed) of the total production of the TKE above waves.

The distribution of the eddy-viscosity is shown in Figure 3.2. The eddy viscosity which follows from the mixing length theory is underestimated compared to the $e - \varepsilon$ model. The details of the K distribution are important as the heat flux is determined by the diffusivity of turbulence above waves. Just above the surface the diffusivity of turbulence is enhanced due to the presence of waves. That enhances the turbulent mixing of sensible heat above waves and the exchange coefficient of heat.

The dependence of the Stanton number on wind speed is assessed in the following way. The open ocean data set of recent simultaneous measurements of wind stress and sensible heat flux (Anderson, 1993) have been chosen. Wind stresses and sensible heat

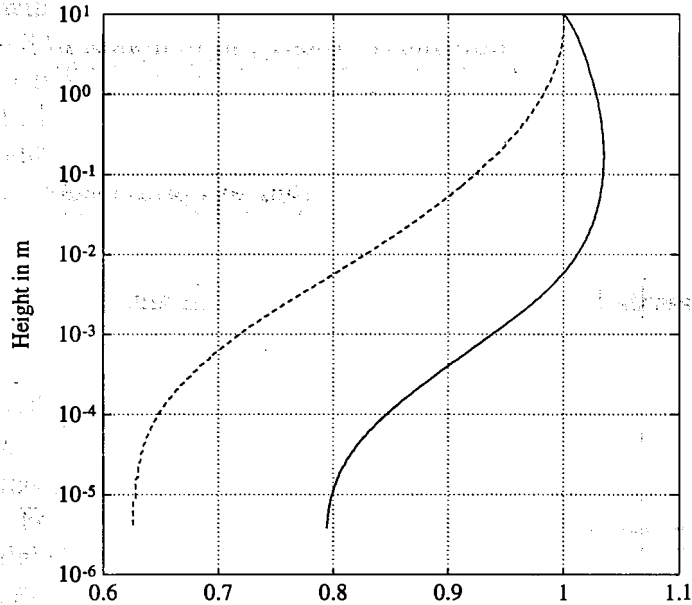


Figure 3.2 : Eddy-viscosity $K/(\kappa z u_*)$. $e-\epsilon$ model (eq. 31) - solid line, mixing length model - dashed line.

fluxes in the experiment were determined by the inertial-dissipation method.

Anderson reports the drag coefficient and Stanton number in the wind speed range of 5-20 m/s. His data show a clear 100% increase of the drag coefficient with wind. The heat flux coefficient is much less dependent on wind speed. However within the scatter his data do not resolve whether C_H or temperature roughness length z_{0t} is independent of wind speed. If the latter is true the Stanton number would increase for more than 30% in the given wind speed range and for the reported drag coefficients.

We need to be able to reproduce the experimental dependence of the drag coefficient C_D on wind speed, which is more or less well established. Comparison of model results and data is shown in Figure 3.3. The regression line of Anderson is for all data in the range $4.5 < U_{10} < 21$ m/s: $10^3 C_D = 0.40 + 0.079 U_{10}$. For data in the range of wind speed $U_{10} > 10$ m/s his regression line is $10^3 C_D = 0.59 + 0.065 U_{10}$, which is in close agreement with Large and Pond (1982) regression: $10^3 C_D = 0.49 + 0.065 U_{10}$. However in the range of $4 < U_{10} < 10$ m/s Large and Pond approximate their data with constant value $10^3 C_D = 1.14$ (standard deviation 0.20). For wind speeds higher than 10 m/s agreement of model results with data is reasonable. In the range of 5-10 m/s, the model gives somewhat higher values of the drag coefficient. The model results in this range correspond better to the measurements of Large and Pond (1982), obtained with the same method as Anderson. Taking into account that conditions of low wind speed introduce more uncertainty into measurements and that the model results do not contradict the other data sets (Large and Pond, 1982), we conclude the overall reasonable agreement of model results with data. The overall increase of the drag coefficient in the wind speed range 5-20 m/s is 80%.

The simultaneously calculated values of the Stanton number should then fall in the cloud of experimental values of C_H . We then argue that the model results establish

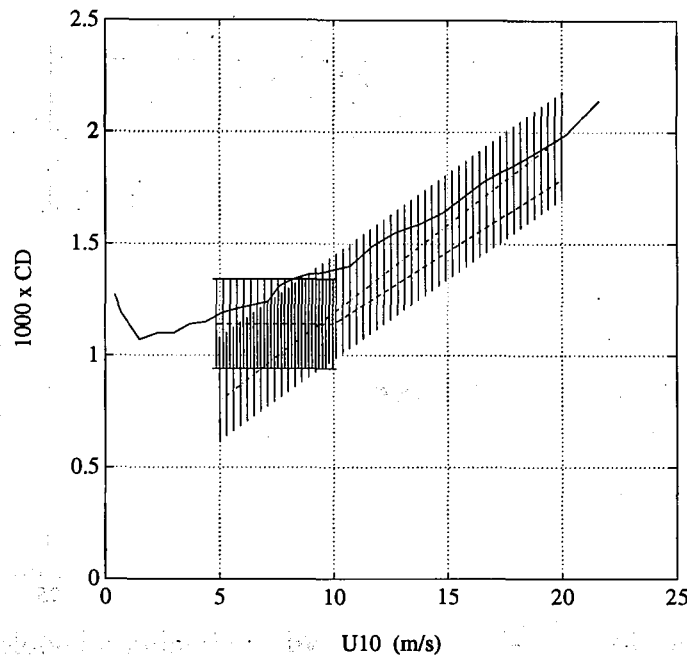


Figure 3.3 : Drag coefficient versus U_{10} . Regression line from Anderson (1993) - dashed-dotted line; his data fall in the shaded area. Regression line from Large and Pond (1982) - dashed line; in the wind speed range 5-10 m/s the standard deviation is shown. Model results - solid line.

the dependence of the Stanton number on wind speed. Modelled and measured values of C_H are shown in Figure 3.4. Considering the scatter of data it is not too surprising that the model results are well within the cloud of data.

In the range of wind speed 3-10 m/s we obtain the Stanton number which is virtually independent of wind speed $C_H = 1 \cdot 10^{-3}$. It increases for about 10% in the range of 10-20 m/s. The increase is smaller than that following from the 'constant roughness lengths' parametrization. Assuming $C_H = 0.029C_D^{1/2}$ which gives $C_H = 10^{-3}$ for the wind speed of 5 m/s we obtain an overall increase in C_H of 30% in the wind speed range of 5-20 m/s. The increase is three times larger than the model results in the same range of wind speed and the difference increases for higher wind speeds. Thus the present theory agrees better with the 'constant Stanton number' parametrization rather than the 'constant roughness lengths' parametrization of sensible heat flux.

In the literature it is argued that for wind speeds higher than 15 m/s the effect of the sea spray evaporation becomes important and increases the exchange coefficients for heat and moisture (Andreas *et al.*, 1995; Fairall *et al.*, 1994). The model results of Fairall *et al.* (1994) show that the contribution of spray to air-sea fluxes becomes comparable to the direct fluxes at wind speed about 35 m/s for sensible heat. Andreas *et al.* (1995) estimate the spray contribution to the heat fluxes to be about 10% at 15 m/s wind speed. However, experimental evidence for such increase is lacking, though only few data are available at high wind speeds. The effect of sea spray is not accounted for by the present model.

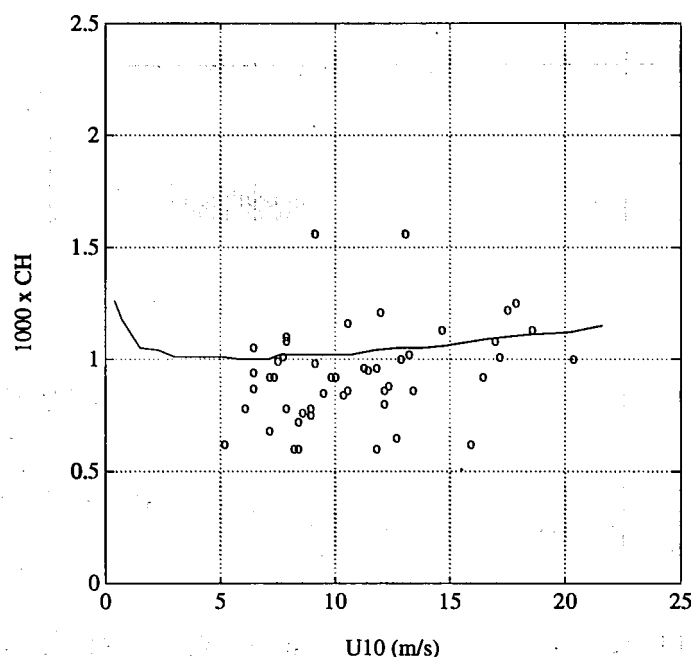


Figure 3.4 : Stanton number versus U_{10} . Circles - data of Anderson (1993), compiled from his figure 8(a). Model results - solid line.

3.3 Air Flow over Waves: Numerical Developments

Numerical wave-forecasting models (such as the WAM model, WAMDI 1988) are based on the idea that the random sea state can be decomposed into a collection of waves with a range of wavelengths and propagating in a range of directions to the wind. Hence such forecast models need to parametrise the processes that control the waves in terms of both the length of the wave and direction of propagation. In particular, the wind supplies energy to the waves and makes them grow, and this energy supply from the wind to the waves needs to be understood for the whole range of wavelengths and propagation directions.

Despite this practical need, most previous studies of air flow over waves have considered only a two-dimensional flow, where the mean wind is perpendicular to crests of the two-dimensional waves. We have extended the previous analysis of Belcher & Hunt (1993) of turbulent air flow over waves that propagate in the same direction as the wind to analyse turbulent air flow over waves that propagate at an angle to the wind as shown in Figure 3.5.

The main result from the analysis is a formula for the rate that energy is transferred from the wind to the waves, including the variation with the angle between the wind and waves. This formula has a complicated dependency on the angle, but when plotted this dependency is fortuitously close to a simple variation currently used in wave forecast models, i.e. that the growth rate varies approximately as $\cos^2\theta$ (see Figure 3.6). Hence our work supports the parametrizations currently used. In particular, the growth rate used for the Reynolds averaged model discussed elsewhere in this report is based on this form of parametrization.

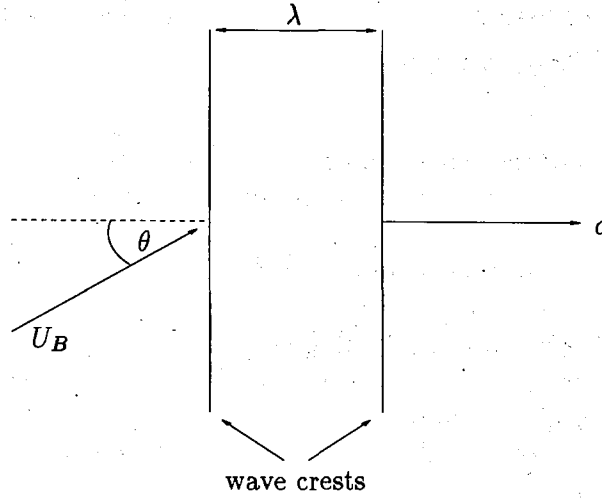


Figure 3.5: Plan view of oblique air flow over two-dimensional waves.

We also developed a numerical model of the interaction between wind and a small amplitude water wave. This model was used to investigate the effects of molecular viscosity on air flow over water waves. Our conclusion was that the molecular viscosity can be important. This finding is surprising because wind blowing over waves is turbulent, which is usually assumed to dominate mixing so that mixing by molecular processes is negligible. However, our detailed study shows that processes very near the air-water interface control the energy supplied by the wind to the waves and that this near-interface region can be strongly affected by molecular viscosity.

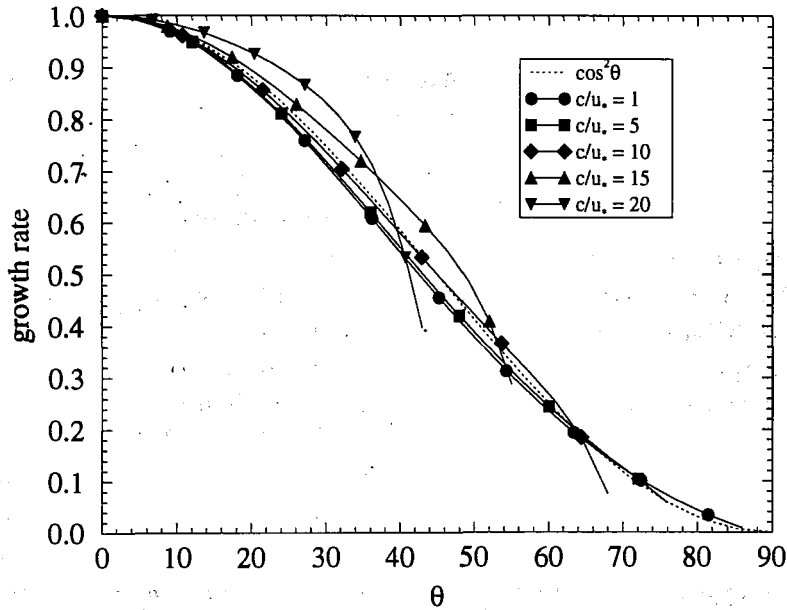


Figure 3.6: Variation of growth rate with angle θ ($kz_0 = 10^{-5}$, and growth rate is normalised on growth rate at $\theta = 0$).

3.4 High frequency / high wavenumber wind-wave spectra and breaking waves

One aspect of ocean surface waves that needs to be better understood is wave breaking. Breaking waves are believed to transfer significant momentum and energy between the atmosphere and ocean and, in rough sea conditions, such breaking waves may be responsible for a substantial fraction of the total gas exchange across the air-sea interface. Hence crucial quantities in air-sea interaction are the statistics of the breaking-wave coverage and their variation with wind speed.

An apparently unrelated aspect of ocean waves is the form and behaviour of the high frequency and high wavenumber parts of the spectra of the wind-waves. These parts of the spectra are observed to have universal forms and hence are believed to be in a dynamical equilibrium. Wave forecasting models such as WAM do not compute explicitly these tails of the spectra, but patch parametrized models onto the resolved part of the spectrum.

The work developed here shows for the first time a link between the character and statistics of breaking waves and the equilibrium ranges of the wave spectra. Data shows that breaking waves have high curvature at their crests, and they are modelled here as waves with discontinuous slope at their crests. Spectra are then dominated by these singularities in slope. The equilibrium range is assumed to be scale invariant, meaning that there is no privileged length scale. This assumption implies that: (i) the sharp-crested breaking waves have self-similar shapes, so that large breaking waves are magnified copies of the smaller breaking waves; and (ii) statistical properties of the distribution of breaking waves, such as the average total length of breaking-wave fronts of a given scale, varies with the scale of the breaking waves as a power law, parametrized here with exponent D .

The two-dimensional wavenumber spectrum of a scale-invariant distribution of such self-similar breaking waves is calculated and found to vary as $\Psi(\mathbf{k}) \sim k^{-5+D}$. The exponent D is calculated by assuming a scale-invariant dynamical balance in the equilibrium range. This balance is satisfied only when $D = 1$, so that $\Psi(\mathbf{k}) \sim k^{-4}$, in agreement with recent data. The frequency spectrum is also calculated and shown to vary as $\Phi(\sigma) \sim \sigma^{-4}$, which is also in good agreement with data. The theory also gives statistics for the coverage of the sea surface with breaking waves, and, when $D = 1$, the fraction of sea surface covered by breaking waves is the same for all scales. Hence the equilibrium described by our model is a *space-filling saturation*: equilibrium at a given wavenumber is established when breaking waves of the corresponding scale cover a given, wind-dependent, fraction of the sea surface.

Although both $\Psi(\mathbf{k})$ and $\Phi(\sigma)$ vary with the same power law, the two power laws arise from quite different physical causes. As the wavenumber, k , increases, $\Psi(\mathbf{k})$ receives contributions from smaller and smaller breaking waves. In contrast, $\Phi(\sigma)$ is dominated by the largest breaking waves through the whole of the equilibrium range and contains no information about the small-scale waves. This deduction from the model suggests a way of using data to distinguish the present theory from previous work.

CHAPTER FOUR

GAS AND MOISTURE EXCHANGE AT AIR-WATER INTERFACES

4.1 Introduction

Prediction of scalar transfer rates at the interface between immiscible, turbulent streams has been of central importance in many industrial operations such as gas absorption, condensation, evaporation, extraction and aeration. Recently, gas, moisture and heat transfer at the ocean-atmosphere interface has begun to receive attention. The primary motivation has come from the need to parametrize coupling fluxes between the ocean and the atmosphere, required by general circulation models used in long term climate studies.

A fundamental understanding of transport processes at gas-liquid interfaces has, however, been slow in coming about, primarily because of the difficulties in making measurements, and in doing computer simulations near mobile and deformable boundaries. In contrast, flows and scalar transport near fluid-solid boundaries is better understood because of intensive investigations over the last two decades.

Be that as it may, the earliest theory for mass and heat transfer was proposed by Lewis and Whitman (1924), who postulated laminar films on each side of the fluid boundary with well-mixed turbulent fluid in the outer regions. The transfer coefficients then, on each side, were inversely proportional to the thickness of the laminar film and directly proportional to the molecular diffusivity. Measurements, however, *e.g.* by Gilliland and Sherwood (1934), suggested that the transfer coefficients, at least on the liquid side, tended to vary as the square root of the molecular diffusivity. This finding has been validated in later work, for example by McManamey *et al.* (1973), and Vivian and King (1964), amongst others. While there is still some controversy as to the precise dependence of the transfer coefficients on molecular diffusivity, nonetheless, there is general agreement that it lies somewhere between the square root and the three-quarters power.

In spite of this, the Lewis-Whitman (1924) film theory is useful, if for no other reason than that it affords a convenient means to visualize the scales controlling the various transport processes. Consider, first, transfer of sparingly soluble gases such

as carbon dioxide and methane to the ocean. At wind speeds below those at which wave breaking occurs, typical gas transfer velocities, controlled by the liquid side, are $\sim O(10\text{cm/hr})$. Since molecular diffusivity of such gases in water or sea water are $\sim O(10^{-5}\text{cm}^2/\text{s})$, it follows from film theory that the main concentration changes occur in layers $\sim O(10^{-2}\text{mm})$ in thickness. For moisture transfer on the air side, transfer velocities are $\sim O(1\text{cm/s})$ and diffusivities are $\sim O(0.1\text{cm}^2/\text{s})$ so that concentration changes occur over regions of $\sim O(1\text{mm})$.

Ripples and capillary waves have wavelengths $O(1\text{cm})$ and it is deformations of these scales that primarily impact frictional drag. Form drag, on the other hand is affected by wavelength $O(1\text{ to }10\text{m})$, though there also is some effect of waves in the capillary-gravity range.

One central consideration during project development was that since scalar transfer occurs over so much smaller scales than the wave motion, it becomes possible to examine the controlling processes, which must be turbulence centered, in isolation from surface deformations that are an order of magnitude, or more, larger in scale. Clearly, capillary wave motions, and their interactions with turbulence, should be taken into consideration. However, in the absence of breaking, consideration of waves with length scales that are much larger may be deferred.

4.2 Scalar transfer models – a brief history

As discussed, the concept of a laminar film adjacent to a boundary, governing transfer rates, was out of line with observations, leading Higbie (1935) to speculate that the transfer processes were akin to unsteady absorption into an essentially laminar fluid for some period, after which the surface element was replenished with fresh bulk fluid. Unlike the theory of Lewis and Whitman, Higbie predicted that mass transfer rates were proportional to the square root of the molecular diffusivity and inversely proportional to the square root of the time period between surface replenishments. Subsequently, Danckwerts (1951) modified this penetration theory to allow a random distribution of surface ages and phrased the theory in terms which were more realistic from the viewpoint of turbulent processes. Nonetheless, the essential Higbie model only changed slightly with regard to the constant of proportionality and still maintained a dependence of the transfer rate, $\bar{\beta}$ (m/s), on the square root of the ratio between the molecular diffusivity, D (m^2/s), and the average time between surface renewals, $\bar{\tau}$, *i.e.* :

$$\bar{\beta} = (D/\bar{\tau})^{1/2} . \quad (4.1)$$

The main unknown then related to the mean time between surface renewals, which needed to be based on a model for the underlying turbulence structure. For example, Fortescue and Pearson (1967) proposed that the time between renewals could be approximated by a scale related to the integral time and velocity scales of the far field turbulence, $\bar{\tau} = \Lambda/\sqrt{u'^2}$, where Λ is the far-field turbulence integral scale and $\sqrt{u'^2}$ is the far-field turbulence velocity scale.

At about this time Banerjee *et al.* (1968), and subsequently Lamont and Scott

(1970), suggested that the time between renewals was related, however, to the Kolmogorov time scale, leading also to an expression for $\bar{\tau}$ of the type $\bar{\tau} = (\nu/\epsilon)^{1/2}$, where ϵ is the turbulent energy dissipation rate close to the interface and ν is the kinematic viscosity. Unlike the model of Fortescue and Pearson where the renewals are thought to be mainly due to the large eddies, Banerjee *et al.* focused on the small eddies in the viscous dissipation range. Both of these so-called large- and small-eddy models predicted the data against which they were compared rather well. The controversy continued for some time until Banerjee (1990) used a theory due to Hunt and Graham (1978) to calculate the surface divergence spectrum and an analytical expression for the effect of eddy Reynolds number on mass or heat transfer rate, in the absence of interfacial shear, as:

$$\frac{\bar{\beta} Sc^{0.5}}{u'_{\infty}} \cong \frac{C}{Re_T} (0.3(2.38 Re_T^{3/4} - 2.14 Re_T^{2/3}))^{1/4} \quad (4.2)$$

Here Sc is the Schmidt number equal to ν/D , u'_{∞} is the far-field integral velocity scale of the turbulence, C is a constant of the order 1, and Re_T is an eddy Reynolds number based on the far-field integral velocity scale, length scale and kinematic viscosity. Equation 4.2 is plotted in Figure 4.1 and one can see that the Fortescue and Pearson (1967) prediction is asymptotic at low eddy Reynolds numbers to the curve whereas the Banerjee *et al.* (1968) prediction is asymptotic at high eddy Reynolds number. It should be noted that the theory proposed in Banerjee (1990) only applies strictly to far-field turbulence that is homogeneous and isotropic, and at an unsheared gas-liquid interface i.e., there is no wind stress imposed. In most practical situations, however, shear is imposed on the interface and the situation is further complicated by the formation of waves. Very little was known about such problems until recently, and it is these topics then that will be discussed in the following sections.

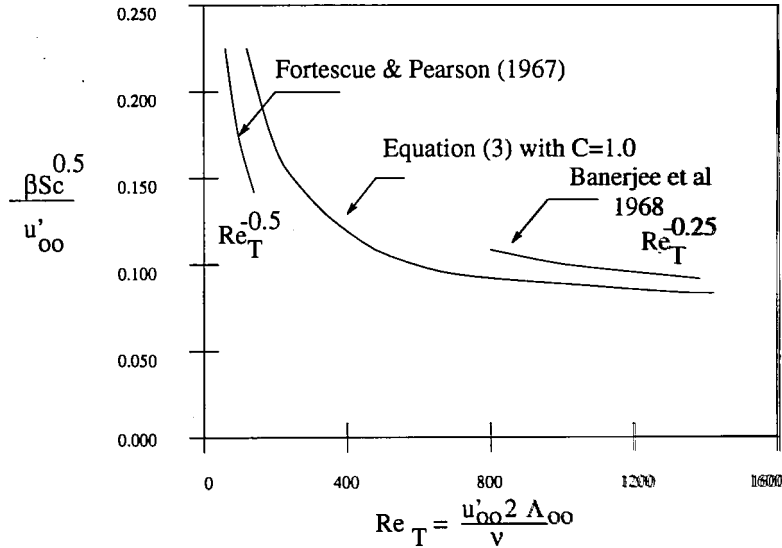


Figure 4.1: Variation of the mass transfer coefficient with turbulent Reynolds number, Eq. 4.2. The models of Fortescue and Pearson (1967) and Banerjee *et al.* (1968) are also reported for comparison.

4.3 Turbulence Structure near flat gas liquid Interfaces

Streaky structures have been identified in wall turbulence since the pioneering experiments of Kline *et al.* (1978) who also observed that low speed regions would periodically be ejected in bursts. It is known that these bursts or ejections, and related sweeps, that come down to the wall region to replace the displaced fluid, strongly influence heat and mass transfer at a wall.

The reason for bursts formation is still unclear, but appears to be related to quasi-streamwise vortices that form very close to the boundary. The quasi streamwise vortices themselves initially appear oriented in the wall-normal direction and spin up between the low-speed streaks and high-speed regions that lie very close to the wall. The mean flow then stretches these vortices in a quasi-streamwise direction. It appears that ejections and sweeps are associated with these quasi-streamwise vortices. The immediate question that arises, then, is whether such structures, observed in wall turbulence, occur near gas-liquid interfaces. Considering that the gas has rather low inertia compared to the liquid, so that fluctuations on the liquid side parallel to the interface can proceed relatively unimpeded, they can in a sense be expected on the gas side since the liquid surface, to a flowing gas, looks much like a wall. However, to the liquid, the interface is almost a slip surface (at least for the higher frequency fluctuations), though mean shear is impressed due to the gas flow. Nonetheless, the boundary conditions at a fluid-fluid interface are very different and it is not clear what is to be expected.

To clarify this situation, Rashidi and Banerjee (1990), carried out a number of experiments in which they investigated the flow structure in a flowing stream of liquid, with and without shear imposed by gas flow. Close to the gas-liquid interface a patchy structure at zero shear and low-speed high-speed streaky structures which are qualitatively similar to those seen near a wall at increasingly higher shear rates were observed. Furthermore, burst-like structures emanating from the gas-liquid interface, much like seen in wall turbulence were recorded. This led Rashidi and Banerjee to conclude that shear rate was the primary determinant of structure in such situations, and the details of the boundary condition were secondary. The finding regarding interfacial bursts and streaks was later confirmed by Komori *et al.* (1993). Nonetheless, there are important quantitative differences in the interface flow field on the liquid side from wall turbulence, though the qualitative features are similar. The criterion for transition from the patchy structures seen at no shear, to the streaky structures was clarified through direct numerical simulation (DNS) by Lam and Banerjee (1992).

Those authors also showed that if sufficient shear is imposed on the gas-liquid interface, then the structure changes dramatically as evident also from the direct numerical simulations of Lombardi *et al.* (1996), carried out as part of this project. Lombardi *et al.* (1996) did a direct numerical simulation where the gas and liquid was coupled through continuity of velocity and stress boundary conditions at the interface. The interfacial plane itself shows regions of high shear stress and low shear stress, with low shear stress regions corresponding to the low speed regions and the high shear stress to the high speed regions. The low shear stress regions are indeed streaky in nature with high shear stress islands. At the edges of the high shear stress regions, vortices are seen to spin up on both sides of the interface. These are initially in the plane normal to the interface but subsequently are stretched in the quasi-streamwise direction by

the mean flow. These quasi-streamwise vortices, known for playing a major role in the ejection-sweep processes observed in wall turbulence, do the same at the gas-liquid interface.

At this point it is worth considering how the high shear stress regions form. This can be clarified by considering a quadrant analysis of the velocity field over the interface in which velocity fluctuations in each quadrant of the Reynolds stresses are correlated with shear stress at the interface. In the first quadrant both the streamwise and interface normal velocity fluctuations are positive. In the second, the streamwise component is negative but the interface normal component is positive. This corresponds to an ejection of low speed fluid. In the third quadrant, both the streamwise and the interface-normal velocity fluctuations are negative, and in the fourth the streamwise component is positive whereas the interface-normal component is negative. The fourth quadrant then corresponds to a sweep in which high-speed fluid is brought towards the interface.

Consider now the correlation of each quadrant of such velocity fluctuations with the interfacial shear stress shown in Figure 4.2 (left) on the gas side. It is clear that sweeps, i.e., in the fourth quadrant, lead to the high shear stress regions whereas ejections lead to the low shear stress regions. This is what is observed in wall turbulence at a solid boundary and therefore the gas sees the liquid surface much like a solid boundary. However, if we look at Figure 4.2 (right), it is immediately clear that no such correlation exists on the liquid side. In fact, all the quadrants have similar behavior with regard to the shear stress regions that occur below the high speed sweeps on the gas side, i.e., the motions that bring high speed fluid from the outer regions to the interfaces on the gas side leads to high shear stress at the interface. Conversely, ejections on the gas side which take low speed fluid away from the interface into the outer flow, strongly correlate with low shear stress regions. The liquid does not behave in this way and does not dominate the pattern of shear stress on the interface. This is of some importance as we will show in a later section.

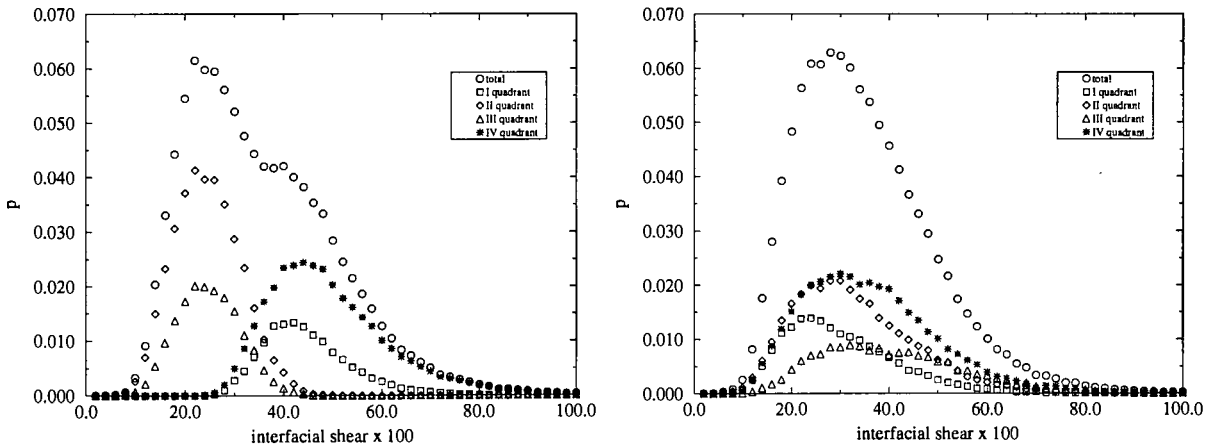


Figure 4.2: Probability of strongly coherent events classes according to quadrant as a function of interfacial shear stress in the region over which the events occur –left: gas; right: liquid.

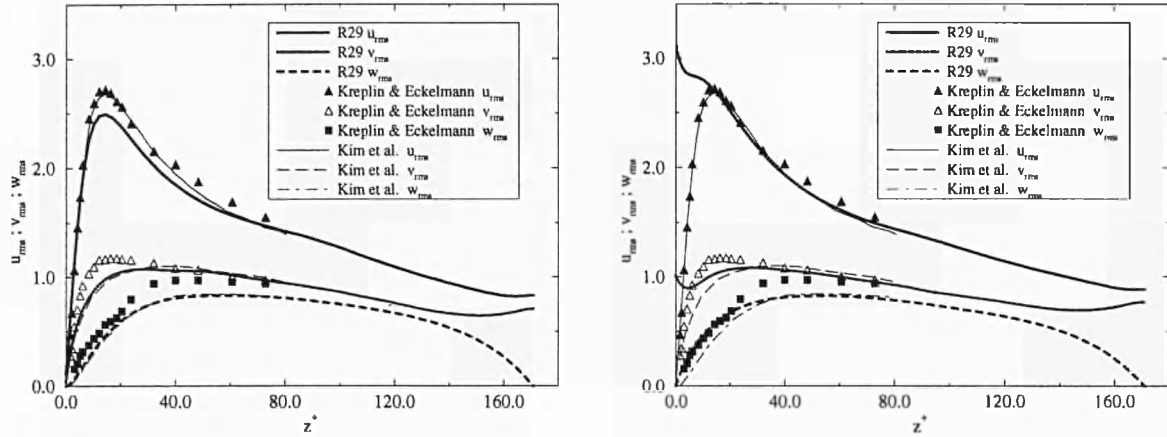


Figure 4.3: Velocity fluctuations in wall turbulence (experimental measurements by Kreplin and Eckelmann, 1979, and DNS by Kim *et al.*, 1987) and at an air-water interface (DNS by Lombardi *et al.*, R29) –left: gas; right: liquid.

The difference between the gas and the liquid phases in the near interface region is further clarified by observing the velocity fluctuations on each side of the interface as shown in Figure 4.3. The left portion of the figure is for the gas whereas the right one is for the liquid. The gas, as is evident, behaves much like flow over a solid wall. The fluctuations are almost identical to that at a solid boundary, in all directions – streamwise, spanwise, and wall-normal. On the other hand, the liquid, as evident from the bottom figure, has the largest fluctuations in the streamwise and spanwise directions right at the interface itself. Indeed, as it was speculated before, it sees the interface virtually as a free slip boundary, except for the mean shear.

Certain other aspects of turbulence on each side of a gas-liquid interface are worth considering. Clearly, ejections and sweeps may be expected to play an important role in determining scalar transfer rates so their frequency of occurrence is of some importance. In the wall region, it is known that ejections and sweeps have a spacing in time that lies between a non-dimensional time of 30 and 90, 90 being the upper-limit which corresponds to those assemblages of ejections and sweeps that are termed bursts. Rashidi and Banerjee (1990) found that on the liquid side of a sheared interface this type of parametrization held. Thus, the qualitative behavior is similar, though within the bursts themselves there are substantial differences between the gas and the liquid sides. This finding, with regard to the time between bursts, which remain about the same as in wall turbulence, is of considerable importance in predicting scalar transfer as discussed later.

4.4 Turbulence structure near wavy surfaces

The previous discussion focused on turbulence phenomena for coupled gas-liquid flows with flat interfaces –a situation close to the experiments of Rashidi and Banerjee (1990). To understand the effects of waves on the gas side –where such effects may be expected

to be more important than on the liquid side,– the flow over a surface with two-dimensional waves (with spanwise crests and troughs) was investigated. The flow situations correspond to the experiments of Buckles and Hanratty (1984), so the results could be checked.

To allow the pseudospectral method to be used for flows over wavy boundaries it was necessary to map the flow field into a rectangular domain. This was done with a nonorthogonal transformation that stretched the surface normal coordinate. To maintain spectral accuracy in the simulations, the solution procedure adopted in the DNS previously described (see Lam and Banerjee (1992)) had to be modified. A projection algorithm was adopted –the details being available in De Angelis *et al.*(1997a,b).



Figure 4.4: Quasi-streamwise vortices scalar indicator.

The waves introduced a streamwise length scale as indicated by the vortex structure shown in Figure 4.4 (here a scalar vortex indicator based on the eigenvector corresponding to the complex eigenvalues of the rate of deformation tensor is used to show the quasi-streamwise vortices). However, when the phase average velocities and shear stresses are removed from the instantaneous field, then typically streaky regions of high speed - low speed flow and shear stress are seen, as indicated in Figures 4.5 and 4.6. The streak spacing is ~ 100 in units nondimensionalized with the frictional drag (removing the form drag component from the total drag). This suggests that turbulence phenomena near the wavy surface may scale with frictional drag, rather than the total drag. On examining the time between sweeps and bursts, a time nondimensionalized with the frictional drag, i.e. $t^+ = t\tau_i/\mu$, is seen to be between 30 and 90, in agreement with what happens at a flat wall. Here τ_i is the frictional drag, i.e. the form drag has been removed from the total.

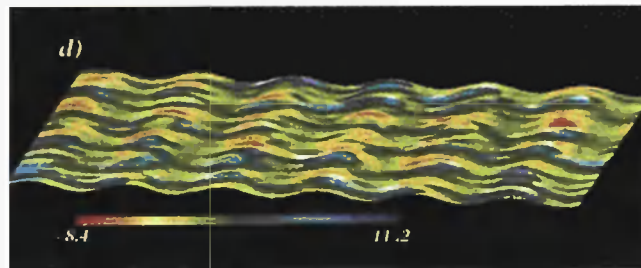


Figure 4.5: Streaky structure at a wavy wall

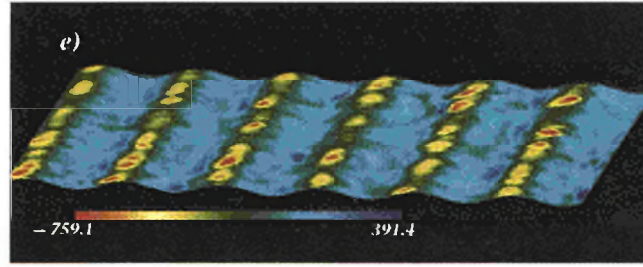


Figure 4.6: Shear stress at a wavy wall.

When simulations are performed for air-water streams coupled across a deformable interface, quasi-3D interfacial waves develop and propagate. The primary deformations are spanwise ripples with bulges imposed by turbulent motions. The streaky nature of the streamwise velocity field near the interface, as well as the shear stress is still retained as shown in Figure 4.7 and 4.8. The numerical results have not been fully analyzed, but the indications are that near-interface turbulence phenomena scale with the frictional drag and kinematic viscosity, as in the case of a wavy wall.

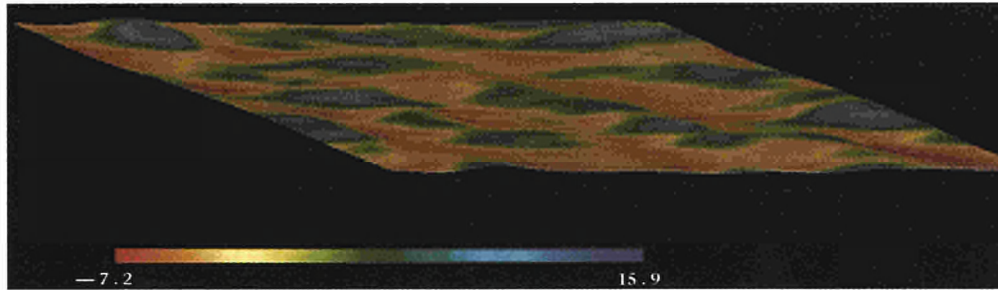


Figure 4.7: Streaky structure at a wavy interface.

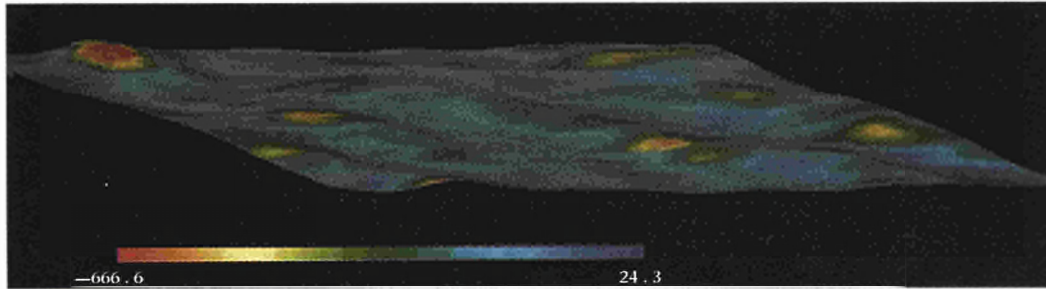


Figure 4.8: Shear stress at a wavy interface.

4.5 Scalar transfer rates

4.5.1 Simulation Results: flat interface

Scalar transfer rates were calculated using the velocity fields discussed in the previous sections. For the computations in which Sc (or Pr) are $\sim O(1)$ the spacing of the collocation points used for the velocity field simulation were also used for the scalar

Table 4.1: Scalar Transfer Calculation Parameters

Sc	Resolved region z^+	Chebyshev modes	β
0.7	171	65	0.097
10	43	65	0.016
3.65	171	129	0.053
25	43	129	0.020

flux calculations, i.e. the scalar concentration equation was solved using the same number of modes in each direction. However, the simulations for higher Sc (or Pr) number required a much finer spacing of collocation points in the interface-normal direction. To achieve this, the region resolved with Chebyshev modes was as indicated in Table 4.1.

Constant concentration boundary conditions were used at the interface – corresponding to the equilibrium concentration for the species being transferred. This is a reasonable assumption and is always used in chemical engineering for sparingly soluble species. The boundary conditions at the outer edge of the resolved region were zero mean concentration and zero normal fluctuating flux.

Contours of the instantaneous scalar fluxes at interfaces are shown in Figures 4.9 and 4.10, and compared with the shear stress at the interface for the gas and the liquid side calculations respectively.

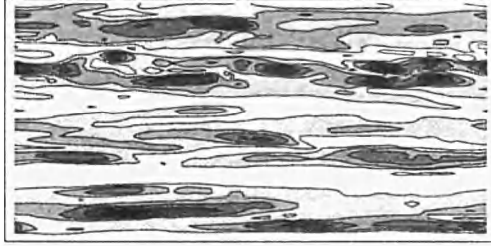


Figure 4.9.a: Mass flux $Sc = 10$ on the gas side.

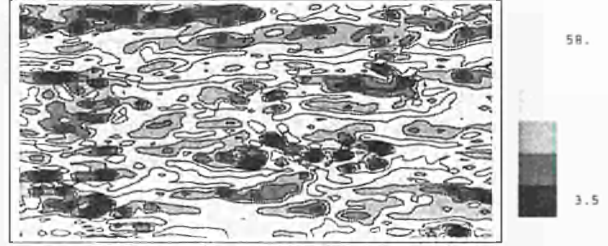


Figure 4.10.a: Mass flux $Sc = 25$ on the liquid side.

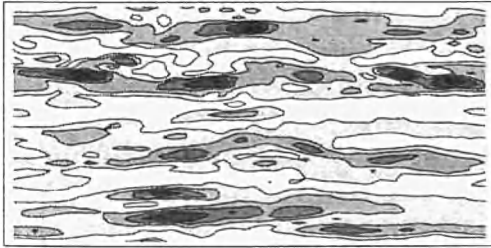


Figure 4.9.b: Shear stress at the interface.

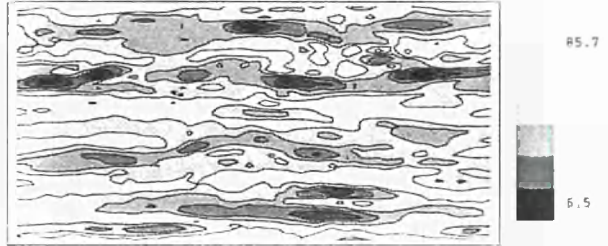


Figure 4.10.b: Shear stress at the inter-

face. It is immediately evident that the gas side fluxes correlate well with the shear stress and this is shown quantitatively in Figure 4.11. On the other hand, the flux field on the liquid side shows a much finer structure (see Figure 4.10) and no such correlation exists.

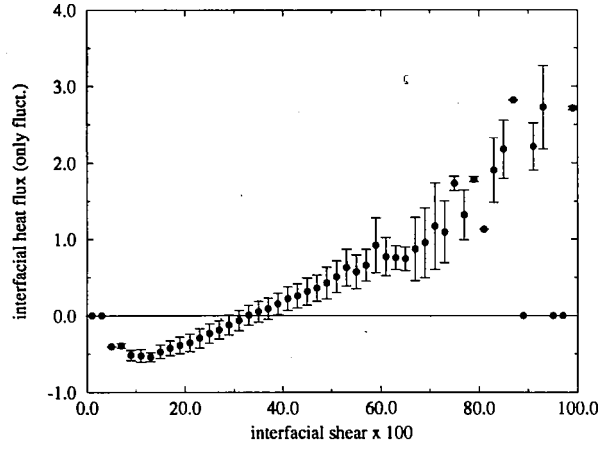


Figure 4.11: Shear stress vs. heat flux fluctuations on the gas side.

It is of interest therefore to understand what processes control the liquid side fluxes. Figure 4.12 shows the instantaneous Reynolds stresses $u'w'$, the interface normal velocity w' , and the scalar transfer coefficient $\beta_t^+ = \beta/u_t^*$ as a function of time in wall units. This is shown for two points at the interface which are typical of all points.

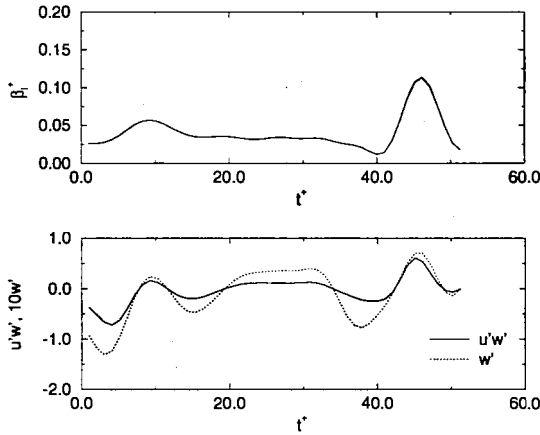


Figure 4.12.a: Time history for the liquid of scalar transfer coefficient, β^+ , and Reynolds stress, $u'w'$.

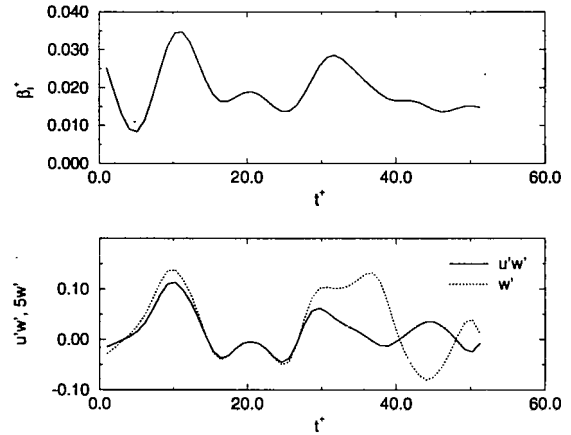


Figure 4.12.b: Time history for the liquid of scalar transfer coefficient, β^+ , and Reynolds stress, $u'w'$.

It is clear that when $u'w'$ is strongly positive and w' is positive (corresponding to a sweep) the scalar coefficient is high. The correlation with the instantaneous Reynolds stress is self-evident, and the sweep essentially renews the interfacial region, giving rise to high scalar transfer rates. Since, in the liquid side, sweeps do not correlate with the high shear stress areas at the interface, therefore strong correlation between scalar transfer rates and interfacial shear stress patterns is not to be expected.

The time period between sweeps can also be estimated from the numerical simulation. On the gas and the liquid side there are between 1 and 3 sweeps, corresponding to 1 “burst”, in about 90 non-dimensional time units (tu_*^2/ν), where $u_* = \sqrt{\tau_i/\rho}$ and τ_i is the interfacial shear stress (equal for both phases). For the gas side, the result is to

be expected, but the liquid side results –though in line with the experiments of Rashidi and Banerjee (1990)– indicate that the main turbulence phenomena in the two fields are uncoupled. This follows because the density and viscosity of the gas and the liquid are different and the dimensional time between the sweeps and bursts are, therefore, very different.

4.5.2 Simulation Results: Wavy surface

The temporally and spatially varying velocity field obtained in the simulation for gas flow over wavy surfaces was provided for solution of the species concentration equation and the scalar transfer rate was determined. To date the calculations have been done with $Sc = 1$ and for the gas side, as the scalar concentration gradients are spread over the thickest layer in this case – and hence could be expected to be most affected by the wavy surface.

The objective of the simulation was to determine the value of β^+ for comparison with the flat interface cases of Table 4.1. Since the surface is wavy, a portion of the total surface stress is due to the form drag, and a portion is due to the frictional drag. The direct numerical simulation allows each component of the drag to be estimated. If we define a velocity scale based on frictional drag as u_* and based on frictional plus form drag as \hat{u}_* , then the simulation gives, $\beta^+ = 0.077$ and $\hat{\beta} = 0.063$.

4.5.3 Scalar flux parametrization

The surface renewal theory of Danckwerts (1951) may be used to parametrize scalar transfer rates on the liquid side, with a time between renewals being between 30 and 90 shear-stress-based non-dimensional time units. The theory was originally developed for “mobile interfaces” in the sense that liquid motions parallel to the interface were relatively unimpeded. The scalar transfer rate is then:

$$\bar{\beta} = (D/\tau^+)^{1/2} \quad (4.3)$$

with $\tau^+ = 30$ to 90 (ν/u_*^2) based on the preceding discussion. This leads to:

$$\frac{\bar{\beta}_l Sc^{0.5}}{u_l^*} = 0.108 \text{ to } 0.158 \quad (4.4)$$

This equation was derived by Banerjee (1990), based on the conjecture that sweeps/bursts controlled scalar transfer rates and that sweep/burst frequencies were similar at a sheared liquid interface to those observed in wall turbulence. Both conjectures are supported by the simulations and experiments.

Equation (4.3) is compared with simulation results for two different Schmidt numbers in Figure 4.13. It is clear that the numerical values agree with the predictions and the Schmidt number dependence is correctly predicted.

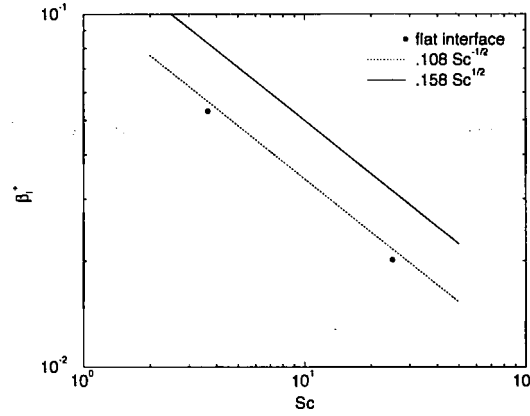


Figure 4.13: Mass transfer coefficient vs Sc number for the liquid.

Equation (4.3) is also compared with wind-wave tank data for SF_6 and CO_2 transfer rates from Wanninkhof and Blivens (1991) and Ocampo-Torres *et al.* (1994) in Figures 4.14 and 4.15 respectively. Again the agreement is good noting that u_* is probably somewhat overestimated as the form drag was not separated out.

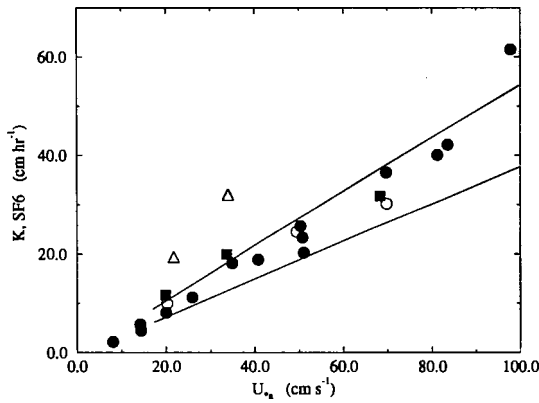


Figure 4.14: Comparison of Equation (4.9) with the data by Wanninkhof and Bliven (1991). The outlying points are large amplitude waves that were breaking. It has been assumed that $\rho_w u_{*w}^2 = \rho_a u_{*a}^2$ in making the plot.

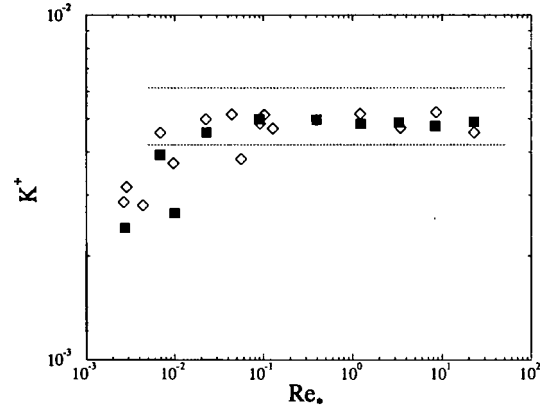


Figure 4.15: Comparison of Equation (4.9) with wind-wave tank gas transfer data (from Ocampo-Torres *et al.*, 1994) assuming $Sc = 660$; here $\beta^+ = \beta_w/u_{*w}$ and $Re_* = u_{*w}h/\nu$.

Turning now to the gas side, the gas sees the liquid much like a solid surface as discussed earlier. So a form of the surface renewal theory modified for such applications, *e.g.* by Banerjee (1971) amongst others, is necessary. This leads to a different dependence in the Schmidt number, and the modified expression is:

$$\frac{\overline{\beta_g} Sc^{2/3}}{u_g^*} = 0.07 \text{ to } 0.09 \quad (4.5)$$

Figure 4.16 compares the expression with DNS results. It is clear that the Schmidt number dependency is correctly predicted, and the numerical values are within the

range of Equation (4.5). Also shown in the figure is β_g^+ and $\hat{\beta}_g^+$ for gas flow over a wavy surface with $Sc = 1$. It is clear that if the frictional drag is used to nondimensionalize β_g , then the results are in line with the equation (4.5), and the wave effects are captured in this formulation. However if β_g is nondimensionalized with the total drag, then the value of the LHS of Equation (4.5) lies well below the prediction.

The lower bound of Equation (4.5) is also compared with the moisture transfer data of Ocampo-Torres *et al.*(1994) in Figure 4.17. The agreement, again, is good.

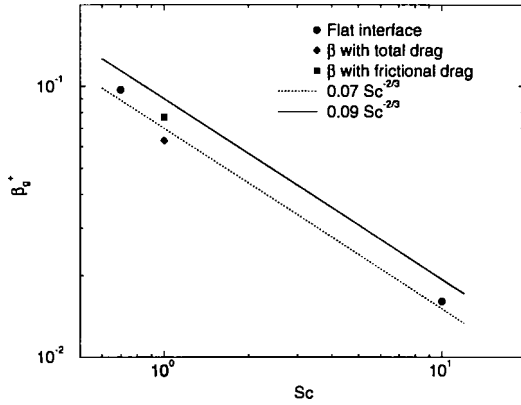


Figure 4.16: Mass transfer coefficient vs Sc number on the gas side.

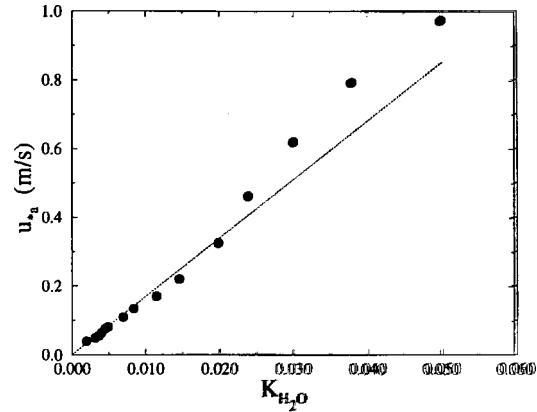


Figure 4.17: Mass transfer coefficient v.s. u_* from Ocampo-Torres *et al.*(1994).

CHAPTER FIVE

SEA SPRAY EFFECTS ON LATENT HEAT EXCHANGE AT THE AIR-SEA INTERFACE

5.1 Introduction

One contribution to the transfer of heat and mass from the ocean surface is via sea spray droplets, large numbers of which are generated by breaking waves, thereby increasing the available interfacial area. However, the question of how significant this mechanism is has sparked some controversy; some researchers (*e.g.* Hasse, 1992) claim that there is no significant enhancement of the fluxes due to spray, except perhaps for hurricane strength winds, whilst others consider it to be important at much lower wind speeds (see for example the exchange between Andreas, 1994 and Hasse, 1994). Recent work (Fairall *et al.*, 1994; Kepert, 1994) has proposed that spray evaporation plays an important role in the development of tropical storms, based on the finding that the early evolution could not be explained without the presence of liquid water droplets. Another reason why the production of droplets is of interest is that they can evaporate to form crystals of sodium chloride which, if carried to the higher regions of the troposphere, become potential nucleation sites for the condensation of water vapour in clouds.

At low wind speeds, the sea surface is flat, but as the wind increases, ripples appear on the surface due to the development of capillary waves. As the wind speed increases further, the waves become larger until they finally become unstable and water tips from the higher regions, a process known as *breaking*. In experiments using wind-wave tanks with short fetches, wave breaking occurs for wind speeds above a critical threshold of about $10\text{--}13\text{ms}^{-1}$. In the open ocean, where there is a much greater fetch, the onset of this phenomenon is more gradual and breaking waves first appear for wind speeds of $2\text{--}3\text{ms}^{-1}$ (Monahan *et al.*, 1986).

Breaking waves can be classified into two main groups, plunging breakers and spilling breakers, and the two classes are illustrated in Figure 5.1. Plunging breakers are the type normally observed on beaches and in this case, the crest of the wave overturns, forming a sheet of water which plunges down in front of the wave, trapping air and generating eddies in the sea. In the open sea, the vast majority of breaking

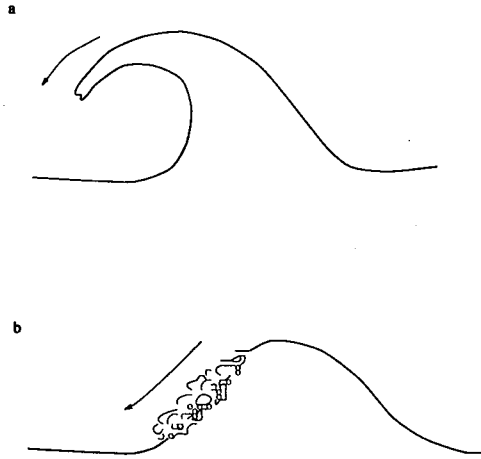


Figure 5.1 : Diagram showing breaking wave. a) Plunging breaker in which crest curls over and falls ahead of wave. b) Spilling breaker in which water flows down face of wave.

waves are spilling breakers, in which a turbulent flow of water moves down the leading face of the wave, entraining air.

Breaking waves, known as whitecaps in the scientific literature, are of interest mainly due to the fact that bubbles result from the entrainment of air, and these subsequently rise to the surface where they burst, producing droplets. Another important effect is that the presence of whitecaps increases the reflectivity of the sea; Stabenon and Monahan (1986) have shown that they make a significant contribution to the total albedo. Bubbles may also increase the transfer rates of soluble gases, and this is discussed by Woolf and Thorpe (1991).

The usual way in which the number of breaking waves is quantified is to use a parameter W , defined as the proportion of the ocean surface visually observed to be covered with whitecaps. The time-averaged whitecap coverage is highest in mid latitude winters, where it can reach 3%, and is lowest in the equatorial regions, where it is less than 0.5%; the global average is in the region of 1%. The whitecap coverage is dependent mainly on wind velocity and analysis of photographic observations by Monahan (1971) found that at wind speeds of less than 4ms^{-1} , W was always less than 0.1%. At higher wind speeds whitecap coverage increases very rapidly. This strong dependence on the wind speed would suggest that the rate at which the spray droplets are produced by wave-entrained bubbles increases dramatically with wind speed.

5.2 Mechanism of droplet generation

The processes which take place as the bubble reaches the surface have been investigated using high speed photography by, amongst others, Kientzler *et al.* (1954), and is illustrated in Figure 5.2. As the bubble emerges from the liquid, a thin film forms at the upper surface of the bubble. This film thins by drainage and then ruptures,

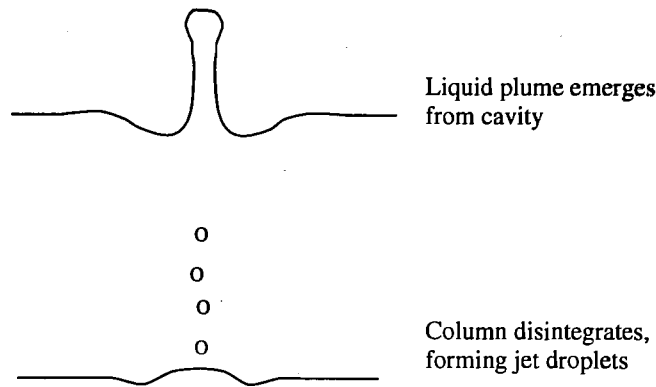


Figure 5.2 : Processes taking place when a bubble reaches water surface.

often producing small “film” droplets. Following this breakage, a narrow liquid column emerges from the centre of the cavity and rises, disintegrating to form “jet” droplets as the result of the development of instabilities. This behaviour has also been studied by Boulton-Stone and Blake (1993) and Decker and de Leeuw (1993) using theoretical models.

Several jet drops are produced by each bubble and are fairly consistently about one tenth the radius of the parent bubble. Since the bubble spectrum peaks at a radius of $50\text{--}100\mu\text{m}$ (Kolovayev, 1976; Cipriano and Blanchard, 1981; Johnson and Cooke, 1979), this suggests a typical droplet radius of several microns. Film droplets are more numerous and are generally smaller, typically $1\text{--}2\mu\text{m}$ in radius (Cipriano and Blanchard, 1981; Woolf *et al.*, 1987), though experiments by Resch and Afeti (1992) have shown that a large number of droplets are also produced in the sub-micron size range. However, sub-micron droplets are too small to have any significant effect on the overall transport rates.

In order to gain a better insight into the bursting of bubbles, a series of experiments was conducted as part of this research programme (Rossodivita *et al.*, 1995, and Rossodivita and Andreussi, 1997). Bubbles were introduced into a 48dm^3 tank of fresh water by injecting air through a porous membrane. By using media of different porosities, the bubble sizes could be varied from 0.6mm to 1.5mm in diameter; the tank was sufficiently deep to enable the bubbles to attain terminal velocity before reaching the surface. An important feature of the experiments was that swarms of bubbles were generated, as would be the case under a breaking wave, whereas most previous investigations have involved the release of bubbles one by one.

Observations of the bubbles were made by photographic image analysis and the droplets were observed by means of a two-component, dual beam Phase Doppler Analyser (see Bachalo, 1990 for a discussion of this technique). The apparatus enabled measurements to be made of the sizes of droplets and their ejection velocities, for droplets with diameters in the range $2\text{--}160\mu\text{m}$.

Figure 5.3 shows the distribution of droplet sizes obtained from these experiments. Measurements reported in the literature (*e.g.* Kientzler *et al.*, 1954) have found that

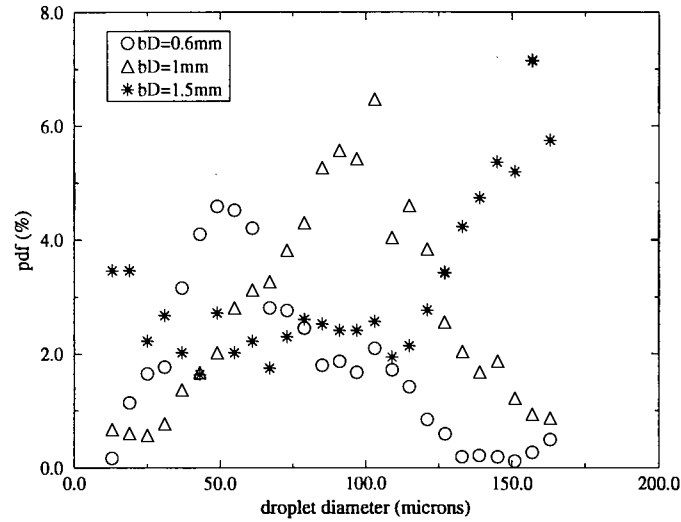


Figure 5.3 : Probability distribution function (pdf) of droplets vs. diameter size (bD=bubble diameter). Height above the interface: 1mm.

jet droplets are generally about one tenth the diameter of the parent bubble; in the present experiments, peaks can be seen at this point for the 0.6mm and 1mm diameter bubbles. For the 1.5mm bubbles, many droplets are generated at this point, but a large number of much smaller droplets are also found; these smaller droplets are likely to be film droplets, which are produced in large numbers by larger bubbles.

The velocity distribution of the droplets is shown in Figure 5.4. It can be seen that the larger bubbles produce droplets with higher upward velocities, and for the 0.6mm bubbles, it can be seen that the distribution peaks at about $60\mu\text{m}$, which would correspond to jet droplets. The absence of a prominent peak in the other two curves is probably due to the fact that larger bubbles generate proportionally more film droplets, which have a wider distribution of ejection angles and sizes.

Bursting bubbles are not the only sources of spray droplets; at higher wind speeds, the drag exerted by the wind causes liquid to be torn directly from the waves. The production of these droplets starts at about 9ms^{-1} and increases dramatically with increasing wind speed. Photographic observations of the production of these droplets have been made by Koga (1981, 1987) using a wind-wave tank. It was found that near to the crest of the wave, where the wind stress is generally highest, small projections develop which then break up to form droplets. The maximum diameter of these droplets was approximately 3mm and was generally no smaller than $20\mu\text{m}$ (Koga, 1981; Monahan *et al.*, 1986). Calculations made by Koga (1987) and by Bortkovskii (1987) have shown that the Kelvin-Helmholtz instability is probably responsible for producing these projections.

Andreas (1992) showed that at higher wind speeds, the droplets with radii in the range $10\text{-}300\mu\text{m}$ would contribute most to the heat fluxes. This size range would be dominated by spume droplets, implying that spume generation is the most important mechanism of droplet generation under these conditions.

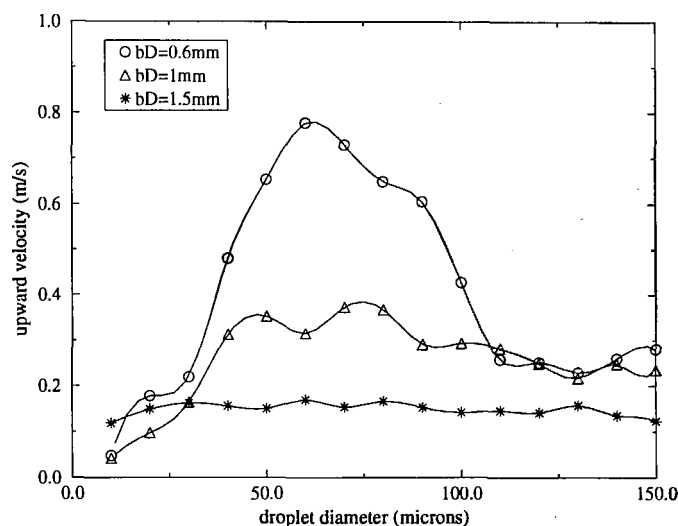


Figure 5.4 : Distribution of droplets upward velocity vs. diameter size (bD=bubble diameter). Nominal height above the interface level: 1mm.

5.3 Droplet production

5.3.1 Method of calculating droplet production

In order to calculate the fluxes due to sea-spray, an obvious pre-requisite must be to have an idea of how many droplets are actually produced. The detailed behaviour and structure of breaking waves is far too complex to allow the calculation by purely theoretical means and so it is necessary to look for assistance in the form of experimental data. Several research programmes have taken measurements of the droplet concentrations and size distributions over the sea (Monahan, 1968; Preobrazhenskii, 1973; DeLeeuw, 1990) and, although the quantity of data is limited, this provides a good starting point for any calculation.

If the sea were pure water, then one could calculate the spray contribution to the fluxes directly from the droplet concentration and size distribution using standard formulae for the rates of evaporation and cooling. The salt content of the sea complicates matters somewhat in that it affects the evaporation rate of water. The relative humidity over the sea is typically about 80% and at this level, droplets shrink by evaporation until they reach about half their original diameter, at which point the sodium chloride concentration is sufficiently high to inhibit any further evaporation.

In addition to the size and number of droplets present, it is therefore necessary to know the droplets' salt content. "Young" droplets will readily evaporate, but "old" ones which have reached equilibrium with the air can no longer exchange heat or mass. However, the available experimental data do not include this information — the sensors made no distinction between young and old droplets — so some means of calculating droplet ages is required. In order to do this, previous researchers have made estimates

of the droplet residence time, the period spent in the air before falling back to the sea. However, the residence time is strongly influenced by the air flow over waves, the nature of which is not only complex and turbulent, but also not well known. It was mentioned earlier that there are wild variations in the predictions of droplet production rates and a major factor behind this is the different assumptions (sometimes unreasonable) that have been made concerning the flight time.

In order to calculate the droplet source term, a model was constructed to track the motion and evolution of sea spray droplets. The model included formulations for the heat transfer around the droplets and the rate of evaporation. The effect of turbulence on the paths taken by the droplets was also taken into account. By simulating a large number of droplets, it was thus possible to predict what concentration profiles would result from the release of a given number of droplets with a particular initial size distribution. Comparisons with data on droplet sizes and concentrations then enabled the source term to be calculated. The methodology is discussed in more detail in the rest of this section.

5.3.2 Flow over waves

The flow over waves is highly turbulent and the velocity of the air at any instant in time can be represented as comprising a mean component and a component due to the turbulent fluctuations. If u and w represent the components in the horizontal and vertical directions respectively, then one can simply write them in the form

$$u = \bar{u} + u' \quad (5.1)$$

$$w = \bar{w} + w' \quad (5.2)$$

where the overbar denotes the time-averaged value and the prime denotes the departure due to the turbulence. The turbulent component can be thought of as being due to the presence of circulating motions superimposed on the mean flow. These motions, known as eddies, are transient phenomena which are primarily generated by at the boundary of a flow, in this case the sea surface. Over the sea, the length of the dominant eddies is about half the distance from the surface and this length is known as the turbulence length-scale, though in practice there exists a wide range of different eddy sizes. Other quantities used to characterise the turbulence are the Lagrangian time-scale, T_L , which represents the lifetime of a typical eddy, and the root mean square value of the velocity fluctuations, σ .

The application of two of these quantities can be illustrated by introducing the Langevin equation:

$$w'(t + \delta t) = \left(1 - \frac{\delta t}{T_L}\right) w' + \sigma_w \left(\frac{2\delta t}{T_L}\right)^{\frac{1}{2}} \gamma \quad \delta t \ll T_L \quad (5.3)$$

This is used to calculate the velocity of a fluid element at a time $t + \delta t$ from a knowledge of its velocity at a previous time t . The first term on the right hand side

can be thought of as being a history or memory effect and the second term as being due to random changes in the turbulence field. γ is a random number with a Gaussian distribution and unit variance (though other shapes are sometimes used) and it is interesting to note that δt has an exponent of one half — a situation not normally encountered in differential equations. Expressions for the components of velocity in the other directions are of the same form.

Let us now consider, from a more physical standpoint, how the turbulence may affect the residence times. One can easily see that in a flow with no turbulence or upwardly moving currents, a droplet will continuously fall toward the sea under the influence of gravity. However, in a turbulent flow, it is likely to encounter eddies which may alter its direction of motion. If the droplet moves into a part of an eddy where the upward fluid motion is greater than its terminal velocity, then it will be carried up to a higher elevation. When the droplet is carried through a number of such eddies, then its residence time will be greatly extended. In fact, the flight path of light particles and droplets is controlled mainly by the turbulence; larger particles, which are too heavy to be lifted against gravity by the eddies are not greatly affected by the turbulence.

The mean flow over a surface is generally expressed as a logarithmic profile (Paulson, 1970; Dyer, 1974). In reality, the flow profile over steep three dimensional waves is rather more complex, but in the absence of suitable alternative models, a logarithmic profile was adopted for the simulations. This is equivalent to assuming that the flow streamlines run parallel to the wave profile, which is not quite the case, especially over steep waves.

5.3.3 Droplet simulations and estimates of droplet production

The movement of droplets was simulated by assuming that they move relative to the air at their terminal fall velocity; this is quite reasonable for the size of droplet under study, though for large droplets inertial effects can be significant. A modified Langevin equation was used to predict the turbulent component of air velocity; the Langevin equation predicts how the turbulence changes *in a frame of reference moving with the fluid*, but we need to know how the turbulence changes in the droplet's reference frame. Since droplets do not exactly follow the streamlines, it is necessary to correct for this and this was done using the model of Edson and Fairall (1994). Equations for the droplet evaporation rate and heat transfer were solved at each time-step to calculate the droplet size and temperature.

Figure 5.7 shows some concentration profiles which were calculated using this approach. Simulations of droplets of different sizes originating at a height of 1m were performed and the resulting vertical concentration profile calculated. Each run tracked the path of 10 000 non-evaporating droplets in a flow field with a wind speed of 22ms^{-1} at 10m. It can be clearly seen that the turbulence causes a significant number of droplets to be carried to higher elevations, particularly the smaller ones.

As discussed earlier, spray droplets originate from two main processes; from bursting bubbles or as a result of water being torn directly from the region of the wave crests. In the case of jet droplets, information on the observed ejection heights was used to

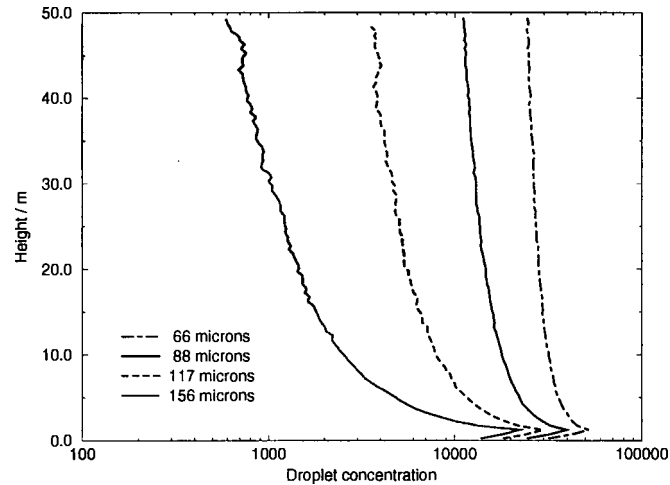


Figure 5.5 : Concentration profile resulting from release of non-evaporating droplets at 1m.

determine their initial velocity and this was used for the initial conditions. It was found that most of the droplets spent very little time in the air before falling back into the water and only a very small proportion reached heights of a few metres. Thus it appeared that this simple model could not explain the large numbers of droplets observed at higher elevations. With spume droplets, the situation regarding the initial velocity is less clear; in the absence of other information, they were assumed to be ejected at speeds of $2u_*$ and at an angle of 30° to the horizontal, which what is found for sand particles which are torn from the ground by the wind (Nalpanis *et al.*, 1993). However, it was found that again only a very small proportion of droplets reached heights significantly above the surface. One possible conclusion from these simulations is that a considerable number of droplets are produced, of which only a tiny minority reach significant elevations. An alternative, and more probable, conclusion is that after formation, droplets are advected well above the surface by air currents which are not modelled in the current simulations.

Investigations showed that the predicted shape of the droplet concentration profile was independent of the height at which droplets were released, for heights above the release point. This meant that it would be reasonable to simulate the droplet transport by considering droplets released at a significant height above the surface. In the simulations, droplets were started off at a height of 1m and their subsequent evaporation and motion tracked. For the initial velocity, it was assumed that the vertical component of the air velocity had a Gaussian distribution and the droplets moved relative to this at their terminal velocity; only upwardly moving droplets were considered — thus the calculated production rate could be thought of as representing the net source flux through a layer 1m above the surface.

The choice of 1m was somewhat arbitrary and was determined partly because of the erratic nature of the measurements below this level. Obviously, predictions for the near-surface concentrations would not necessarily be valid, but under conditions of whitecapping and high wind, this region would be expected to be saturated and therefore spray would not significantly enhance the heat and mass transfer here. The main advantage of simulating droplets released at higher elevations was the saving in

computer time, since it was no longer necessary to track large numbers of droplets which rapidly fell back into the sea in order to obtain trajectories for the few that reached appreciable heights.

The next step was to apply the code to situations for which field measurements of the droplet concentration and size distribution were available. Due to the strong dependence of the wave structure on the fetch and history of the wind field, only data taken from over the sea were considered. Examination of the literature on measurements of droplet concentrations led to the selection of the data of DeLeeuw (1986, 1990) and Smith *et al.* (1993). These sets of data contained sufficient information to calculate the production rate and it was considered that the experiments had been carefully performed.

DeLeeuw's data were collected in the North Atlantic and the North Sea and involved the use of a rotating collector with a silicone coating to capture spray droplets. The craters left in the coating were later inspected under a microscope and the concentration and sizes of the droplets were inferred. Data were collected over a wide range of wind speeds and measurements made at four different wind speeds were used in this work. In the field trials, the droplets were divided into a number of size bands, spaced logarithmically, and the same size bands were used for the simulations. The model was used to track the evolution of a release of a large number of droplets in a particular size band and so determine what concentration profiles would result. For releases of droplets in the largest size bands, the model predicted that these droplets only contributed significantly to concentrations in the original size band. For releases from the smallest size bands, the droplets had sufficient time to evaporate significantly and the release would give rise to droplet concentrations in a few different size bands; solution of a set of simultaneous equations then yielded the production rates.

Figure 5.8 shows the calculated rate of production as a function of droplet initial diameter; all wind speeds are for a height of 10m. It can be seen that, with one exception, the rate increases with wind speed, with this increase being most pronounced for the larger droplets. For both the 11ms^{-1} and 15.5ms^{-1} cases the source term was found to vary roughly as $d_d^{-2.7}$. The values for the 12.8ms^{-1} wind speed are much higher than would be expected from the other sets of data; the reason for this is not clear, but it could be that the conditions had been changing, in which case history effects could be responsible. It should also be noted that due to an equipment malfunction, no data for the humidity were obtained for the 22ms^{-1} case. Initially, the simulations were performed assuming a relative humidity of 80%, but it was found that no initial size distribution could explain the observed size distribution; the results in the graph were obtained using a value of 95%, and a sensitivity analysis showed that the error arising from using an incorrect humidity would be less than about 50%.

The data of Smith *et al.* were taken on a tower located on the tip of an island, using an optical detection method. The data cover a higher range of wind speeds than those of DeLeeuw, but do not include measurements of the larger drops. Simulations were again undertaken to calculate the droplet production rates from the data, and the results again showed a strong increase in the rate of droplet generation with wind speed, especially for the larger droplets — the slope of the curve for the $80\mu\text{m}$ droplets suggests a dependency of roughly U_{10}^6 . Other researchers have also found a rapid variation with wind speed, for example experiments in a wind/wave tank by Lai and Shemdin (1974) indicated that the droplet production rate varied as u_*^4 , and Andreas *et al.* (1995) proposed a model in which the dependence varied approximately as u_*^3 .

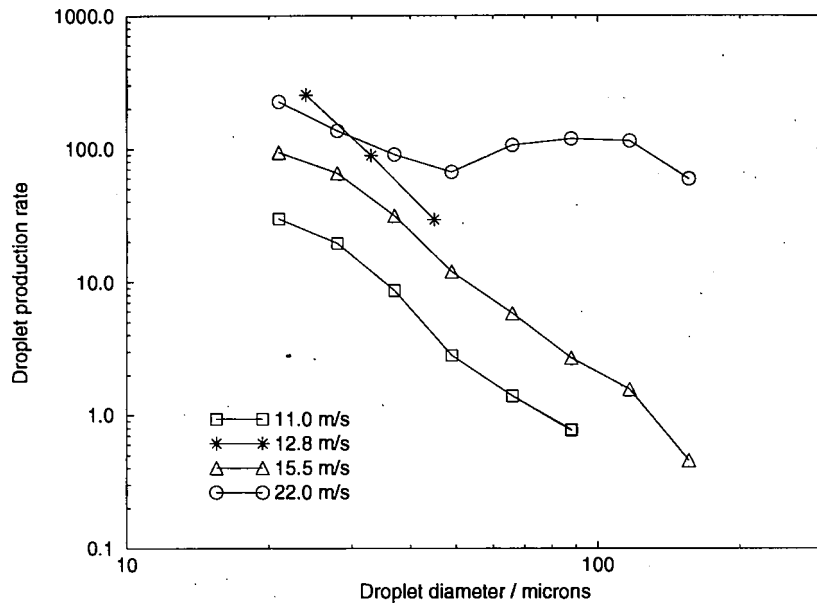


Figure 5.6 : Droplet generation rate calculated from data of DeLeeuw. Units are $\text{m}^{-3} \mu\text{m}^{-1} \text{s}^{-1}$. Parameter is wind speed.

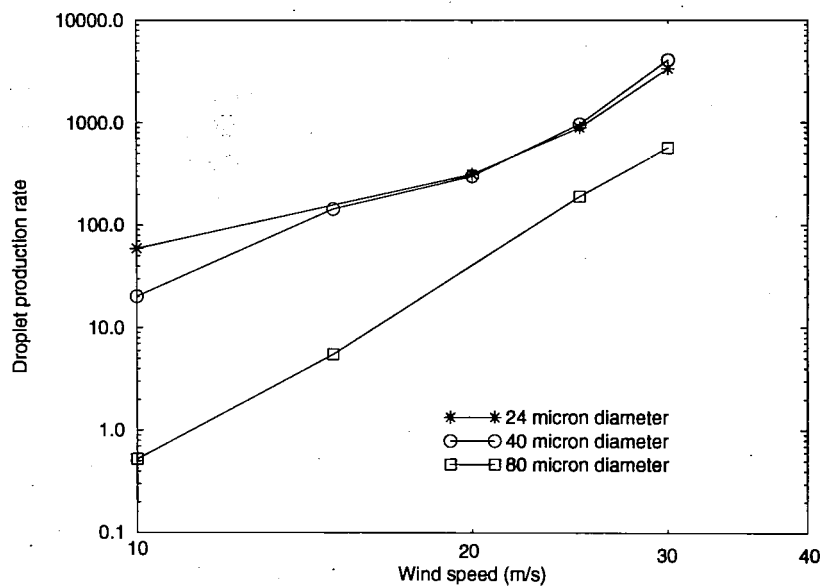


Figure 5.7 : Droplet generation rate calculated from data of Smith *et al.* Units are $\text{m}^{-3}, \mu\text{m}^{-1}, \text{s}^{-1}$. Parameter is droplet diameter.

Air temp	Sea temp	Relative humidity	Total flux	Flux for $z > 2\text{m}$	Flux for $z > 5\text{m}$	DeCosmo model
15	12	80	5.2	3.8	2.7	17.8
15	12	90	2.9	2.6	2.1	101
27	29	80	7.8	4.2	2.7	515
-10	0	80	4.3	2.6	1.9	191

Figure 5.8 : Latent heat fluxes predicted for different conditions by droplet evaporation and with DeCosmo's model.

The results obtained were then used to address the question of whether the spray contributes significantly to the overall latent heat and mass fluxes. Calculations were made of the spray latent heat transfer at 11ms^{-1} and 22ms^{-1} , using the respective curves in Figure 5.7 for the droplet generation function, over the range of sizes for which this had been calculated. In order to gain an idea of where the transfer was taking place, the contributions taking place above 2m and above 5m were also calculated. Comparisons were then made with the fluxes calculated using the formulation of DeCosmo (1991) relative to the overall heat flux at the air-sea interface. Results for four cases, representing typical conditions over tropical oceans, mid-latitude waters and polar seas are reported in Fig. 5.8; the mass exchange is not given since it is proportional to the latent heat transfer are shown in Figure 5.8. It was found that the fluxes were only a few watts per square metre — this compares with values often of the order of hundreds of watts per square metre (depending on the temperature difference) calculated with DeCosmo's formula.

The results also showed that the main contribution was from the larger ($>60\mu\text{m}$) droplets, which would be mainly spume droplets. Since the production rate of these droplets appears to increase very rapidly with wind speed, one can expect that droplets would make a very substantial contribution to the heat and moisture budgets under storm conditions. Also, it is clear that much of this exchange takes place well away from the sea surface. This is significant as many authors have claimed that the presence of spray does not significantly enhance transfer rates as an increase in evaporation leads to an increase in humidity, suppressing further evaporation. However, if the evaporation takes place over a deep layer, this is not so likely to be the case.

There are a number of potential sources of error in the calculation of the droplet generation rate; one major source is from experimental errors in the data on which these calculations are based, another lies with the idealised model used for simulating the droplet motion. However, without more experimental data and a better understanding of the flow over waves, it is difficult to improve on this — in particular, caution should be used in extrapolating the production rates presented here to other conditions.

CHAPTER SIX

CONCLUSIONS AND FUTURE DIRECTIONS

6.1 Wave-Climate Models

There is continuing uncertainty as to the effects of anthropogenic activities in long-term climate. In particular, from the early 1800s there has been an effective increase of about 50 % in greenhouse gases (Lindzen, 1994). However, because of the delays associated with the heat capacity of the oceans, it will perhaps be decades before climate changes can be identified in the data. The historical record suggests long ocean delays, which in turn suggests that the climate response to increasing greenhouse gas concentrations would be far from what might be the "equilibrium state". With regard to activities that generate greenhouse gases, ocean delay has a major impact on whether we pursue a "business as usual" scenario (Houghton *et al.*, 1990) or take Draconian measures to curtail generation. Ocean delay, of course, depends crucially on exchanges with the atmosphere, i.e. the couplings.

Be that as it may, there are also significant uncertainties in translating anthropogenic production of greenhouse gases into atmospheric concentrations. Again, there are deviations from equilibrium concentrations, part of this being associated with absorption into the oceans.

To clarify these issues, large-scale computer simulations of climate have been undertaken. The atmospheric and oceanic circulation calculations have become increasingly detailed, but the models coupling the two –except perhaps in some regional simulations like ECAWOM– have remained primitive. This, to some extent, has come about because improved representations of the coupling require calculation of the global wave field, which adds significantly to the computing resources required for climate simulations. Nonetheless, the rapid growth in computational capability, and in particular, the advent of massively parallel machines, suggests that more sophisticated coupled modules, such as the regional model ECAWOM, will become feasible on a global scale. This, in turn, should lead to more reliable long-term climate simulations, provided that well-validated models for the air-sea exchanges are available.

The policy implications of more dependable simulations are enormous. Not only do these impact activities that generate greenhouse gases, but also impact, as an example,

mitigatory and control measures that might be necessary for low-lying coastal areas. This is because an early indicator of greenhouse-gas-related climate effects may well be increases in the frequency and intensity of severe storms, and storm surges, and increase of severity in the wave climate. For the European Union, with its relatively large coastal areas and population, as well as significant offshore oil-gas production, these matters are therefore of great interest.

Turning now to work undertaken for the PISA project, the main findings, and indications as to where work might be focused in the future, are summarized in the following paragraphs. We start with developments related to wave forecasting, which also clarifies areas where more understanding of wind-wave momentum coupling is necessary, and move on to momentum exchange, energy and species exchange, and finally, discuss the effect of sea spray on latent heat/moisture exchange.

Some of the main findings of the PISA project have been reported at a conference titled "Wind-over-Wave Couplings: Perspectives and Prospects", held at University of Salford, April 8-10, 1997. Specifically, these are the papers by Hunt, Cohen, Belcher and Wood (1997), De Angelis, Lombardi, Andreussi and Banerjee (1997a), Heimbach, Bauer, Hasselmann, Hasselman and Lionello (1997), Belcher and Vassilicos (1997), and Makin (1997). These were invited lectures and are published along with other invited lectures by Oxford University Press.

The overall conclusion of the collaboration is that the multidisciplinary nature of the consortium proved beneficial, and substantial progress was made by the collaboration between meteorologists, oceanographers, fluid dynamicists and chemical engineers. The results will be applied in future generation coupled-atmosphere-wave-ocean models of the ECAWOM type, as well as being useful in many industrial sectors where interfacial transport processes are important, *e.g.* the chemical and metallurgical industries.

6.2 Wave Forecasting

Detailed knowledge of the two-dimensional wave spectrum is necessary for many applications, including ship routing, offshore activities, the construction of reliable wave climatologies, and most crucially, an improved understanding of air-sea interaction processes and the development of coupled atmosphere-wave-ocean models. The synthetic aperture radar is at present the only instrument capable of providing such data continuously, and with global coverage.

However, to reliably retrieve ocean wave spectra from observed SAR image spectra, the nonlinear image distortion due to orbital motion effects must be taken into account. This problem has been successfully solved by an improved retrieval algorithm based on an efficient inversion of a closed nonlinear forwards transformation relation. The application of the algorithm in assimilation schemes such as the optimal interpolation scheme or the Green's function methods yields not only an update of the global two-dimensional wave spectral field, but provides also corrections of the driving wind field. The wind field corrections obtained with these schemes were found to be mutually consistent and agreed with other data obtained through GTS.

A scheme based on the adjoint technique was also developed. Studies performed with its one-dimensional predecessor showed that it represents a powerful tool for

model tuning. However, to decide unambiguously upon the parametrizations of the individual source terms of the energy balance equation, more complex two-dimensional sea-state measurements are necessary together with highly accurate wind fields. Such data are available from the SWADE experiment. Besides these high resolution reanalysis products, sea-state measurements from different instruments, including directional wave buoys and airborne radars, provide an ideal data set for testing, evaluating and optimizing alternative model source terms -a future activity!

A further step towards an integrated data assimilation scheme comprising both wind and wave fields is achieved with the development of the coupled ECAWOM model. Besides its use in an integrated operational data assimilation scheme it also represents a powerful tool for testing alternative model source terms obtained through the improved knowledge of air-sea interaction processes.

The statistical analysis of 2 1/2 years of ERS-1 data yields good overall agreement of the ERS-1 retrievals with the WAM computations with respect to net significant wave height. However, small but systematic discrepancies between the modeled and retrieved wave heights for wind-sea and swell systems suggest that the WAModel physics can still be improved. The WAModel has too strong dissipation at low frequencies and too strong wind input source term.

The information contained in the ERS-1 spectral retrievals needs to be further investigated to identify the origins of the deviations found in this first exploratory statistical analysis. The cross-validation with existing altimeter data and with data retrieved from NOAA helps in assessing and improving the quality of sea-state measurements from space and of numerical atmosphere and wave models.

6.3 Wind-Wave Momentum Coupling

Several studies were conducted as part of the PISA project in order to improve our understanding of wind-wave momentum coupling. In the first, a one-dimensional model, using the Reynolds-averaged (two-equation, $k - \epsilon$) formulation, was applied to the air-flow over waves. Explicit account was taken of the wave-induced momentum and heat flux, and these depended crucially on the wave growth rate and spectrum parametrizations. The spectrum was patched together with an energy-containing part proportional to the inverse wave age taken to the power of 0.55, and had an age-independent tail. The growth rate parametrization also used a $\cos^2 \theta$ dependence on wave angle to the wind, and different expressions for waves travelling slower than the wind, and faster than the wind. The wave-induced stress was assumed to decay exponentially with distance above the waves, and wave number.

The results obtained indicated an increasing proportion of the drag was attributable to form drag, as wind speed increased. The calculated drag coefficients appeared to be within the range of the observed data and increased with wind speed -but it should be noted that the data do not contain measurements of the wave spectrum and growth rate. As form drag accounts for a large portion of the total drag at higher wind speeds, the parametrization of the growth rates and spectrum becomes central to validating the calculations.

The model also resulted in an expression for heat exchange in which the Stanton

number was relatively constant with wind speed -perhaps in line with the field data, but these were too scattered to allow reliance to be placed in them. An interesting aspect of the model is that it takes account of the difference in mechanism between momentum and heat exchange at the sea surface. Momentum fluxes are substantially affected by the organized wave-induced motions and hence there is a substantial increase in the drag coefficient as wind velocity increases, leading to substantial increases in total drag coefficient with wind velocity. On the other hand, heat is transported only by the turbulent flux and the effect of waves only comes indirectly through effects on the turbulent diffusivity. To first order, this occurs through production of turbulence from dissipation of the wave-induced motion near the wave surface-but the effect is much weaker than the direct impact of wave-induced motion on the momentum flux-hence the relative constancy of the Stanton number with wind speed in contrast to the rapid increase of the total drag coefficient. These aspects are further validated by the direct numerical simulations of heat and mass exchange discussed later. Furthermore, the large-eddy simulations for flow over waves, performed as part of the project, but of insufficient resolution to be conclusive, also supports these findings. Improved parametrization of backscatter has been developed by Salvetti and Banerjee (1995) and will be implemented in subgrid scale models for LES in future.

The one-dimensional model, perhaps in a somewhat simplified form, is suitable for incorporation in ECAWOM or any other coupled-atmosphere-wave-ocean model. In any case, it clarifies the importance of understanding wave growth and the high wave number tails of the wave spectrum -subjects taken up in the next paragraph.

To better understand wave growth, a theoretical study of turbulent air flow over waves traveling at an arbitrary angle to the wind was undertaken. The study extended the work of Belcher and Hunt (1993) in which two main regions were identified. In an inner region adjacent to the wave surface, the wave-induced turbulence was considered to be in local equilibrium with the wave-induced shear. In the outer region the turbulent eddies are thought to be rapidly distorted and are not in local equilibrium with the shear. Mastenbroek *et al.* (1995) used the second-order Launder *et al.* (1975) closure to show that the Belcher-Hunt predicted rapid decay of the wave-induced stress with distance above the waves, and the relationship of the decay to the height of the inner region, is verified. The wave growth rates of oblique flows were found to be flatter at small angles than $\cos^2 \theta$ and to fall off more rapidly for larger angles -for a given c/u_* - c being the phase speed, u_* is the friction velocity and θ is the angle to the wind. A striking aspect of the results, which requires further validation, is that for higher values of c/u_* , the waves with the largest growth rate move at nonzero angles to the wind! Another interesting aspect is that when the growth rate is normalized with its value at $\theta = 0$, and plotted for various c/u_* , the envelope approximates the $\cos^2 \theta$ dependence, which is the angular dependence commonly used in wave-forecasting models. The effects of waves of arbitrary three-dimensional shape need still to be analyzed, but may be possible to investigate using Fourier superposition. The results of the analysis still have to find their way into the one-dimensional modelling described previously - and this is planned for the future.

A study of the high frequency/high wave number parts of the wind wave spectrum was also undertaken, as this part is important in many air-sea exchange processes, but are not computed by wave-forecasting models. These parts of the spectra are observed to have universal forms and thought to be in dynamical equilibrium. From the analysis, assuming that breaking waves have discontinuous slopes at their crests - as

observed, it appears the equilibrium range is dominated by these singularities in slope. Further assuming a scale invariant dynamical balance in the equilibrium range leads to a spectrum with $\sim k^{-4}$ variation, in agreement with recent data. The frequency spectrum also shows $\sim \sigma^{-4}$ variation, again in agreement with data. Although these vary with the same power laws, the reasons are different. As the wavenumber, k , increases, the spectrum receives contributions from smaller breaking waves, whereas the frequency spectrum is dominated by the longest breaking waves and contains no information about small-scale waves. This deduction suggests a way to test the theory and distinguish it from previous work – an activity of interest for the future.

6.4 Heat and Mass Exchange

Turning back to exchange of heat and species (CO_2 , moisture) at the air-sea interface, we consider first transfer velocities at continuous interfaces. Since the thickness containing resistances to the exchanges are $\sim O(1 \text{ mm})$ or less, it is possible to resolve by direct numerical simulation (DNS). In this regard, note that wind shear leads to a vortex sheet on each side of such an interface and these are remarkably resistant to perturbations in outer regions. (This is why wall turbulence is so difficult to disrupt by oscillations imposed on the outer flows). Because the regions of interest are so thin compared to the interfaces, the first DNS were done for coupled gas-liquid flows with flat interfaces in order to understand the dominant phenomena. This immediately clarified that the air sees the interface something like a wall from the view point of the near-interface turbulence because of the high inertia of the liquid. The water however, sees the interface something like a slip surface with regard to velocity fluctuations because of the low inertia of the air. Thus the interfacial velocity patterns were dominated by liquid side events – since high velocity gradients developed on the gas side. A parallel theoretical study using rapid distortion theory supported this view.

This insight was also in line with simulation of scalar transfer rates which gave transfer velocity which varied as $Sc^{-2/3}$ on the air side, but as $Sc^{-1/2}$ on the liquid side (Sc is the Schmidt or Prandtl number which is the ratio of kinematic viscosity or momentum diffusivity – to mass or heat diffusivity). The $Sc^{-1/2}$ dependence is appropriate for “clean” interfaces – surfactant accumulation could change the dependence to something closer to the air side. DNS were also done for flow over wavy surfaces (of capillary wave characteristics) and fully-deformable cases where the interface was allowed to develop capillary waves. Some of the results from these very computer-intensive simulations are still being analyzed, but it appears clear that the results on the scalar transfer velocities are proportional to friction velocities. Thus the total drag, which contains a form drag component, should not be used to calculate the friction velocity. This finding is also in line with the Reynolds-averaged studies on heat exchange reported in an earlier paragraph. The form drag must be separated out and only the frictional drag used. This arises because the phenomenon dominating scalar exchange are sweep/bursts. A direct correlation between such events and high transfer velocities is evident in the DNS in all cases – both on the air side and the water side.

For sufficiently turbulent streams the sweep/burst events occur with frequencies that are much higher than the frequency of capillary waves, and scale primarily with

the frictional drag and viscosity. This understanding leads to “turbulence-centered” parametrizations that imply transfer velocities $\propto Sc^{-1/2}u_{*L}$ on the water side, and $\propto Sc^{-2/3}u_{*G}$ on the air side. The range of the proportionality constants are also predictable. Note that the u_* s are strictly to be based on frictional drag. Such parametrizations show remarkable agreement with wind-wave tank experiments, where waves were superimposed on the flow and measurements made in regions where wave growth rates were very small – i.e. form drag was low. However to apply them to field data, the sea state and wave growth rates must be known, and as discussed when discussing momentum exchange, form drag accounts for a significant portion of the total drag in such situations. Thus the field data could be expected to lie below the wind-wave tank data, unless the correlation was strictly against the frictional drag velocity – which would have to be estimated for each field situation. A further reduction may occur in the ocean – particularly at low wind velocities – due to surfactant accumulation.

To summarize, the preliminary findings, pending further analysis of the fully deformable interface DNS, clarify the dependence of the transfer velocities on Sc , different on the air and water sides, and show proportionality to the frictional velocity (i.e. based on the frictional stress). Furthermore it is clear that the mechanisms governing the exchange are related to turbulence phenomena and the effect of waves enter only indirectly through the additional dissipation injected by turbulence production through wave-induced stresses.

6.5 Exchange Processes due to Marine Spray

The work on the fluxes due to spray droplets which contained both an experimental and a theoretical component. The experiments involved making observations of droplets formed by rising clouds of bubbles bursting at the liquid surface. Measurements of the sizes and velocities of the droplets were taken and analyzed. Comparisons showed that the ejection velocities were of the order of those reported in the literature, the difference being that other researchers have generally used individual bubbles rather than clouds of bubbles, as is found under breaking waves.

A model was constructed to track the motion and evaporation of droplets over a turbulent sea surface. Using data for the concentration and size distribution of droplets over the sea, this was then used to calculate the rate at which droplets of different sizes are produced for a range of different wind speeds. The results showed that the generation of droplets increased very rapidly as the wind speed increased, this increase being most dramatic for the larger droplets, most of which would be spume drops. With a knowledge of the source term, estimates of the contributions to the latent heat and moisture fluxes were then made; at a wind speed of 22ms^{-1} , it was found that the latent heat fluxes due to droplet evaporation were an order of magnitude less than the total fluxes which have been measured. However, most of the contribution was from the larger droplets ($>60\mu\text{m}$) and, although there is not sufficient data to quantitatively predict how the production rate of these will increase with wind speed, the results of this work strongly suggest that above about 30ms^{-1} , the droplets will play an important role in the exchange processes. Such high winds are normally associated with tropical storms.

The approach taken toward the calculation of the droplet source term and hence the fluxes requires experimental data on the droplet concentration over the ocean and an understanding of the air flow over the sea surface. These have proved to be the limiting factors in the estimation of the source term; our research has found that the most important effects of sprays will be at high wind speeds, with most of the transfer being due to the large drops — the few data which were available for high wind speeds were mainly for small drops. The acquisition of high quality data to fill this gap would lead to much more reliable estimates of the fluxes under storm conditions. Also, the air flow over waves at high wind speeds is very poorly understood, which necessitates the use of grossly simplified models for the air flow. Clearly, further research on sea spray formation at high wind speed, and particularly measurements under storm conditions is desirable.

6.6 Future Work

The results summarized in the present report allow the main objective of the project -the development of a module for the coupling fluxes at the air-sea interface to be fully attainable. Future work can then start from this module and its use to assess the effects of wave-related processes on climate change. The interface module can be incorporated in the coupled atmosphere-wave-ocean model ECAWOM, which has been developed in a parallel project. To this end, ECAWOM can be modified and used to elucidate the impact of various models -particularly with regard to wave-related processes. Numerical experiments can also be conducted with ECAWOM to elucidate effects of model changes and resolution on climate.

In the development of the module, further theoretical and numerical simulation work will be required to improve the parametrization schemes relative to the fluxes of momentum, heat and mass. In particular, the wind-wave coupling model, based on the rapid distortion theory, needs to be extended to include effects of wave three-dimensionality.

The scalar flux models will incorporate wave effects through changes in the near surface turbulence structure. As both momentum and the scalar fluxes occur at length scales that require understanding of the high wave number tail of the ocean-wave spectrum, an assessment of data in this regard will also be necessary.

Finally, parametrization schemes relative to the coupling fluxes in the case of wave breaking need to be further developed. This problem appears to be difficult also because of the limited amount of reliable data available. It seems possible that the results obtained in a parallel project supported by the EU and the increasing amount of data published in the open literature may shed new light on the exchange processes at the air-sea interface in presence of marine sprays.

REFERENCES ¹

- Anderson, R.J. (1993) "A study of wind stress and heat flux over the open ocean by the inertial-dissipation method", *J. Phys. Oceanogr.*, **23**, 2153-2161.
- Andreas, E.L. (1992) "Sea spray and the turbulent air-sea heat fluxes", *J. Geophys. Res.* **97** No. C7 pp. 11429-11441.
- Andreas, E.L. (1994) 'Comments on "On the contribution of spray droplets to evaporation" by Lutz Hasse. *Boundary-Layer Meteorology*, **68**, pp. 207-214.
- Andreas, E.L., Edson, J.B., Monahan, E.C., Rouault, M.P. and Smith, S.D. (1995) "The spray contribution to net evaporation from the sea: A review of recent progress" *Boundary-Layer Meteorology*, **72**, pp. 3-52.
- Bachalo, E. (1990) "Methods for measuring the size and velocity of spheres by dual-beam light-scatter interferometry", *Applied Optics*, **19** 3.
- Banerjee, S., Rhodes, E. and Scott, D.S. (1968) "Mass transfer through falling wavy liquid films in turbulent flow", *Ind. Eng. Che. Fundamentals*, **7**, 22.
- Banerjee, S. (1971) "A note on turbulent mass transfer at high Schmidt numbers", *Chem. Eng. Science*, **26**, 989-990.
- Banerjee, S. (1990), "Turbulence structure and transport mechanisms at interfaces", *Proc. 9th Int. Conf. Heat Transfer*, 1, 395-418, Hemisphere Press, N.Y.
- Banerjee, S. (1995a), "Structure and transport processes in free-surface turbulence", plenary lecture, in *Two-Phase Flow Modelling and Experimentation*, ed. G.P. Celata and R.K. Shah, 1 13-22, Edizioni ETS, Pisa, Italy.
- Banerjee, S. (1995b), "Turbulent heat and mass transfer at gas-liquid interfaces", plenary lecture, *Proceedings of the Second ISHMT-ASME Heat and Mass Transfer Conference*, Karnataka, India.
- Barzel, G., Long, R.B., Hasselmann, S. and Hasselmann, K. (1993) "Wave model fitting using the adjoint technique". In: *Proceedings of the Conference on air-sea interaction*, Marseille, June 1993.
- Barzel, G., (1994) "Optimierung eines Seegangmodells mit der Adjungierten Methode", PhD thesis, University of Hamburg (MPI für Meteorologie, Examensarbeit Nr. 26).
- Bauer, E., Hasselmann, S., Hasselmann, K. and Graber, H. C. (1992) "Validation and assimilation of Seasat altimeter wave heights using the WAM wave model", *J. Geophys. Res.* **C97**, 12671-1268.
- Bauer, E., S. Hasselmann and K. Hasselmann (1996a), "An operational wave forecast system using wind and wave data"; in: *Proceedings of the 2nd ERS Applications Workshop, London, 6-8 December 1995*, ESA SP-383.

¹NOTE: Publications starting with "-" have been generated by this EC-project

- Bauer, E., S. Hasselmann and K. Hasselmann (1996a), "An operational wave forecast system using wind and wave data"; in: *Proceedings of the 2nd ERS Applications Workshop, London, 6-8 December 1995*, ESA SP-383.
- Bauer, E., K. Hasselmann, I.R. Young and S. Hasselmann (1996b) "Assimilation of wave data into the wave model WAM using an impulse response function method", *J. Geophys. Res.* **C101**, 3801-3816.
- Bauer, E. and P. Heimbach (1996c), "Comparison of ERS-1 SAR wave mode data with Altimeter data from TOPEX/POSEIDON and ERS-1", Submitted to *J. Geophys. Res.*
- Bauer, E. and Staabs, C. (1996) "Statistical properties of global significant wave heights and their use for validation", *J. Geophys. Res.*, in press.
- Belcher, S.E. & Hunt, J.C.R. (1993) "Turbulent shear flow over slowly moving waves", *J. Fluid Mech.*, **251**, 109-148.
- Belcher, S.E. and Vassilicos, J.C. (1997), "Breaking waves and wind-wave spectra", *Wind-over-Wave Couplings: Perspective and Prospects*, University of Salford, Oxford University Press, in press.
- Belcher, S.E. and Vassilicos, J.C. (1997), "Breaking waves and the equilibrium range of wind wave spectra", *J. Fluid Mech.*, to appear.
- Belcher, S.E. (1997), "Turbulent shear flow over oblique waves", to be submitted to *Boundary-Layer Met.*
- Beux, F. and Banerjee, S. (1996), "Numerical simulation of three-dimensional two-phase flows by means of a level set method", *Computational Fluid Dynamics '96*, J. Wiley & Sons Eds, p 563-569.
- Blanc, T.V. (1985), "Validation of bulk-derived surface flux, stability, and roughness results due to the use of different transfer coefficient schemes", *J. Phys. Oceanography*, **15**, 650-659.
- Blanchard, D.C. (1982) "The production, distribution, and bacterial enrichment of sea-salt aerosol", *Proc. of the NATO advanced institute on the air-sea exchange of gases and particles*, Durham, New Hampshire, 19-30 July 1982. D. Reidel Pub., Colorado.
- Bortkovskii, R.S. (1987) "Air-sea exchange of heat and moisture during storms". Revised English Edition (Ed. E.C. Monahan) D. Reidel, Dordrecht.
- Boulton-Stone, J.M. and Blake, J.R. (1993) "Gas bubbles bursting at a free surface" *J. Fluid Mech.*, **254**, pp. 437-466.
- Bradley, E.F., Coppin, P.A. and Godfrey, J.S. (1991), "Measurement of sensible and latent heat flux in the Western Equatorial Pacific Ocean", *J. Geophys. Res.*, **96** (Supplement), 3375-3389.
- Broecker, H.C., and Siems, W. (1984), "The role of gas bubbles for gas transfer from water to air at higher wind speeds", in *Gas Transfer at Water Surfaces*, ed. W. Brutsaert and G.H. Jirka, Reidel, Mass, 229-238.
- Brüning, C., Hasselmann, S., Hasselmann, K., Lehner, S., Gerling, T. (1994) "First evaluation of ERS-1 synthetic aperture radar wave mode data", *Global Atmos. Ocean System* **2**, pp. 61-98.
- Buckles, J. and Hanratty, T. (1984) "Turbulent flow over large-amplitude wavy surfaces", *J. Fluid Mech.*, **140**, 27-44.
- Businger, J.A. (1973), "Turbulent transfer in the atmospheric surface layer", *Workshop on Micrometeorology*, ed. D.A. Haugen, Am. Met. Soc. 67-98.
- Cardone, V.J., Graber, H.C., Jensen, R.E., Hasselmann, S., and Caruso, M.J (1996), "In search for a surface wind field in SWADE IOP-1: Ocean wave modelling Perspective"; *Global Atmos. Ocean System*, in Press.

- Caudal, G. (1993), "Self-consistency between wind stress, wave spectrum, and wind-induced wave growth for fully rough air-sea interface", *J. Geophys. Res.*, **98**, C12, 22743-22752.
- Chalikov, D.V. and Makin, V.K. (1991) "Models of the wave boundary layer", *Boundary-Layer Met.*, **56**, 83-99.
- Chalikov, D.V. and Belevich, M.Yu. (1993) "One-dimensional theory of the wave boundary layer", *Boundary-Layer Met.*, **63**, 65-96.
- Cipriano, R.J. and Blanchard, D.C. (1981) "Bubble and aerosol spectra produced by a laboratory 'breaking wave'", *J. Geophys. Res.*, **86**, No. C9, pp. 8085-8092.
- Cohen, J.E. and Belcher, S.E. (1997), "Turbulent shear flow over fast moving waves", Submitted to *J. Fluid Mech.*
- Danckwerts, P.V. (1951) "Significance of liquid film coefficients in gas absorption", *Ind. Eng. Chem.*, **43**, 1460, 1951.
- De Angelis, V., Lombardi, P., Andreussi, P. and Banerjee, S. (1997a) "Microphysics of scalar transfer at air-water interfaces", *Wind- over-Wave Couplings: Perspective and Prospects*, University of Salford, Oxford University Press, in press.
 - De Angelis, V., Lombardi, P. and Banerjee, S. (1997b), "Direct numerical simulation of turbulent flow over a wavy wall", *Physics of Fluids*, **9** N8, 2429-2442.
 - De Angelis, V. and Banerjee, S. (1997c), "Microphysics of turbulent transport processes at gas-liquid interfaces", Winter Annual Meeting ASME, Invited paper to be published in Proceedings.
- De Leeuw, G. (1986) "Vertical profiles of giant particles close above sea surface", *Tellus*, **38B**, pp. 51-61.
- De Leeuw, G. (1990) "Profiling of aerosol concentrations, particle size distributions and relative humidity in the atmospheric surface layer over the North Sea", *Tellus*, **42B**, pp. 342-354.
- Decker, H. and De Leeuw, G. (1993) "Bubble excitation of surface waves and aerosol droplet production: a simple dynamical model", *J. Geophys. Res.*, **98**, No. C6, pp.10223-10232.
- DeCosmo, J. (1991), "Air-sea exchange of momentum, heat and water vapor over whitecap sea states", *Technical Report ONR Grant N00014-85-K-0123*, Ph.D. Thesis., University of Washington, Seattle, WA 98195, p. 212.
- DeCosmo, J., Katsaros, K.B., Smith, S.D., Anderson, R.J., Oost, W.A., Bumke, K. and Grant, A.L.M. (1996) "Air-sea exchange of sensible heat and water vapor over whitecap sea states", *J. Geophys. Res.*, in press.
- Dyer, A.J. (1974) "A review of flux profile relationships", *Boundary-Layer Met.*, **7**, pp. 363-372.
- Edson, J.B. and Fairall, C.W. (1994) "Spray droplet modelling. I. Lagrangian model simulation of the turbulent transport of evaporating droplets", *J. Geophys. Res.*, **99**, pp. 25295-25311.
- Fairall, C.W., Kepert, J.D. and Holland, G.J. (1994) "The effect of sea spray on surface energy transports over the ocean", *TGAOS*, **2**, 121-142.
- Fortescue, G.E. and Pearson, J.R.A. (1967) "On gas absorption into a turbulent liquid", *Chem. Eng. Science*, **22**, 1163.
- Francey, R.J. and Garratt, J.R. (1979) "Eddy flux measurements over the ocean and related transfer coefficients", *Boundary-Layer Met.*, **14**, 153-166.
- Garratt, J.R. (1977) "Review of drag coefficients over oceans and continents", *Mon. Weather Rev.*, **105**, 915-929.
- Geernaert, G.L. (1990) "Bulk parameterizations for the wind stress and heat fluxes", *Surface Waves and Fluxes*, Vol. 1, G.L. Geernaert and W.J. Plant, Eds., Kluwer Academic, 336pp.

- Giering, R. and Kaminski, T. (1996) "Recipes of adjoint code construction", *MPI-Report* Nr. 212, Max-Planck-Institut für Meteorologie, Hamburg. Submitted to *ACM Transactions on Mathematical Software*.
- Gilliland, E.R. and Sherwood, T.K. (1934), "Diffusion of vapors into air streams", *Ind. Eng. Chem.*, **26**, 516.
- Hansen, J., Fung, I., Lacis, A., Rind, D., Lebedeff, S., Ruedy, R. and Russell, G. (1988) "Global climate changes as forecast by Goddard Institute for Space Studies: three-dimensional model", *J. Geophys. Res.*, **93**, 9364-9391.
- Hansen, B., Brüning, C. and Staabs, C. (1994) "Global comparison of significant wave heights derived from ERS-1 SAR wave mode, ERS-1 altimeter and TOPEX altimeter data". In: *Space at the Service of our Environment, Proceedings of the Second ERS-1 Symposium*, Hamburg, FRG, Oct. 1993. ESA SP - 361.
- Harris, J.A., Belcher, S.E., and Street, R.L. (1996), "Linear dynamics of wind waves in coupled turbulent air-water flow - 2", *J. Fluid Mech.*, **308**, 219-254.
 - Hasse, L. (1992) "On the contribution of spray droplets to evaporation", *Boundary-Layer Meteorology*, **61**, pp. 309-313.
 - Hasse, L. (1994) "Reply to Andreas (1994)", *Boundary-Layer Meteorology*, **69**, pp. 335-339.
 - Hasselmann, K. (1991), "Ocean circulation and climate change", *Tellus*, **43B**, 82-103.
 - Hasselmann, K. and Hasselmann, S. (1991) "On the nonlinear mapping of an ocean wave spectrum into a synthetic aperture radar image spectrum and its inversion", *J. Geoph. Res.* **96** 10713- 10729.
 - Hasselmann, K., Heimbach, P. and Hasselmann, S. (1996) "Application of near real-time ERS-1 SAR wave mode data". In: *Oceanology International 1996*, Conference and Exhibition, Section 2: "The global ocean - towards operational oceanography"; Conference Proc. Vol. 3, pp. 181-196; Brighton, 6-8 March 1996.
 - Hasselmann, S., Brüning, C., Hasselmann, K. and Heimbach, P. (1996a) "An improved algorithm for the retrieval of ocean wave spectra from SAR image spectra", *J. Geoph. Res.* **C101**, 16615-16629.
 - Hasselmann, S., Lionello, P. and Hasselmann, K. (1996b) "An optimal interpolation assimilation scheme for wave data", *J. Geoph. Res.*, in press.
 - Hasselmann, S., Bennefeld, C. and Heimbach, P. (1996c) "Algorithm for retrieving ocean wave spectra from SAR image spectra". To appear as *Technical Report* (1997) of the German Climate Computing Centre (DKRZ), Hamburg, FRG.
 - Heimbach, P., Hasselmann, S., Brüning, C. and Hasselmann, K. (1996a) "Application of wave spectral retrievals from ERS-1 SAR Wave Mode data for improved wind and wave field analyses". In: *Proceedings of the 2nd ERS Applications Workshop*, London, 6-8 December 1995, ESA SP-383.
 - Heimbach, P., Hasselmann, S. and Hasselmann, K. (1996b) "Statistical comparison of ERS-1 SAR wave mode data with the WAM model over a 3 year period". Submitted to *J. Geoph. Res.*.
 - Heimbach, P., Bauer, E., Hasselmann, S., Hasselman, K., Lionello, P. (1997), "Use of near real-time ERS-1 SAR wave mode image spectra for wind and wave analyses", *Wind-over-Wave Couplings: Perspective and Prospects*, University of Salford, Oxford University Press, in press.
 - Hersbach, H. (1996) "The adjoint of the WAM model", KNMI Scientific Report, 97-01.
 - Hersbach, H. (1997) "Application of the adjoint of the WAM model to inverse wave modeling". Submitted to *J. Geoph. Res.*.
 - Hewer, F.E. and Wood, N. "The effective roughness length for scalar transfer in neutral conditions over hilly terrain", Submitted to *Quarterly Journal of the Royal Meteorological Society*.

- Higbie, R. (1935) "The rate of absorption of a pure gas into a still liquid during short period of exposure", *Trans. Am. Inst. Chem. Eng.*, **31**, 365.
- Houghton, J.T., Jenkins, G.J. and Ephraums, J.J. (1990) "Climate change. The IPCC Sci. Assessment", Cambridge Univ. Press, Cambridge.
- Hunt, J.C.R. and Graham, J.M.R. (1978) "Free stream turbulence near plane boundaries", *J. Fluid Mech.*, **84**, 209.
- Hunt, J.C.R., Cohen, J.E., Belcher, S.E., Wood, N. (1997) "Turbulent flow over growing waves", *Wind-over-Wave Couplings: Perspective and Prospects*, University of Salford, Oxford University Press, in press.
- Janssen, P.A.E.M. (1989) "Wave-Induced Stress and the Drag of Air Flow over Sea Waves", *J. Phys. Oceanogr.*, **19**, 745-754.
- Johnson, B.D. and Cooke, R.C. (1979) "Bubble populations and spectra in coastal waters: A photographic approach", *J. Geophys. Res.* **84**, No. C7, pp. 3761-3766.
- Kepert, J.D. (1994) "Heat and moisture budget of the tropical cyclone boundary layer", Submitted to: *J. Atmos. Sci.*.
- Kientzler, C.F., Arons, A.B., Blanchard, D.C. and Woodcock, A.H. (1954) "Photographic investigation of the projection of droplets by bubbles bursting at a water surface", *Tellus* **6** No. 3 pp. 1-7.
- Kim, J., Moin, P., and Moser R. (1987) "Turbulence statistics in fully developed channel flow at low Reynolds number," *J. Fluid Mech.* **177**, 133.
- Kline, S.J., Reynolds, W.C., Schraub, F.A. and Runstadler, P.W. (1978) "The structure of turbulent boundary layers", *J. Fluid Mech.*, **70**, 741.
- Koga, M. (1981) "Direct production of droplets from breaking wind-waves - its observation by a multi-colored overlapping exposure technique", *Tellus* **33**, pp. 552-563.
- Koga, M. (1987) "Characteristic features of a wind wave field with occasional breaking, and splashing droplets at high winds", In: *Oceanic Whitecaps and their Role in Air-Sea Exchange Processes* (pp. 129-145), ed. E.C. Monahan and G. Mac Niocaill, D. Reidell, Norwell, Mass.
- Kolovayev, P.A. (1976) "Investigation of the concentration and statistical size distribution of wind-produced bubbles in the near-surface ocean layer", *Oceanology* **15**, pp. 659-661.
- Komen, G.J., Cavaleri, L., Donelan, M., Hasselmann, K., Hasselmann, S. and Janssen, P.A.E.M. (1994) "Dynamics and modelling of ocean waves", Cambridge University Press, Cambridge, UK, 560 pp.
- Komori, S., Murakami, Y. and Ueda, H. (1989), "Relationship between surface-renewal and bursting motions in an open channel flow", *J. Fluid Mech.*, **203**, 103.
- Komori, S., Nagaosa, R. and Murakami, Y. (1993) "Direct numerical simulation of three-dimensional open-channel flow with zero-shear gas-liquid interface", *Phys. Fluids*, **A5**(1), 115-125.
- Kondo, J. (1975), "Air sea bulk transfer coefficients in diabatic conditions", *Boundary Layer Meteorolog.*, **9**, 91-112.
- Kondo, J. (1976) "Parameterization of turbulent transport in the top meter of the ocean", *J. Phys. Oceanogr.* **6**, 712-720.
- Kreplin, H. and Eckelmann, H. (1979) "Behavior of the three fluctuating velocity components in the wall region of a turbulent channel flow," *Phys. Fluids* **22**, 1233.
- Lai, R.J. and Shemdin, O.H. (1974) "Laboratory study of the generation of spray over water", *J. Geophys. Res.*, **79**, pp. 3055-3063.
- Lam, K. and Banerjee, S. (1992) "On the condition of streak formation in a bounded turbulent flow", *Phys. Fluids*, **A4**(2), 306-320.

- Lamont, J.C. and Scott, D.S. (1970) "An eddy cell model of mass transfer into the surface of a turbulent liquid", *AIChE J.*, **16**, 1215.
- Large, W.G. and Pond, S. (1982) "Sensible and latent heat flux measurements over the ocean", *J. Phys. Oceanogr.*, **12**, 464-482.
- Launder, B.E., Reece, G.J. and Rodi, W. (1975) "Progress in the development of a Reynolds-stress turbulent closure", *J. Fluid Mech.*, **68**, 537-566.
- Lewis, W.K. and Whitman, W.G. (1924) "The principles of gas absorption", *Ind. Eng. Chem.*, **16**, 1215.
- Lindzen, R.S. (1994) "Climate dynamics and global change", *Ann. Rev. Fluid Mech.*, **26**, 353.
- Lionello, P., Günther, H. and Janssen, P.A.E.M. (1992) "Assimilation of altimeter data in a global third generation wave model", *J. Geophys. Res.* **C97**, 14453-14474.
- Liss, P.S., and Merlivat, L. (1986), "Air-sea gas exchange rates: Introduction and synthesis", In: *Air-sea Exchange of Gases and Particles* (Ed. P.S. Liss and W.G. Slinn) 241-299. D. Reidel, Dordrecht.
- Liu, W.T., Katsaros, K.B. and Businger, J.A. (1979), "Bulk parametrization of air-sea exchanges of heat and water vapour including the molecular constraints at the interface", *J. Atm. Sci.*, **30**, 1722-1735.
- Lombardi, P., De Angelis, V. and Banerjee, S. (1996) "Direct numerical simulation of near-interface turbulence in coupled gas-liquid flow", *Phys. Fluids*, **8**, 1643-1665.
- Makin, V.K. (1989) "The dynamics and structure of the boundary layer above sea", Senior doctorate thesis, Inst. of Oceanology, Acad. of Sci. USSR, Moscow, 417 pp.
- Makin, V.K. (1990) "Deviation of the mean wind speed profile above waves from the logarithmic distribution", *Izv. Atmos. Ocean Phys.*, **26**, 322-324.
- Makin, V.K., Kudryavtsev, V.N. and Mastenbroek, C. (1995) "Drag of the sea surface", *Boundary-Layer Meteorol.* **73**, pp. 159-182.
- Makin, V. (1997) "Dynamical coupling of waves with the atmosphere", *Wind-over-Wave Couplings: Perspective and Prospects*, University of Salford, Oxford University Press, in press.
- Manabe, S., and Wetherald, R.T. (1987), "Large-scale changes in soil wetness induced by an increase in atmospheric carbon dioxide", *J. Atm. Sci.*, **44**, 1211-1235.
- Mastenbroek, C., Makin, V.K., Garat, M.H. and Giovanangeli, J.P. (1995) "Experimental evidence of the rapid distortion of turbulence in the air flow over water waves", *Memorandum KNMI*, 00-95-01, submitted to *J. Fluid Mech.*
- McMananey, W.J., Davies, J.T., Woolen, J.M. and Koh, J.R. (1973), "The influence of molecular diffusion on mass transfer between turbulent liquids", *Chem. Eng. Science*, **28**, 1061.
- Merlivat, L., and Memery, L. (1983), "Gas exchange across an air-water interface: Experimental results and modelling of bubble contribution to transfer", *J. Geophys. Res.*, **88**, No. C1, 707-724.
- Monahan, E.C. (1968) "Sea spray as a function of low elevation wind speed", *J. Geophys. Res.*, **73**, No. 4, pp. 1127-1137.
- Monahan, E.C. (1971) "Oceanic whitecaps", *J. Phys. Oceanogr.*, **1**, pp. 139-144.
- Monahan, E.C., Spiel, D.E. and Davidson, K.L. (1986) "A model of marine aerosol generation via whitecaps and wave disruption". In: *Oceanic Whitecaps and their Role in Air-Sea Exchange Processes* (pp. 167-174), ed. E.C. Monahan and G. Mac Niocaill, D. Reidell, Norwell, Mass.

- Murphy, P.P., Fedey, R.A., Gammon, R.H., Harrison, D.E., Kelly, K.C. and Waterman, L.S. (1991), "Assessment of the air-sea exchange of CO_2 in the South Pacific during Austral autumn", *J. Geophys. Res.*, **96**, 20, 455-465.
- Nalpanis, P., Hunt, J.C.R. and Barret, C.F. (1993) "Saltating particles over flat beds", *J. Fluid Mech.*, **251**, pp. 661-685.
- Ocampo-Torres, F.J., Donelan, F.J., Woollen, J.M. and Koh, J.R. (1994) "Laboratory measurements of mass transfer of carbon dioxide and water vapor for smooth and rough flow conditions", *Tellus Series B*, 46:16.
- Paulson, C.A. (1970) "The mathematical representation of wind speed and temperature profiles in the unstable atmospheric boundary layer", *J. Appl. Meteorol.*, **9**, pp. 857-861.
- Phillips, O.M. (1977) "Dynamics of the Upper Ocean", 2nd ed. Cambridge University Press, 336 pp.
- Pond, S., Phelps, G.T., Paquin, J.E., McBean, G. and Stewart, R.W. (1971) "Measurements of the turbulent fluxes of momentum, moisture and sensible heat over the ocean", *J. Atmosph. Sci.*, **28**, 901-917.
- Preobrazhenskii, L. Yu. (1973) "Estimate of the content of spray-drops in the near-water layer of the atmosphere", *Fluid Mechanics — Soviet Research*, **2**, pp. 95-100.
- Rashidi, M. and Banerjee, S. (1990) "The effect of boundary conditions and shear rates on streaks formation and breakdown in turbulent channel flow", *Phys. Fluids*, **A2**, 1827.
- Resch, F. and Afeti, G. (1992) "Submicron film drop production by bubbles in seawater", *J. Geophys. Res.*, **97**, No. C3. pp. 3679-3683.
- Rossodivita, A., Ciandri, P., Tanzini G. and Andreussi P. (1995) "Characterization of the aerosol produced by bubbles bursting at a free surface", Third International Symposium on Air-Water Gas Transfer, Heidelberg, July 24-27.
 - Rossodivita, A. and Andreussi P. (1997) "Characterization of droplets produced by bubbles bursting at the air-sea interface", Submitted to *J. Geoph. Res.*.
 - Salvetti, M.V. and Banerjee, S. (1995) "A priori tests of a new dynamic subgrid-scale model for finite difference large-eddy simulations", *Physics of Fluids*, **7**, 2831.
 - Salvetti, M.V., Zang, Y., Street, R.L., and Banerjee, S. (1996), "Large-eddy simulation of decaying free-surface turbulence with dynamic mixed subgrid-scale models", Proceedings of the Twenty-First Symposium on Naval Hydrodynamics, Trondheim, Norvegia, June 24-28, 1996.
 - Salvetti, M.V., Zang, Y., Street, R.L., and Banerjee, S. (1997), "Large-eddy simulation of free-surface decaying turbulence with dynamic subgrid-scale models", *Physics of Fluids*, in press.
- Smith, S.D. (1980) "Wind stress and heat flux over the ocean in gale force winds", *J. Phys. Oceanogr.*, **10**, 709-726.
- Smith, S.D. (1988) "Coefficients for sea surface wind stress, heat flux and wind profiles as a function of wind speed and temperature", *J. Geophys. Res.*, **93**, C12, 15467-15472.
- Smith, S.D. and Anderson, R.J. (1988) "Bedford institute of oceanography eddy flux measurements during HEXMAX", in *Proceedings of the NATO Advanced Workshop: Humidity exchange over the sea: main experiment (HEXMAX), analysis and interpretation*, eds. W.A. Oost, S.D. Smith and K.B. Katsaros, Dellenhove, Epe, The Netherlands, 14- 21.
- Smith, S.D. (1989), "Water vapour flux at the sea surface", *Boundary Layer Meteorolo.*, **47**, 277-293.
- Smith, M.H., Hill, M.K., Park, P.M. and Consterdine, I.E. (1990) "Aerosol concentraions and estimated fluxes over the sea", in: *Modelling the Fate and Influence of Marine Spray* Proceedings of a workshop held 6-8 June 1990, Luminy, Marseille, France.

- Smith, S.D., Anderson, R.J., Oost, W.A., Kraan, C., Maat, N., DeCosmo, J., Katsaros, K.B., Davidson, K.L., Bumke, K., Hasse, L. and Chadwick, H.M. (1992) "Sea surface wind stress and drag coefficients: the HEXOS results", *Boundary-Layer Meteorol.*, **60**, 109-142.
- Smith, M.H., Park, P.M. and Consterdine, I.E. (1993) "Marine aerosol concentrations and estimated fluxes over the sea", *Q. J. R. Meteorol. Soc.*, **119**, pp. 809-824.
- Stabeno, P.J. and Monahan, E.C. (1986) "The influence of whitecaps on the albedo of the sea surface". In *Oceanic Whitecaps and their Role in Air-Sea Exchange Processes* (pp. 261-266), ed. E.C. Monahan and G. Mac Niocaill, D. Reidell, Norwell, Mass.
- Stouffer, R.J., Manabe, S. and Brian, K. (1989), "Interhemispheric asymmetry in climate response to a gradual increase of atmospheric CO_2 ", *Nature*, **342**, 660-662.
- Stretch, D., Belcher, S.E. and Hunt, J.C.R., "Interaction between turbulence on either side of gas-liquid interface", in preparation.
- Takahashi, T. (1989), "The carbon dioxide puzzle", *Oceanus*, **32**, 22-29.
- Vivian, J.E. and King, C.J. (1964), "Diffusivities of slightly soluble gases in water", *AIChE J.*, **10**, 221.
- WAMDI Group (Hasselmann, S. *et al.*), (1988) "The WAM model – a third generation wave prediction model", *J. Phys. Oceanogr.* **18**, pp. 1775-1810.
- Wang, C.S., and Street, R.L. (1978) "Transfers across an air-water interface at high wind speeds: the effect of spray", *J. Geophys. Res.*, **83**, No. C6 pp. 2959-2969.
- Wanninkhof, R.H. and Bliven, L.F. (1991) "Relationship between gas exchange, wind speed, and radar backscatter in a large wind wave tank", *J. of Geophys. Res.*, **96**(C2), 2785-2796.
- Washington, W.M., and Meehl, G.A. (1984), "Seasonal cycle experiment on the climate sensitivity due to a doubling of CO_2 with an atmospheric general circulation model coupled to a simple mixed-layer ocean model", *J. Geophys. Res.*, **89**, 9475-9503.
- Washington, W.M., and Meehl, G.A. (1989) "Climate sensitivity due to increased CO_2 : experiments with a coupled atmosphere and ocean general circulation model, *Climate Dynamics*, **4**, 1-38.
- Woolf, D.K., Bowyer, P.A. and Monahan, E.C. (1987) "Discriminating between the film-drops and jet-drops produced by a simulated whitecap", *J. Geophys. Res.*, **92**, pp. 5142-5150.
- Woolf, D.K. and Thorpe, S.A. (1991) "Bubbles and the air-sea exchange of gases in near-saturation conditions", *Journ. Marine Res.*, **49**, pp. 435-466.
- Wu, J. (1993) "Production of spume drops by the wind tearing of wave crests: The search for quantification", *J. Geophys. Res.* **98**, No. C10 pp. 18221-18227.

European Commission

EUR 18356 — Investigations of the coupling fluxes at the air-ocean interface

Edited by Paolo Andreussi and Sanjoy Banerjee

Luxembourg: Office for Official Publications of the European Communities

1998 — viii, 73 pp. — 21 x 29.7 cm

ISBN 92-828-4878-7

Price (excluding VAT) in Luxembourg: ECU 10

BELGIQUE/BELGIË
Jean De Lannoy Avenue du Roi 202/Koningslaan 202 B-1190 Bruxelles/Brussel Tél. (32-2) 538 43 08 Fax (32-2) 538 08 41 E-mail: jean.de.lannoy@infoboard.be URL: http://www.jean-de-lannoy.be
La librairie européenne/De Europese Boekhandel Rue de la Loi 244/Wetstraat 244 B-1040 Bruxelles/Brussel Tél. (32-2) 295 26 39 Fax (32-2) 735 08 60 E-mail: mail@libeurop.be URL: http://www.libeurop.be
Moniteur belge/Belgisch Staatsblad Rue de Louvain 40-42/Leuvenseweg 40-42 B-1000 Bruxelles/Brussel Tél. (32-2) 552 22 11 Fax (32-2) 511 01 84
DANMARK
J. H. Schultz Information A/S Herstedvang 10-12 DK-2620 Albertslund Tlf. (45) 43 63 23 00 Fax (45) 43 63 19 69 E-mail: schultz@schultz.dk URL: http://www.schultz.dk
DEUTSCHLAND
Bundesanzeiger Verlag GmbH Vertriebsabteilung Amsterdamer Straße 192 D-50735 Köln Tel. (49-221) 97 66 80 Fax (49-221) 97 66 82 78 E-Mail: Vertrieb@bundesanzeiger.de URL: http://www.bundesanzeiger.de
ΕΛΛΑΔΑ/GREECE
G. C. Eleftheroudakis SA International Bookstore Panepistimiou 17 GR-10564 Athina Tel. (30-1) 331 41 80/1/2/3/4/5 Fax (30-1) 323 98 21 E-mail: elebooks@netor.gr
ESPAÑA
Boletín Oficial del Estado Trafalgar, 27 E-28071 Madrid Tel. (34) 915 38 21 11 (Libros), 913 84 17 15 (Suscrip.) Fax (34) 915 38 21 21 (Libros), 913 84 17 14 (Suscrip.) E-mail: clientes@com.boe.es URL: http://www.boe.es
Mundi Prensa Libros, SA Castelló, 37 E-28001 Madrid Tel. (34) 914 36 37 00 Fax (34) 915 75 39 98 E-mail: libreria@mundiprensa.es URL: http://www.mundiprensa.com
FRANCE
Journal officiel Service des publications des CE 26, rue Desaix F-75727 Paris Cedex 15 Tél. (33) 140 58 77 31 Fax (33) 140 58 77 00
IRELAND
Government Supplies Agency Publications Section 4-5 Harcourt Road Dublin 2 Tel. (353-1) 661 31 11 Fax (353-1) 475 27 60 E-mail: opw@iol.ie
ITALIA
Licosa SpA Via Duca di Calabria, 1/1 Casella postale 552 I-50125 Firenze Tel. (39-55) 064 54 15 Fax (39-55) 064 12 57 E-mail: licosa@fbcc.it URL: http://www.fbcc.it/licosa
LUXEMBOURG
Messageries du livre SARL 5, rue Raiffeisen L-2411 Luxembourg Tél. (352) 40 10 20 Fax (352) 49 06 61 E-mail: mdl@pt.lu URL: http://www.mdl.lu
Abonnements: Messageries Paul Kraus 11, rue Christophe Plantin L-2339 Luxembourg Tél. (352) 49 98 88-8 Fax (352) 49 98 88-444 E-mail: mpk@pt.lu URL: http://www.mpk.lu

NEDERLAND
SDU Servicecentrum Uitgevers Christoffel Plantijnstraat 2 Postbus 20014 2500 EA Den Haag Tel. (31-70) 378 98 80 Fax (31-70) 378 97 83 E-mail: sdu@sdu.nl URL: http://www.sdu.nl
ÖSTERREICH
Manz'sche Verlags- und Universitätsbuchhandlung GmbH Kohlmarkt 16 A-1014 Wien Tel. (43-1) 53 16 11 00 Fax (43-1) 53 16 11 67 E-Mail: bestellen@manz.co.at URL: http://www.austria.EU.net:81/manz
PORTUGAL
Distribuidora de Livros Bertrand Ld.* Grupo Bertrand, SA Rua das Terras dos Vales, 4-A Apartado 60037 P-2700 Amadora Tel. (351-1) 495 90 50 Fax (351-1) 496 02 55
Imprensa Nacional-Casa da Moeda, EP Rua Marquês Sá da Bandeira, 16-A P-1050 Lisboa Codex Tel. (351-1) 353 03 99 Fax (351-1) 353 02 94 E-mail: del.incm@mail.telepac.pt URL: http://www.incm.pt
SUOMI/FINLAND
Akateeminen Kirjakauppa/Akademiska Bokhandeln Keskuskatu 1/Centralgatan 1 PL/PB 128 FIN-00101 Helsinki/Helsingfors P./fn (358-9) 121 44 18 F./fax (358-9) 121 44 35 Sähköposti: akatilaus@akateeminen.com URL: http://www.akateeminen.com
SVERIGE
BTJ AB Traktörvägen 11 S-221 82 Lund Tfn (46-46) 18 00 00 Fax (46-46) 30 79 47 E-post: btjeu-pub@btj.se URL: http://www.btj.se
UNITED KINGDOM
The Stationery Office Ltd International Sales Agency 51 Nine Elms Lane London SW8 5DR Tel. (44-171) 873 90 90 Fax (44-171) 873 84 63 E-mail: ipa.enquiries@theso.co.uk URL: http://www.theso.co.uk
ÍSLAND
Bokabud Larusar Blöndal Skólavörðustíg, 2 IS-101 Reykjavík Tel. (354) 551 56 50 Fax (354) 552 55 60
NORGE
Swets Norge AS Østenjoveien 18 Boks 6512 Etterstad N-0606 Oslo Tel. (47-22) 97 45 00 Fax (47-22) 97 45 45
SCHWEIZ/SUISSE/SVIZZERA
Euro Info Center Schweiz c/o OSEC Stampfenbachstraße 85 PF 492 CH-8035 Zürich Tel. (41-1) 365 53 15 Fax (41-1) 365 54 11 E-mail: eics@osec.ch URL: http://www.osec.ch/eics
BĂLGARIA
Europress Euromedia Ltd 59, blvd Vitosha BG-1000 Sofia Tel. (359-2) 980 37 66 Fax (359-2) 980 42 30 E-mail: Milena@mbx.cit.bg
ČESKÁ REPUBLIKA
ÚSIS NIS-prodejna Havelskova 22 CZ-130 00 Praha 3 Tel. (420-2) 24 23 14 86 Fax (420-2) 24 23 11 14 E-mail: nkposp@dec.nis.cz URL: http://usiscr.cz

CYPRUS
Cyprus Chamber of Commerce and Industry PO Box 1455 CY-1509 Nicosia Tel. (357-2) 66 95 00 Fax (357-2) 66 10 44 E-mail: info@ccci.org.cy
EESTI
Eesti Kaubandus-Tööstuskoda (Estonian Chamber of Commerce and Industry) Toom-Kooli 17 EE-0001 Tallinn Tel. (372) 646 02 44 Fax (372) 646 02 45 E-mail: einfo@koda.ee URL: http://www.koda.ee
HRVATSKA
Mediatrade Ltd Pavla Hatza 1 HR-10000 Zagreb Tel. (385-1) 43 03 92 Fax (385-1) 43 03 92
MAGYARORSZÁG
Euro Info Service Európa Ház Margitsziget PO Box 475 H-1396 Budapest 62 Tel. (36-1) 350 80 25 Fax (36-1) 350 90 32 E-mail: euroinfo@mail.mata.v.hu URL: http://www.euroinfo.hu/index.htm
MALTA
Miller Distributors Ltd Malta International Airport PO Box 25 Luqa LQA 05 Tel. (356) 66 44 88 Fax (356) 67 67 99 E-mail: gwirth@usa.net
POLSKA
Ars Polona Krakowskie Przedmiescie 7 Skr. pocztowa 1001 PL-00-950 Warszawa Tel. (48-22) 826 12 01 Fax (48-22) 826 62 40 E-mail: ars_pol@bevy.hsn.com.pl
ROMÂNIA
Euromedia Str. G-ral Berthelot Nr 41 RO-70749 Bucuresti Tel. (40-1) 315 44 03 Fax (40-1) 315 44 03
RUSSIA
CCEC 60-letiya Oktyabrya Av. 9 117312 Moscow Tel. (7-095) 135 52 27 Fax (7-095) 135 52 27
SLOVAKIA
Centrum VTI SR Nám. Slobody, 19 SK-81223 Bratislava Tel. (421-7) 531 83 64 Fax (421-7) 531 83 64 E-mail: europ@ttb1.sltk.stuba.sk URL: http://www.sltk.stuba.sk
SLOVENIA
Gospodarski Vestnik Dunajska cesta 5 SLO-1000 Ljubljana Tel. (386) 611 33 03 54 Fax (386) 611 33 91 28 E-mail: europ@gvestnik.si URL: http://www.gvestnik.si
TÜRKİYE
Dünya Infotel AS 100, Yil Mahallesi 34440 TR-80050 Bagcilar-Istanbul Tel. (90-212) 629 46 89 Fax (90-212) 629 46 27 E-mail: infotel@dunya-gazete.com.tr
AUSTRALIA
Hunter Publications PO Box 404 3067 Abbotsford, Victoria Tel. (61-3) 94 17 53 61 Fax (61-3) 94 19 71 54 E-mail: jpdavies@ozemail.com.au
CANADA
Les éditions La Liberté Inc. 3020, chemin Sainte-Foy G1X 3V Sainte-Foy, Québec Tel. (1-418) 658 37 63 Fax (1-800) 567 54 49 E-mail: liberte@mediom.qc.ca
Renouf Publishing Co. Ltd 5369 Chemin Canotek Road Unit 1 K1J 9J3 Ottawa, Ontario Tel. (1-613) 745 26 65 Fax (1-613) 745 76 60 E-mail: order.dept@renoufbooks.com URL: http://www.renoufbooks.com

EGYPT
The Middle East Observer 41 Sherif Street Cairo Tel. (20-2) 393 97 32 Fax (20-2) 393 97 32 E-mail: order_book@meobserver.com.eg URL: www.meobserver.com.eg
INDIA
EBIC India 3rd Floor., Y. B. Chavan Centre Gen. J. Bhosale Marg. 400 021 Mumbai Tel. (91-22) 282 60 64 Fax (91-22) 285 45 64 E-mail: ebic@glasbm01.vsnl.net.in URL: http://www.ebicindia.com
ISRAËL
ROY International 41, Mishmar Hayarden Street PO Box 13056 61130 Tel Aviv Tel. (972-3) 649 94 69 Fax (972-3) 648 60 39 E-mail: royil@netvision.net.il
Sub-agent for the Palestinian Authority:
Index Information Services PO Box 19502 Jerusalem Tel. (972-2) 627 16 34 Fax (972-2) 627 12 19
JAPAN
PSI-Japan Asahi Sanbancho Plaza #206 7-1 Sanbancho, Chiyoda-ku Tokyo 102 Tel. (81-3) 32 34 69 21 Fax (81-3) 32 34 69 15 E-mail: books@psi-japan.co.jp URL: http://www.psi-japan.com
MALAYSIA
EBIC Malaysia Level 7, Wisma Hong Leong 18 Jalan Perak 50450 Kuala Lumpur Tel. (60-3) 262 62 98 Fax (60-3) 262 61 98 E-mail: ebic-kl@mof.net.my
PHILIPPINES
EBIC Philippines 19th Floor, PS Bank Tower Sen. Gil J. Puyat Ave. cor. Tindalo St. Makati City Metro Manila Tel. (63-2) 759 66 80 Fax (63-2) 759 66 90 E-mail: eccpcor@globe.com.ph URL: http://www.eccp.com
SOUTH KOREA
Information Centre for Europe (ICE) 204 Woo Sol Parktel 395-185 Seogyo Dong, Mapo Ku 121-210 Seoul Tel. (82-2) 322 53 03 Fax (82-2) 322 53 14 E-mail: euroinfo@shinbiro.com
THAILAND
EBIC Thailand 29 Vanissa Building, 8th Floor Soi Chidlom Ploenchit 10330 Bangkok Tel. (66-2) 655 06 27 Fax (66-2) 655 06 28 E-mail: ebicbkk@ksc15.th.com URL: http://www.ebicbkk.org
UNITED STATES OF AMERICA
Bernan Associates 4611-F Assembly Drive Lanham MD20706 Tel. (1-800) 274 44 47 (toll free telephone) Fax (1-800) 865 34 50 (toll free fax) E-mail: query@bernan.com URL: http://www.bernan.com
ANDERE LÄNDER/OTHER COUNTRIES/AUTRES PAYS
Bitte wenden Sie sich an ein Büro Ihrer Wahl / Please contact the sales office of your choice / Veuillez vous adresser au bureau de vente de votre choix

NOTICE TO THE READER

Information on European Commission publications in the areas of research and innovation can be obtained from:

◆ **CORDIS, the Community R & D Information Service**

For more information, contact:

CORDIS Customer Service, BP 2373, L-1023 Luxembourg

Tel. (352) 44 10 12-2240; fax (352) 44 10 12-2248; e-mail: helpdesk@cordis.lu

or visit the website at <http://www.cordis.lu/>

◆ **Euroabstracts**

The European Commission's periodical on research publications, issued every two months.

For more information, contact:

RTD help desk, European Commission, DG XIII, L-2920 Luxembourg

Fax (352) 43 01-32084; e-mail: rtd-helpdesk@lux.dg13.cec.be

Price (excluding VAT) in Luxembourg: ECU 10



OFFICE FOR OFFICIAL PUBLICATIONS
OF THE EUROPEAN COMMUNITIES

L-2985 Luxembourg

ISBN 92-828-4878-7



9 789282 848784 >